M.Sc. Thesis

EIT InnoEnergy – SELECT
Environomical Pathways for Sustainable Energy Systems

Design and upscaling of a demo CSP parabolic trough plant utilizing molten salt as heat transfer fluid

Author:	Luca Gentile
Supervisor:	prof. Ivette Rodriguez
External supervisor:	prof. Frank Dinter
Internal Examiner:	prof. César Alberto Valderrama Ángel
Session:	July 2017

Escola Tècnica Superior
d'Enginyeria Industrial de Barcelona

Universitat Politècnica de Catalunya, Spain
in collaboration with
Stellenbosch University, South Africa

M. Sc. SELECT is a cooperation of:
KTH: Royal Institute of Technology, Stockholm, Sweden | UPC: Universitat Politècnica de Catalunya · BarcelonaTech, Barcelona, Spain
IST: Instituto Superior Técnico, in Lisbon, Portugal | TU/e: Eindhoven University of Technology, Eindhoven, the Netherlands
AGH: University of Science and Technology, Krakow, Poland | PoliTo: Politecnico di Torino, Turin, Italy

Acknowledgments

The present work represents the Thesis for the Innoenergy SELECT Master's Programme, whose final year has been spent at the Universitat Politècnica de Catalunya, Barcelona, Spain. It is the result of a three-months internship as internal researcher at the Stellenbosch University, South Africa.

I would like to express my gratitude to Mr. Louis Jestin, for the initial help to create a fruitful collaboration with the Stellenbosch University and the EPPEI Master's Programme.

I would like to thank Professor Frank Dinter, supervisor in South Africa, for his constant help, motivation and enthusiasm during my experience in Stellenbosch. With him, I would like to acknowledge the STERG research group for its support.

I would like to thank Professor Ivette Rodriguez for giving me the opportunity to perform my Master's thesis under her guidance, providing me with essential help and showing continuous willingness.

My deepest gratitude to Professor César Alberto Valderrama Ángel, for his assistance thoughout this final year, and to the whole Innoenergy staff.

On a personal level, there are several people this work is dedicated to. To my father, for having taught me the importance of hard work and tenacity. To my mother, for her sincere happiness towards life. To my sister, friend and guidance throughout my whole life. To my entire family, for its encouragement. To all my friends, stronger than any distance. To all the students I met during these two years, for all I learnt from them. To the people of Sweden, Spain and South Africa, that made me feel like home.

Abstract

Electricity in South Africa is mostly produced by polluting coal-fired power plants. The availability of solar resource is vast and its utilization in the CSP technology is more than promising. When coupled with thermal energy storage, these systems can provide firm and dispatchable energy, covering both base- and peak- demand. The current state-of-the-art is based on the utilization of parabolic trough collectors and thermal oil as heat transfer fluid (HTF). The use of molten salt (MS) in the solar field would substantially increase the upper temperature limit, up to 600 °C, with consequent performance enhancement and cost reduction. LCOE down to 11 c$/kWh and power block efficiencies up to 40% can be achieved. The Molten Salt Parabolic Trough (MSPT) technology would be able to increase the flexibility grid, facilitating the integration of stochastic renewable energy sources and reducing the dependency on fossil fuels.

The main challenge related to the utilization of the MS is its high melting point, which requires the outlining of an appropriate free-protection strategy. Since the technology is not proven on a commercial scale, a demonstration plant should be built to address the main issues and reduce the financial and technological risk. Eskom, the national public utility, is addressed for the construction of a single loop, integrated with a two-tank storage and a steam generation system. It will be based in one of its properties, close to Johannesburg. Four HelioTrough collectors, equipped with Rioglass receivers will be used to ensure high performance and material resistance at elevated temperatures. During night operation, the recirculation of the HTF through the cold storage would maintain the fluid temperature above reasonable limits, without the need of expensive electric heat tracing system. A 3-hour storage and nigh mass flow of 4 kg/s can provide the freeze-protection service, with no additional capital or ongoing cost. Draining with the use of compressed air and by gravity could be considered in case of major faults.

The investment cost of the plant is estimated to be 47,540,797 R (3.7 M$), with yearly O&M expenditure is equal to 542,543 R (around 42,000 $).

Once the demonstration loop will have tested the MSPT performance and reliability, the plant should be upscaled to 100 MW_e. A solar-multiple of 3 and a 15-hour storage system could ensure capacity factors up to 75%, providing fast-ramping base load and competing with the less flexible coal-production. Placing the plant in the central area of the country would represent a good trade-off between solar resource availability and diversification of the production. A I-layout would facilitate the draining procedure and reduce the pressure losses in the piping. Dry-cooling would minimize the water consumption and the overall environmental impact.

MSPT systems represent a frontier technology, whose large-scale implementation would have important business benefits for Eskom, placing the company in a central industrial position. An initial public-private partnership with foreign companies would be beneficial for risk sharing and knowledge transfer. On the long-term, all the South Africa industrial actors can be involved realization of competitive industry, based on the export of technology-intensive goods. Job creation and GDP contribution are two additional important benefits.

The MSPT technology proved to be one of the main ways to ensure a sustainable future in South Africa, from an environmental, social and business standpoint.

Table of Contents

Glossary

Latin symbols	
A	Area [m^2]
c_p	Specific heat capacity
d	Diameter [m]
f	Friction factor
G	Mass velocity [m^2/s]
k	Thermal conductivity [W/mK]
L / l	Length [m]
$\dot{m}$	Mass flow [kg/s]
N	Number
Nu	Nusselt nu,ber
p	Pressure [Pa]
Pr	Prandtl number
$\dot{q}$	Specific heat flux [W/m^2]
$\dot{Q}$	Heat flux [W]
Ra	Rayleigh number
Re	Reynolds number
T	Temperature [K]
U	Overall heat transfer coefficient [W/m^2K]
u / v	Velocity [m/s]
V	Volume [m^3]
W	Width

Greek Symbols	
α	Absorptivity
α (with subscript)	Heat transfer coefficient [W/m^{2}K]
ε	Emissivity
η	Efficiency
ρ	Density/Reflectivity
σ	Surface tension
σ_b	Stefan-Botzmann constant [W/m^{2}K^4]
τ	Transmissivity

Subscripts	
ab	Absorber
amb	Ambient
av	Average
br	Brackets
cd	Conduction
cv	Convection
rad	Radiation
eva	Evaporation
ex	External
f	Fluid
g	Glass
in	Inner
ml	Logarithmic mean
N	Nominal

Subscripts	
o/out	Outer
opt	Optical
rad	Radiation
s	Storage/shell
std	Standard
t	Tube

Abbreviations	
CSP	Concentrating Solar Power
DSG	Direct Steam Generation
GDP	Gross Domestic Product
HTF	Heat Transfer Fluid
IAM	Incidence Angle Modified
IPP	Independent Power Produced
IRP	Integrated Resource Planning
LCOE	Levelized Cost Of Electricity
MSPT	Molten Salt Parabolic Trough
O&M	Operation and Maintenance
PPP	Public-Private Partnership
R&D	Research and Development
REIPPP	Renewable Energy Independent Power Producer Procurement Programme
RES	Renewable Energy Sources
SCA	Solar Collector Assembly
SCE	Solar Collector Element
TMY	Typical Meteorological Year

List of Figures

List of Tables

1. Introduction and literature review

1.1. Motivation and scope of the present study

In South Africa, most of the electricity is currently produced by polluting coal power stations. The demand is expected to grow in the near future and, due to increasing presence of renewable energy sources (RES) in the energy mix, the supply will have to be more flexible. The availability of renewable sources is massive, with one of the highest yearly solar irradiation in the world. Among all the solar-based technologies, Concentrating Solar Power (CSP) seems to be the best for the South African scenario. In fact, when coupled with thermal energy storage, firm and dispatchable electricity can be provided, replacing expensive peaks production. Parabolic-trough collectors represent the most mature and widespread CSP technology, which has shown technical reliability since the '80s. The main limitations of these systems are related to the heat transfer fluid (HTF) utilized: thermal oil. Even if characterized by a low freezing point, its stability is limited to 400 °C, substantially reducing the potential efficiency of the power block. Furthermore, the fluid utilized for storage purposes, usually molten salt (MS), is not exploited to its highest potential, since it has operating temperatures up to 600 °C. Therefore, it seems to be reasonable to use MS directly in the collectors, in order to increase efficiencies and heat storage capacities. The main concern related to this application is the high freezing point. A careful design of the plant and freeze protection strategy should be outlined. A well-designed innovative technology demonstration programme over an extended period needs to be developed, geared towards research and development (R&D), with the aim of cost reduction [1]. The first step for a successful development of the technology is the realization of a demonstration plant, able to prove both feasibility and reliability of the system. The national public utility, Eskom, is addressed for the realization of the plant. In fact, the uncertainties related to a new technology would hinder the participation of solely private actors. Eskom would have the possibility to be a first mover, placing itself in a central position within the international industrial landscape. The pubic-private partnership with foreign companies is essential, ensuring knowledge and expertise transfer, and shared risks.

The main purpose of this work is to propose a design for a demonstration plant located in South Africa utilizing the MSPT (Molten Salt Parabolic Trough). In Chapter 1, an extensive literature review will be performed, in order to justify the decisions taken for the design of the plant. The actual design will be presented in Chapter 2. All the main components will be considered, both on the salt and water side. An annual simulation will be used to size the heat storage system to provide enough heat during low irradiation periods to avoid freezing of the salt, without the need of expensive electric heat tracing system. The simulation of the daily behavior of the plant will be also presented. Chapter 3 will be dedicated to a first cost estimation, while, in Chapter 4, suggestions for the future scale-up will be proposed. An analysis of the business potential and of the main macro socio-economic benefits for South Africa will be included in Chapter 5, underlining the main social aspects related to the described technology. Finally, conclusions will be drawn in Chapter 6.

1.2. Concentrating Solar Power (CSP) technology

1.2.1. Basic principles

Concentrating Solar Power (CSP) technology involves the utilization of mirrors or lenses to concentrate direct beam solar radiation into a receiver, in order to convert it into useful heat [2]. The heat is collected by a fluid and can be utilized directly or to produce electricity or fuels, according to the downstream technology utilized [3]. Unlike low-temperature solar systems, the portion of radiation that has been diffused by the presence of clouds or dust cannot be exploited. As a result, areas with a high number of clear-sky days should be selected as preferable sites [2].

The first utility-scale CSP plants were installed in California between 1986 and 1991 [4]. They have demonstrated their reliability throughout the whole operational life, but no additional installations were proposed during low fossil fuel price periods. Due to cost escalation of the conventional sources in the 2000s, the technology has returned to be central [4].

A CSP plant is composed by three major subsystems [5]:

- The solar field, where the solar energy is concentrated and collected by the Heat Transfer Fluid (HTF). The HTF is usually water, oil or molten salts. In the two last cases, additional heat exchangers are required for the steam production.
- The power block, where the produced steam is used to move a turbine and produce electricity. Common steam Rankine cycles are usually employed.
- Thermal energy storage (TES), which is used to store excess energy collected during high-irradiation periods to be utilized in night-time. It can provide dispatchable energy also when the solar resource is scarce.

If the plant availability should be further enhanced, it can be functionally integrated with fossil fuel stations to create hybrid systems [5]. Depending on the way the solar energy is collected and transferred to the heat transfer fluid, four different technologies can be considered. They are briefly described in the next paragraphs, as in [5].

1.2.2. Parabolic Trough (PT) collectors

Parabolic Trough collectors currently represent the most mature CSP technology, being the first system utilized in the SEGS (Solar Energy Generating Systems) plants in California. It is commercially proven and it has shown to be consistent when connected to the electric grid. They utilize parabolic-shaped mirrors to concentrate the sunlight into a linear receiver placed in the focal line of the parabola (see Figure 1.1). The assembly of mirrors and the receiver are mounted on a frame that tracks the sun on one axis [2].

The main HTFs utilized are steam and thermal oil, but, how it will be described in the present analysis, the potential of employing molten salt is currently under study. When TES is coupled to the system, molten salt is used also as storage medium. The PT technology will be utilized for the demonstration plant, due to its reliability and bankability. A state-of-the art will be presented in detail in section 1.4.

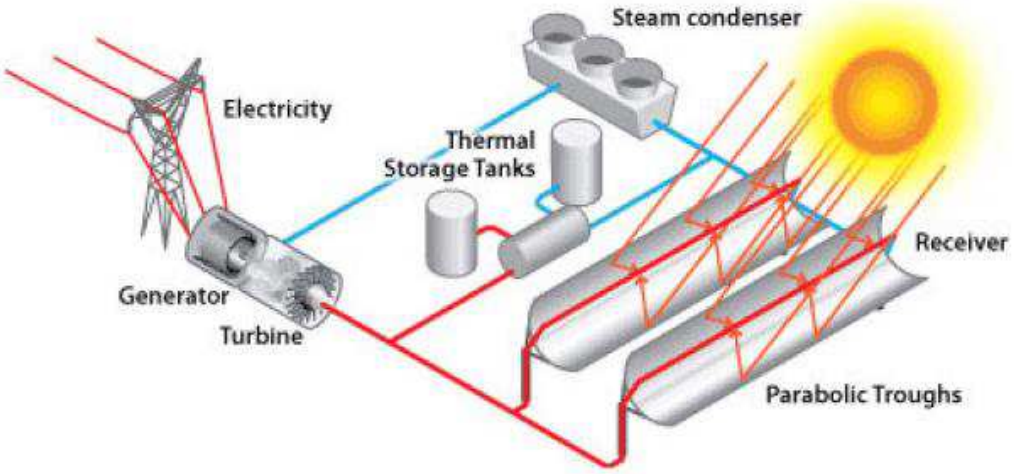

Figure 1.1: CSP parabolic trough plant [5]

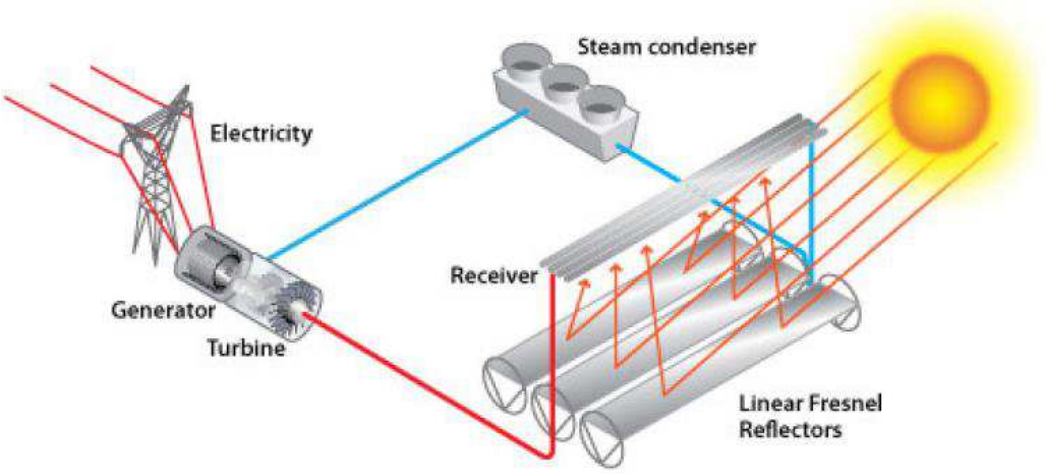

Figure 1.2: CSP Linear Fresnel power plant [5]

1.2.3. Linear Fresnel (LF)

The Linear Fresnel technology is quite similar to the PT, since they share common principles in both arrangement and operation [3]. The solar field is composed by an array or flat mirrors, which reflects the beam radiation onto linear absorbers, mounted on a 10-15 m tall tower, as shown in Figure 1.2. The reflectors are positioned to approximate a parabolic shape, but they track the sun individually. Thus, the receiver is stationary and there is no need of rotating couplings between the receiver and the piping [2]. The main challenge is represented by the mutual shadowing of adjacent reflectors at low solar angles [3].

Typically, water with Direct Steam Generation (DSG) is utilized as heat transfer fluid, but molten salt has been studied to increase the performance of the system [6]. Typical systems operate in the temperature range 50-400 °C, concentrating the beam radiation 10-40 times [3].

The technology is not as mature as PT, but it is currently under development.

1.2.4. Power Tower technology

Also known as Central Tower, the Power Tower technology utilizes a flied of two-axes tracking mirrors called heliostats to concentrate the sunlight onto a receiver place on the top of a tower (Figure 1.3). The light is concentrated in the range of 600-1 000 times, achieving working fluid temperature of 500-800 °C. Both figures are higher than the one characterizing the parabolic trough technology, with consequent higher thermal efficiencies. Various heat transfer fluids can be considered, such as steam, air and molten salt. The last one is usually preferred, since it can be easily and effectively coupled with large thermal storage systems and it is characterized by stability at very high temperatures. The technology is considered mature after the successful operation of different plants worldwide. One of the main example is represented by the Gemasolar power plant, located in Seville, Spain. With 20 MW of installed capacity and 15 hours of storage, the plant can operate at nominal condition up to 5 000 hours per year [7].

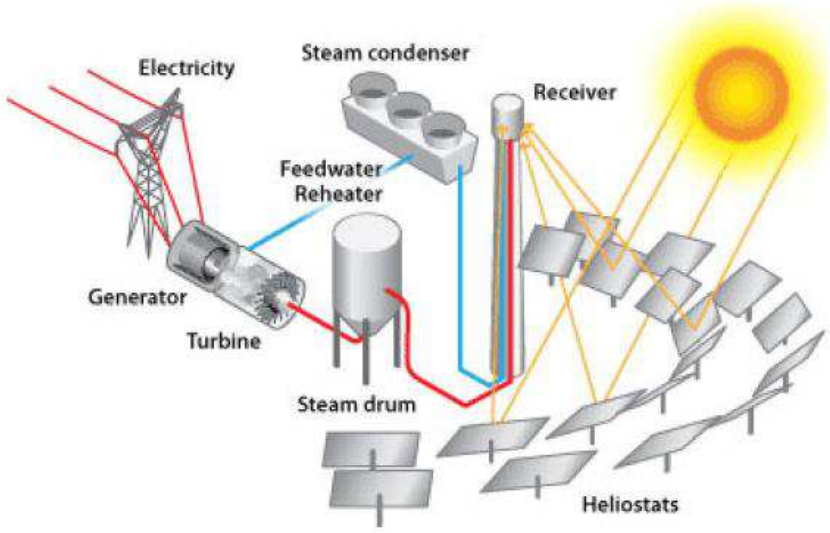

Figure 1.3: CSP central tower power plant [5]

1.2.5. Parabolic Dish

The Parabolic Dish (or Dish engine) technology exploits the geometric properties of a parabola as a 3-D paraboloid, as pictured in Figure 1.4. After being tracked with a two-axes system, the reflected beam radiation is concentrated to a point-focus receiver. The absorber is mounted on an arm at the focal point of the reflector and can reach temperature up to 1 000 °C, with light concentration of 1 000 times [3] [2]. It contains a motor-generator combination that usually operates using a Stirling engine or a micro gas turbine. Due to high tracking efficiency, high operation temperature and high efficiency conversion cycles, the Parabolic Dish is the most efficient CSP technology. Furthermore, the collectors are highly modular and can be utilized in rural and remote areas (even on terrains with grades up to 5 %), with minimum water requirements. The biggest disadvantage is that the heat is directly converted into electricity, limiting storage possibilities [8]. It is also the least commercially mature technology and only

small units (10-25 kW) are currently constructed [2].

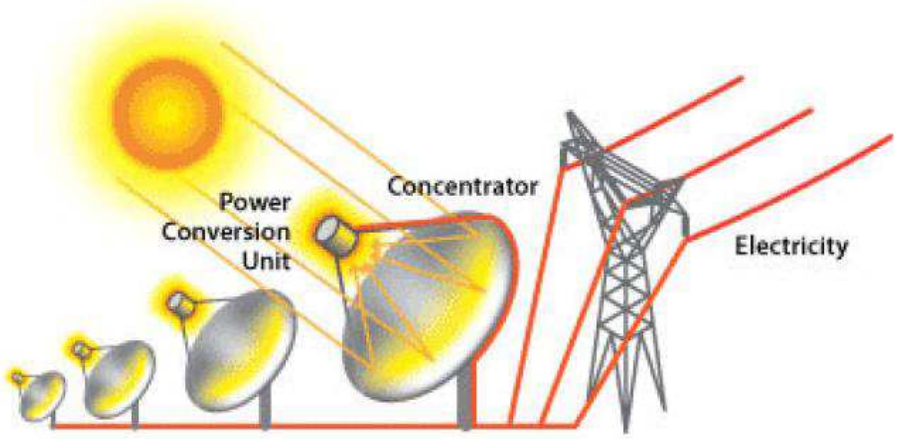

Figure 1.4: CSP parabolic dish plant [5]

1.2.6. Main advantages of CSP

CSP technology presents unique features compared to other RES. It has the main advantage of being dispatchable, providing firm and flexible production [9] [4]. The term "flexibility" refers to the minimum power the plant can operate. This aspect is particularly important since, when shut down, the plant might require a considerable amount of time to re-start the operation, limiting its availability [4]. Flexible power production is a key element for a system that is progressively moving towards a high share of RES in the electricity mix [9]. As underlined by [4], CSP can represent a valid alternative to hydropower stations, being characterized by higher storage efficiencies, over 95 %. Furthermore, the steam turbine of the power block can act as spinning reserve for overall grid stabilization for several seconds, in case of unforeseen outages. Compared to conventional power plants, no fuel consumption is needed to keep the plant warm, if enough energy is stored in the storage system. A CSP steam cycle can be up to four time faster during the start-up, compared to a conventional coal cycle. Finally, reactive power can be exchanged with the grid, ensuring constant voltage control [9].

The main barrier hindering a large-scale utilization of CSP plants is its high capital cost compared to both conventional and more mature RE systems. Typical cost of OCGT (Open Cycle Gas Turbines) is in the order of 600 $/kW, while supercritical coal plants can be as high as 2,500 $/kW. Nuclear power is usually more capital intensive, with initial expenditures of about 5,000 $/kW. On the other hand, CSP plant cost can range from 4,600 $/kW, for a PT system with no thermal energy storage, to 10,500 $/kW, for a Solar Tower plant with 15 hours of storage [8]. More than 80 % of the Levelized Cost Of Electricity (LCOE), or rather the electricity price to break even at the end of the lifetime of the plant, is composed by capital cost. Consequently, it is stable for the entire lifetime. According to the most recent projections, the cost will be competitive with natural gas by 2020 and with coal by 2025, due to both economy of scale and improved manufacturing. It is already a cleaner and more cost-effective solution than oil. Overall, the CSP technology represents a solution with same technical quality

but enhanced economic stability compared to conventional fossil-fuel fired power plants [4].

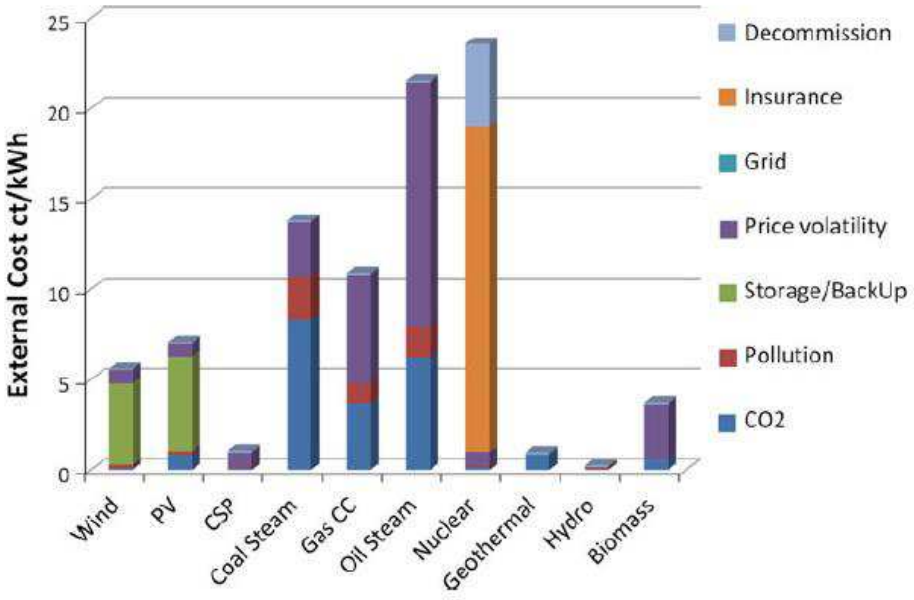

Figure 1.5: Comparison of the external costs for different energy sources [4]

Compared to other RES, Concentrating Solar Power is considered less mature, with a total installed capacity worldwide of 3 GW in 2013, compared to 300 GW and 100 GW for wind power and PV (photovoltaics), respectively [4]. However, the comparison between the different technologies usually does not take into consideration the cost related to infrastructure and grid update. Stochastic energy sources always need pump storage or the back-up from conventional power plants, which should operate between full and minimum load, with adverse implications on efficiency, durability and fuel consumption. In their study, [4] compared different energy technology internalizing all the external costs, such as carbon emission, pollution, storage needed, transmission upgrade, price volatility, decommissioning and insurance cost. As it can be observed in Figure 1.5, CSP represents one of the most valuable systems under this perspective.

When the environmental impacts are considered, lifecycle GHG emissions and land requirements should be analyzed. The total carbon emissions for CSP technology are similar to other RES, around 14 g/kWh. The two main alternatives to cover peak and base demand, gas and coal, are characterized by 422 and 978 g/kWh, respectively. Moreover, the release of the other harmful pollutants is limited to a minimum [10]. The land requirement is usually similar to the one characterizing PV, around 8-15 km^2/TWh, but much smaller than the one needed by wind power (up to 41 km^2/TWh) [10]. These figures are one or two orders of magnitude higher than the ones for conventional power plants. However, mining, transport infrastructure and eventual carbon capture and sequestration have to be considered [4]. Overall, CSP is the best RES in terms of environment and related external socioeconomic costs.

1.2.7. Worldwide CSP market

The development of the CSP technology is driven by different emerging markets, such as China, India, Northern Africa, Southern Africa and Middle East. It has its origin in the Solar Energy Generating Systems (SEGS) established in the Mojave Desert, in California, in the 1980s, as previously mentioned [9].

China is one of the leaders in CSP technology patenting, owning no less than one third of the total patents. It claims to be able to reach 3 GW of installed capacity by 2020. In order to achieve this ambitious target, the country is establishing an efficient value chain. Other countries have similar goals for the near future: India is determined to reach 10 GW by 2020, Saudi Arabia 25 GW by 2030 and Qatar 1.8 GW by 2020. In 2010, the USA invested 2 billion $ in the Abengoa Solana Project, to create one the largest parabolic trough solar power plant in the world, which started its operation in 2013. In Europe, Spain was the first country to introduce a feed-in-tariff for CSP in 2002, in order to foster a large-scale deployment of the technology. However, this incentive was cancelled in 2012 for new applicants and no awarded to plants beyond 2355 MW. The Spanish and American plants have demonstrated to be able to operate on demand, also during low irradiation periods, thanks to the integration with efficient molten salt-based storage systems. In Italy, ENEA was one of the first movers, utilizing a specially designed and patented receiver for the use of molten salt as heat transfer fluid at high temperature [9].

All the countries involved in the development and improvement of the CSP systems have enhanced their learning curve, reducing the overall cost. Further cost reduction will be driven by market opportunities and use of frontier technologies.

1.3. Renewables in South Africa

In South Africa, the electricity generation is controlled by Eskom, the national electricity company, which is responsible for about 96 % of the supply [11]. Compared to the other countries of the Southern Africa Development Community (SADC), South Africa is characterized by a higher electricity access, higher installed capacity and consumption per GDP (Gross Domestic Product). As a result, it produces roughly 80 % of the electricity consumed in whole region, acting as a net exporter [12]. According to the most recent statistics available, 252 578 GWh are produced per annum, of which 249 919 GWh are consumed domestically [13]. The national electricity mix is strongly dependent on coal, which is used as bulk fuel for the clear majority of the annual production (more 90 %), with 14 power stations in operation, for a total of 38.5 GW of installed capacity [11]. This is because South Africa presents the majority of economically extractable coal reserves [12] [14]. Four fast-ranging Open Cycle Gas Turbines (OCGT) utilizing thermal oils, with a total capacity of 2 426 MW, are used only during peak hours or emergency situations, due to their extremely high operational costs [11]. Besides the fossil fuel resources, the country is characterized by an enormous potential in terms of RES [15]. More than 2 500 hours of sunshine are recorded every year and most of the country is classified as semi-arid, with large expanses of flat terrain with high solar irradiation, ideal for a large-scale deployment of solar energy. Furthermore, the presence of the ocean all around the country creates optimal conditions to exploit wind power massively

[16]. However, only 0.8 % of the total annual production is covered by these two resources. Solid mass and waste represent the largest renewable energy contributor, mainly used for heat production. The generation mix includes also two conventional hydroelectric plants and three hydro pumped storage schemes, to cover the demand not met by the base-load power stations. Their combined capacity amounts to 2 732 MW. Finally, Eskom operates the first African nuclear plant, characterized by a production capability of around 2 GW.

The annual electricity consumption by resource is reported in Figure 1.6 [13].

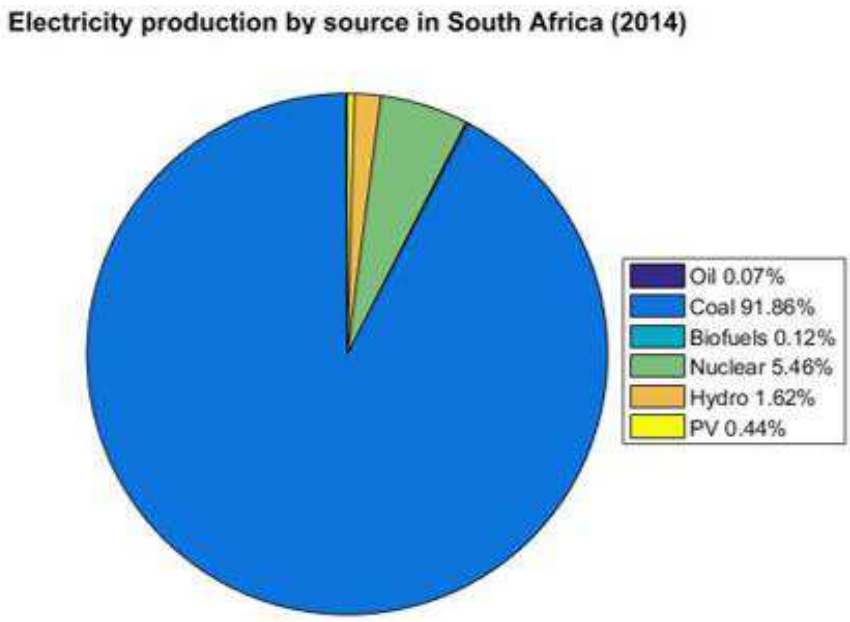

Figure 1.6: Electricity production by source in South Africa [13]

According to several authors, the current extensive exploitation of the coal reserves cannot last in the long-term. [12] and [14] the Southern African region is close to its peak annual consumption and a further increase in demand could lead to shortfalls already in 2018. The installed diesel-powered gas turbines are seen as a mitigating agent for the recent margin problems, but their high running cost could have many adverse implications in the electricity price. In the next paragraphs, the policy supporting a large-scale implementation of RES systems will be presented, together with the potential that the CSP could have in the South African landscape.

1.3.1. Renewable Energy Policy in South Africa

The need of a sustainable energy future is underlined in the cornerstone document of the South African Republic, the Constitution written in 1996. The economic growth should not be untied from the environmental conservation but, on the contrary, the natural resources should be an essential mean to boost the social development [16]. Historically, three main documents can be identified as fundamental for understanding the role of the RES in the national policy: the White Paper on Energy Policy, the White Paper on Renewable Energy and the National Climate Change Response White Paper Policy. These three main policies can be seen as part

of the National Development Plan, a holistic vision for future growth and development. One of the main goals is to return to a state of continued and uninterrupted electricity supply, increasing the generation reserve margin. Under this perspective, the 2010 Integrated Resource Plant (IRP) for electricity 2010-2030 is a fundamental document. It continuously allocates the generation growth, based on electricity demand change, new development in technology and fuel options, scenarios for carbon mitigation strategies and affordability of electricity. The REIPPP (South African Renewable Energy Independent Power Producer Procurement Programme) is a programme of the national Department of Energy that implements the RE allocation in the IRP. Independent Power Producer (IPP) submit bids for the systems that they intend to build, ensuring a competitive tendering procedure [17]. The 2016 IRP update calls for doubling electricity generation, mainly from coal, nuclear, RES (including hydro imported): by 2030, 52 GW should be added to the current portfolio, 17.8 of which from wind, solar, biomass, small-scale hydro, biogas and 2.6 GW from large-scale hydro [18]. CSP represented less than 10 % of RE allocation, with 1050 MW selected since 2011 and no further expansion considered after 2020 [19] [18]. Nuclear energy is seen as able to cover the baseload, while reducing the coal usage. In the other hand, PV and wind energy are expected to produce 14 % of the electricity by 2030, with gas used to cover the peaks [18]. Under the current policy situation, it does not seem feasible to consider further CSP capacity expansion. However, it is opinion of the author that such as study must be accomplished, for the following reason:

- The IRP is continuously updated and if CSP plants operating in South Africa (see section 1.3.2) will prove to be reliable, the technology will have to be considered.
- The use of coal-fired power plants cannot be considered an everlasting option for South Africa: the integration of stochastic sources in the electricity mix, such as wind and PV energy, will require the system to be highly flexible to variation in supply.
- The strong commitment of South Africa to climate change (reduction of greenhouse gas emissions, GHG, by 34% by 2020, and 42% by 2025 [18]) cannot be guaranteed if the potential of CSP is not exploited at its maximum.
- Finally, the pursue of a sustainable future, able to ensure local involvement and social equality, must consider RE as main sources, due to massive local availability.

The operating CSP plants in SA, and the main advantages and barriers for this large-scale implementation will be highlighted in the following paragraphs.

1.3.2. CSP in South Africa: current situation and overall potential

Being part of the so-called “solar belt” (zone with latitude lower than 40°), the geographical position of South Africa is highly favorable to the exploitation of solar energy [20] . The solar resource is vast, with values up to up to 3 000 kWh/m^2 per year in the Northern Cape [12]. This figure places the country among the top-3 nations for solar resource worldwide, which, in some cases, this is almost 50 % better than Spain and California [1] [16]. According to [21], 2 000 kWh/m^2 per year can be considered as the threshold to ensure economic viability of the project.

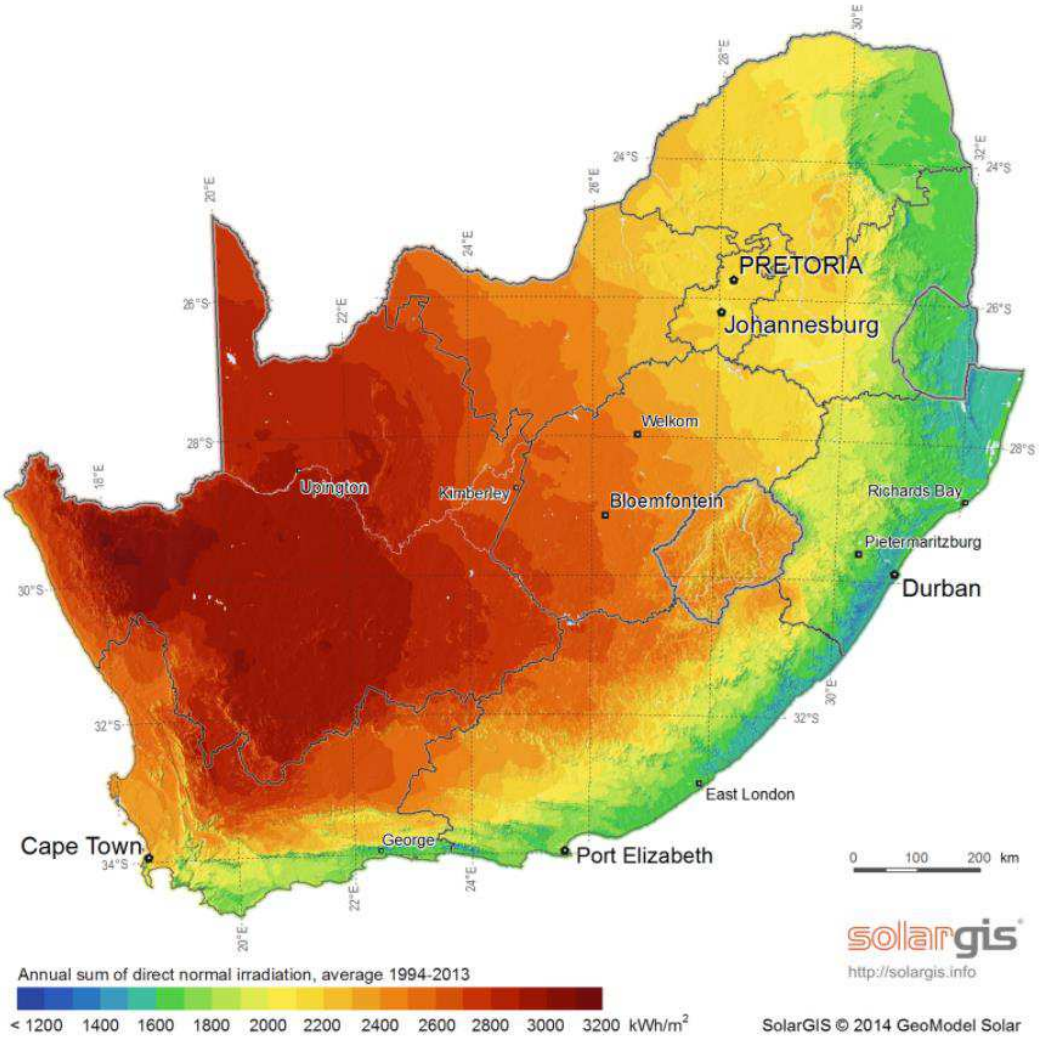

Figure 1.7: Annual solar irradiation in South Africa [23]

Table 1.1: Operating CSP power plants in South Africa [22]

Plant	Technology	Capacity	HTF	Storage	Capacity factor
KaXu Solar One	Parabolic Trough	100 MW	Thermal oil	Two-tank indirect with molten salt (2.5 h)	38 %
Khi Solar One	Power Tower	50 MW	Water/steam	Pressure vessel with saturated steam (2 h)	40 %
Bokpoort	Parabolic Trough	50 MW	Thermal oil	2-tank indirect with molten salt (9.3 h)	52 %

As it can be appreciated in Figure 1.7, most of the areas in South Africa exceed this value. Moreover, vast semi-desert areas are present, with large land availability *[21]*. Three CSP plants are operating in South Africa, while four are under construction, mainly considering parabolic trough systems with thermal oil as heat transfer fluid and located in the Northern Cape. Table 1.1 shows the main characteristics of the operating plants *[22]*.

1.3.3. Potential of CSP technology in South Africa

The reliability of Concentrating Solar Power plants has been proven by more than 20 years of operation in the United States and in Spain. The availability of solar radiation in South Africa is one of the highest worldwide, with an overall CSP potential around 40 GW [9]**.** A plant located in South Africa would perform better than one in Spain, due to its proximity to the equator, reducing the maximum losses related to sun position [23]. A large-scale adoption of solar systems would also entail several benefits for the overall electric system. According to [14], South Africa is currently overestimating the coal resource: peak consumption will be experienced within the next decade and 90 % of the recoverable amount will be completely depleted by mid-century. For this reason, a diversification of the current electricity generation mix would be valuable because of frequent maintenance backlogs, high fuel expenses, geographical concentration and long build periods of existing Eskom's coal-fired power plant [17]. Furthermore, enhancing the reserve margin would be beneficial for the overall grid stability and security of supply [14]

Due to the high flexibility and reduce ramping time required by the power block, CSP plants can be also utilized to replace high-cost emergency generation, which, according to the current IRP, will be mostly covered by diesel-fueled OCGT. The South African load profile is recognized as being noticeably predictable and, if coupled with proper energy storage, a solar plant would be able to provide high-value dispatchable energy on demand [24] [12].

The plant could operate as baseload or to cover the peaks. Baseload power plants will be characterized by higher capacity factors, since they will produce more time. However, they will be characterized by higher cost (due to bigger solar field and storage system) and they will receive, in average, a smaller payment per kWh produced. In the present study, the potential of the CSP technology to reduce the dependency from coal is set as primary and, therefore, the upscaled plant will be designed to cover the base load (see Chapter 4).

From an economic perspective, CSP is the only dispatchable generation that will not suffer from rising fuel prices and cost vulnerability. Since the main part of the cost is related to the initial investment, the financial risk is not linked to external aspects [8]. Due to their dispatchability, CSP power plants can facilitate the integration of other stochastics renewable sources, such as PV and wind, which usually requires a difficult optimization considering different technologies [12]. Consequently, the expected future increase of the electricity price, due to higher demand and limited fuel availability, could be efficiently hindered by a high exploitation of RES, which are characterized by a marginal cost close to zero [4]. CSP will be the main contributors in GHG emissions reduction in South Africa [20]. The industrial landscape offers the possibility to South Africa for being a first mover and becoming a regional R&D (Research and Development) hub [12]. The UNEP (United Nations Environmental Programme) 2014 report has placed SA among the top 10 countries in RES investment,

representing the 10th biggest solar market in the world [16]. The business potential related to CSP technology will be discussed in Chapter 5. Finally, CSP, presenting a better match with existing manufacturing capabilities, can benefit from a higher degree of local inclusion [12]

1.4. State-of-the-art of the Parabolic Trough technology

The CSP technology based on the utilization of parabolic trough collectors is considered to be the most mature solar power design. With a total of 354 MW installed, the SEGS plants have been a valuable landmark for the development and commercial deployment of this technology. Three plants are still in operation, highlighting the level of credibility and confidence towards these systems. They are characterized by light structures and relative high efficiencies. The mirrors are made by sheets of reflective material (usually silvered acrylic), which is bent in a parabolic shape. Each mirror is usually referred to as a Solar Collector Element (SCE). Long troughs are usually composed by several mirrors, creating a Solar Collector Assembly (SCA). The modules are supported from the ground by simple pedestals. The structure is usually subjected to wind drag and it must be robust enough to prevent deviations from normal insolation [3]. Thermal stresses and self-weight are also causes of deformation [25]. The receiver, a black metal pipe encased in a glass tube to limit thermal losses, is mounted on the focal line. Its design its crucial for efficient heat transfer and load management [3].

Currently, the heat transfer fluid utilized is synthetic oil, whose operating temperature is limited to 400 °C due to stability reasons. The steam is usually produced at around 370 °C, limiting the overall efficiency of the power block [26]. In the next sections, the different components will be described briefly.

1.4.1. The structure

In order to achieve a perfect parabolic shape with high optical efficiency, highly precise assembly is required, with design tolerance around ± 2 mm. The overall design should minimize the torsion at the ends of the collector and transfer the torque when the sun is tracked. The steel structure is usually covered with galvanization process, in order to be protected from corrosion agents [27].

Different designs can be considered [28]:

- Use of a central space frame called torque box, which provides good rigidity and prevents torsion. It ensures good performance under moderate wind speeds, but it is characterized by high assembly cost, due to high number of steel profiles.
- Use of a central steel tube (torque tube). It is usually cheaper, but subjected to deformation by gravity (bending) and wind loads (torsion).
- Use of a metallic space frame. No assembly jig is required, but it relies in the accuracy of the preformed parts.

A quality control procedure is of fundamental during the process, ensuring perfect alignment of parallel rows to avoid solar tracking errors [28]. The support structure is made of steel and aluminum. The latter is usually preferred, since it is characterized by higher specific stiffness,

lighter density and consequent lower energy consumption for tracking [27]. The assembly line is applied to mount the collector component and it can be done by a low-skilled workforce [27].

1.4.2. The mirrors

The main type of mirror utilized in commercial PT design is the curved black-silvered low-iron thick-glass one. Polished sheet metal or silver-coated films can be considered in alternative [28]. The fabrication of the mirrors is a cost-intensive process [27].

1.4.3. The solar receiver

The solar receiver tube is the key component of the CSP plant, since its performance has critical consequences in the overall system efficiency [29]. It is composed by two concentric pipes: an inner steel pipe containing the heat transfer fluid and an outer glass tube made of a low-iron borosilicate glass, to increase the transmittance of solar radiation [28]. The outer surface of the steel pipe is an optically selective surface, with high absorptance in the solar spectrum and low emittance in the infra-red radiation range [26]. The absorber is coated with three different layers, to increase absorptivity and reduce thermal losses. A metal with low thermal emissivity is used as inner layer, while the second layer is composed by a mixture of ceramic and metal (Cermet), which enhances the solar absorption. Finally, an anti-reflective coating is deposited to maximize the optical performance [27]. The receiver can be evacuated or non-evacuated [26]. The first option is considered for temperature above 300 °C, where the need of heat loss reduction might be significant. The cost of an evacuated receiver is around 950 $/unit, justifying its utilization only at high temperatures. Getters placed between the receiver and the cover are used to absorb gas molecules passing from the fluid to the annulus though the pipe wall, in order to maintain the vacuum condition [28].

Stainless steel bellows are required to compensate the different thermal expansion of the glass and the steel at elevated temperature [28]. Advanced glass-to-metal welding techniques are used to connect the glass tube to the bellows [27]. The welding represents a weak point in the receiver, which must be protected with an aluminum shield from the concentrated radiation to avoid high thermal and mechanical stresses [28]. Main manufacturers are Schott, Siemens and Archimede Solar Energy (ASE) [28]. In Figure 1.8, a simplified representation of the solar receiver is pictured.

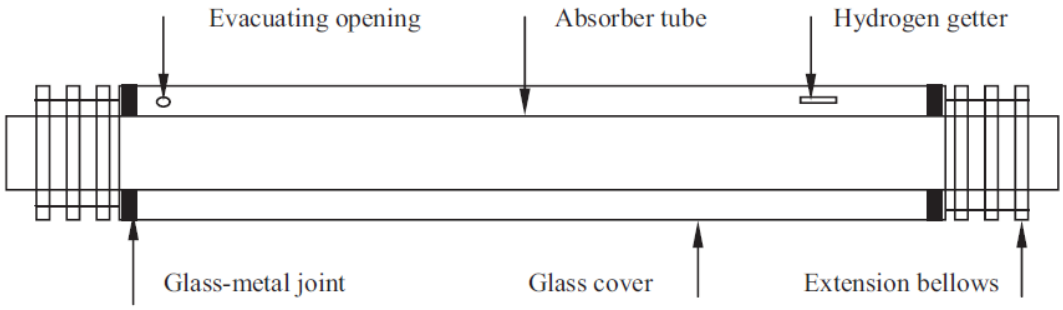

Figure 1.8: Simplified representation of the solar receiver [28]

1.4.4. Tracking system

The solar tracking device must keep the collector towards the sun direction, with substantial influence on the SCA performance [28] [25]. Three main components can be identified: the hydraulic system, needed to rotate the collector around its own axis, the electric motor-gearbox and the local control unit. The tracking mechanisms can be based either on photocells sensors or on astronomical algorithms [27].

1.4.5. Main geometrical and performance parameters

In the recent years, the main technical improvements related to the parabolic trough collectors are oriented towards the increase of the aperture area, in order to maximize the energy gain. Typical length can reach almost 250 m for each SCA, usually composed by 10 SCE. The width is around 6-7 meter, resulting in aperture areas larger than 1 500 m^2 [30] [31].
The geometric concentration ratio C_g is the ratio between the collector aperture area A_{SCA} and the total absorber tube surface A_{tube} [28]:

$$C_g = \frac{A_{SCA}}{A_{tube}} = \frac{W \cdot l_{tube}}{\pi \cdot d_{ab,o} \cdot l_{tube}} = \frac{W}{\pi \cdot d_{ab,o}} \quad (1.1)$$

Where W represents the width of the collector, l_{tube} the total length of the absorber tube and $d_{ab,o}$ its outer diameter. Typical concentrations range around 25-35, but recent designs can reach values close to 70.

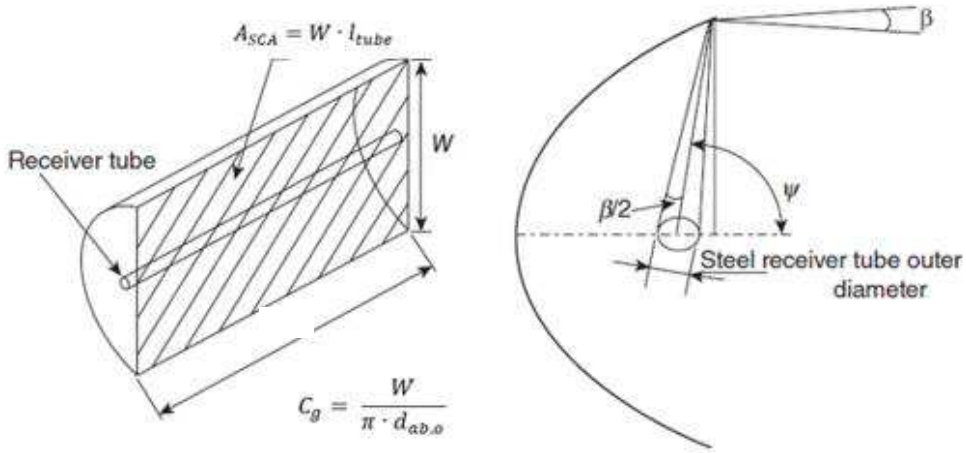

Figure 1.9: Geometric parameter of a PTC, adapted from [29]

The acceptance angle β is the maximum angle that can be formed by two rays on a plane transversal to the collector aperture in such a way that, when they are reflected by the mirrors, they intercept the absorber pipe. The wider the acceptance angle is, the less accurate the tracking system must be. The minimum acceptance angle is 0.53°, which represents the average solid angle with which the solar disk is seen from the Earth. If lower than this limit, the

collector would always lose part of the Direct Normal Irradiation (DNI). Recommended values are between 1-2°.
The rim angle Ψ is calculated as function of the focal distance f and the width:

(1.2) $$tan\,\Psi = \frac{8 \cdot f \cdot W}{W^2 - 16 \cdot f^2}$$

Smaller rim angles reduce the aperture area needed, while large values entail an enlarged reflective surface, without significant increase of useful area on the aperture plane. Typical values are in the range 70-100°. In Figure 1.9, these parameters are described graphically.
Not all the solar radiation intercepted by the mirror area reaches the absorber and an optical efficiency should be considered [28]. The part of the reflected radiation that does not reach the receiver is quantified by the intercept factor. It considers the imperfection of the reflectors (microscopic errors), the imperfections in the parabolic shape (macroscopic errors), the mechanical deformation of the collector, the presence of the flexible bellows and the shadowing of the tube supports. The peak optical efficiency is around 75 %. Finally, it has to be considered that this efficiency depends on the angle of incidence. The Incidence Angle Modifies (IAM) is the ratio between the optical efficiency at a given angle and the optical efficiency at angle of incidence equal to zero and it is a function of the incidence angle itself:

(1.3) $$IAM(\theta) = \frac{\eta_{opt(\theta \neq 0)}}{\eta_{opt(\theta = 0)}}$$

Where η_{opt} is the optical efficiency and θ is the incidence angle. The value of the optical efficiency and of the IAM for the case under study will be described in section 2.1.2.

1.4.6. Operation and maintenance

The main activities related to operation and maintenance of a parabolic trough field are related to the washing and the periodic measurement of the reflectivity of the mirrors. The mirror soiling is highly site-specific, which can have a substantial impact on the performance of the system. During summer, in Spain, the reflectivity decreases 0.0025 % per day during two weeks after washing. For this reason, specially-designed mirror washers utilizing demineralized water are used, collecting water from a tank truck that pumps it at 200 bar. If the mirrors are not very dirty, simple demineralized water curtains may be used. The average water consumption is estimated to be 0.7 l/m^2 [28].
The breakage of the mirrors does not occur very frequently (less than 0.1 % per year), since they are designed to sustain wind speeds up to 100 km/h. If a mirror breaks, the falling pieces might break the glass cover and damage the absorbed, with important economic consequences [28].
Other important activities are the period check of the collector alignment, the periodic maintenance of the ball-joints and the annual analysis of the properties of the heat HTF [28].

1.5. Thermal energy storage (TES)

CSP power plants with thermal energy storage maintain the highest marginal economic value [32]. This is due to the fact a highly efficient is able to store excess production during high irradiation periods and to deliver it at times of greatest need, reducing the typical complication in usage of solar energy [3]. Utilizing the current technology, round-trip efficiencies of 98 % can be achieved [8].

In general, the energy storage system is not essential for proper operation of the plant. However, it presents several fundamental advantages [28]:

- More hours of operation and increased capacity factor of the CSP plant. In this way, the cost of the resulting produced electricity is more competitive.
- Increased dispatchability of the plant, with favorable implications for the electric grid.
- Enhanced performance of the plant during cloud periods, reducing steep transients.
- Avoided damages of the steam turbines, acting as a buffer and reducing the number of starts and stops of the power block. Consequently, the lifetime of the system is elongated substantially.

In the most recent systems, a two-tank system utilizing molten salt as storage medium has been chosen as the most suitable technology for both parabolic trough and solar tower systems. It is considered a to-date commercially viable option for high-temperature applications [33]. The heat is stored in sensible form, exploiting the temperature difference between the “cold” tank, usually at 290 °C, and the “hot” tank, whose temperature depends on the fluid utilized in the solar field. If thermal oil is used, the upper temperature is limited to 390-400 °C. On the other hand, with molten salt, temperatures up to 550-575 °C can be considered, with no additional heat exchanger requirements (direct system) [32]. Immersed electric heaters are placed inside the tanks to avoid the solidification of the salts [32].

Suitable materials resistant to elevated temperatures should be chosen for the construction of the tanks. Carbon and stainless-steel alloys present proper corrosion resistance and mechanical strength to resist up to 650 °C [32].

Currently, slightly less than 50 % of the installed plats has a TES. However, due to the maturity of the systems utilizing molten salts, 80 % of the plants under construction presents a storage system (88 % if only parabolic trough and solar tower systems are considered) [8].

1.6. Heat transfer fluids

Historically, water and thermal oil have been the main heat transfer fluids utilized in the parabolic trough power plants. Innovative solutions aiming at reducing the cost of the produced electricity propose to employ molten salts.

The use of water in parabolic troughs for direct steam generation can be detected from the first SEGS, back in the 1980s. The system results to be simplified and characterized by improved efficiency. However, the scarcity of water in the desert regions represents the main challenge, together with the corrosion potential of the steam at elevated temperatures. Furthermore, the

use of pressure vessel as storage systems set a limit on the availability of back-up energy, which cannot cover periods longer than 1-2 hours. For these reasons, it is not usually considered in the most recent systems [34].

Mineral, silicone and synthetic oils have been tested and used in CSP applications. They present constant thermal conductivity and low corrosivity over a wide range of temperatures. Thermal oils are stable only up to 400 °C and highly expensive. Due to high vapor pressure, they cannot be utilized at storage media. Moreover, they are flammable and toxic [34].

The term “molten salts” is used to designate liquids obtained from the fusion of an inorganic salt [35]. They are excellent heat transfer fluids, since thermally stable at very high temperatures (over 500 °C) and with comparable properties to water, such as viscosity and low vapor pressure. Common used salts are based on nitrates and nitrites, but current research is focusing in the addition of other components to decrease the high boiling point. They are neither toxic nor flammable and they can be used both as storage medium and heat transfer fluid [34]. In the next sections, their choice as operating fluid will be justified.

1.6.1. Advantages in the utilization of molten salt

The main characteristics of the molten salts have been summarized by [34]:

- Low viscosity, enhancing the heat transfer efficiency.
- Low vapor pressure (< 1 atm), resulting in easier and safer storage.
- Thermal stability over 500 °C, enabling production of high-temperature steam. This aspect entails higher efficiencies in the power block and higher electricity production.
- High heat capacity, which reduces the size of the heat storage system.
- High thermal conductivity.
- No toxicity or flammability [26].
- Low cost compared to thermal oils.
- No soil-permeability with consequent no danger for the underground water [36]
- High melting point. It marks the lowest allowable temperature and a safe margin has to be ensured at any time [35].

The use of molten salts as heat transfer fluid is the result of a growing pressure for technological innovation and cost reduction in the RES power plants [37] [3]. Shifting from the use of thermal oil to molten salts can enable significant increase in the operating temperatures, reaching Rankine cycle efficiency up to 40 %, compared to 37.6 % currently achieved with oils at 393 °C [38]. This aspect is also beneficial for the TES, since a higher temperature difference between the two tanks increases the energy density. Temperatures up to 575 °C can be considered in the hot tank, resulting in 2.75 more energy stored in the same volume compared to the base-case employing oils [37] [38]. The absence of intermediate heat exchangers reduces the specific system cost [39].

According to many authors, the use of molten salts as HTF would result in lower LCOE. Matino & Maccari [29] report reduction potential in the range 20-45 %, depending on solar field dimensions, optimized heat collector elements, solar irradiation and other site-specific conditions. A similar figure is presented by [40], who foresees reduction in order of 20 % and

higher capacity factors. Kearney et al. [38] report a less optimistic prediction, with a forecasted decrease in the cost of the electricity produced of 18 %. A molten salt PTC plant with 6-hour storage can reduce the cost of the TES by 43.2 %, of the solar field by 14.8 % an, overall, of the LCOE by 9.8-14.5 % [41]. LCOE as low as 11 c$/kWh can be obtained utilizing the most recent collectors with an optimized storage size [37]. Additional cost reduction could be achieved with economy of scale [37].

Plant operation, administration and power block maintenance costs are unchanged compared to the utilization of oil but, as it will be better described afterwards, special attention should be put on the freezing protection strategy [42]. It is essential to underline that all the overmentioned economic advantages are related to the presence of a storage system, which is the key element to provide a competitive advantage [43].

1.6.2. Challenges

The main challenge related to the utilization of molten salts in the solar field is the high melting point (120-220 °C), compared to the one characterizing the thermal oils (3 °C) [26] [3]. Innovative freezing protection methods and increased O&M requirements are a direct consequence [38]. In Chapter 2, this issue will be directly addressed.

Due to higher density compared to the oils, higher pumping power is needed [28]. The operation at higher temperatures results in higher losses in the solar field and in the piping system, with reduced efficiency in the conversion from solar to thermal energy [40]. Furthermore, expensive header pipe materials should be selected to ensure long-term durability [38]. The high-temperature resistance of the selective coating is of primary importance and innovative solar receivers should be designed for this application. This could increase the capital cost of the solar collectors [26]. Decomposition of the molten salt may take place and insoluble products may form. They tend to plug valves, pipes and heat transfer surfaces, undermining the optimal performance of the system [39].

According to [34], corrosion of the storage container and the piping alloys is an important problem to consider. Corrosion implies interaction with existing stresses related to mechanical and thermal loading, causing Stress Corrosion Cracking (SCC) in prone materials [33]. Chloride impurities, responsible of the adhesion degradation of the oxide scale to metal surface, which makes possible the corrosion attack at the base material, should be avoided and an upper limit of 0.6 % is set for the chloride content [38] [33].

Current R&D is focusing on the cost reduction of sealing ball joints and on the development of selective surfaces able to ensure durability and satisfactory performance at high temperatures. As underlined by [38], the technology must be preliminary proven by a prototype, which will be designed in the next sections.

1.6.3. Choice of the molten salt

Different molten salts present different properties, which can be more or less favorable for the solution of the drawbacks previously described. However, the choice of the perfect salt is not easy, since all the main thermophysical properties show significant differences when presented by different authors [35]. The uncertainty of thermal conductivity and viscosity can have a strong effect on the choice of the equipment, such as area of the heat exchangers

needed for steam production. The cost implications are clear. A trade-off between high melting point and stability at elevated temperatures should be pursued. Figure 1.10 shows the melting points of different alkali nitrates and other relevant mixtures.

"Solar Salt" ($NaNO_3$ 60 % - KNO_3 40 %)

The binary mixture of sodium and potassium nitrates have been commonly used in commercial CSP applications. It remains in thermally stable liquid phase at temperatures up to 600 °C and nickel alloys with 15.20 % chromium content are usually chosen to ensure safe operation. The melting point lies around 220 °C. The chloride ions coming from impurities can be a concern for the corrosion attack but in commercial grades alkali-nitrates this concern is limited. The components can be mined or produced synthetically [44]. Due to its proven reliability, it is the best candidate for a first trial in the solar field [34].

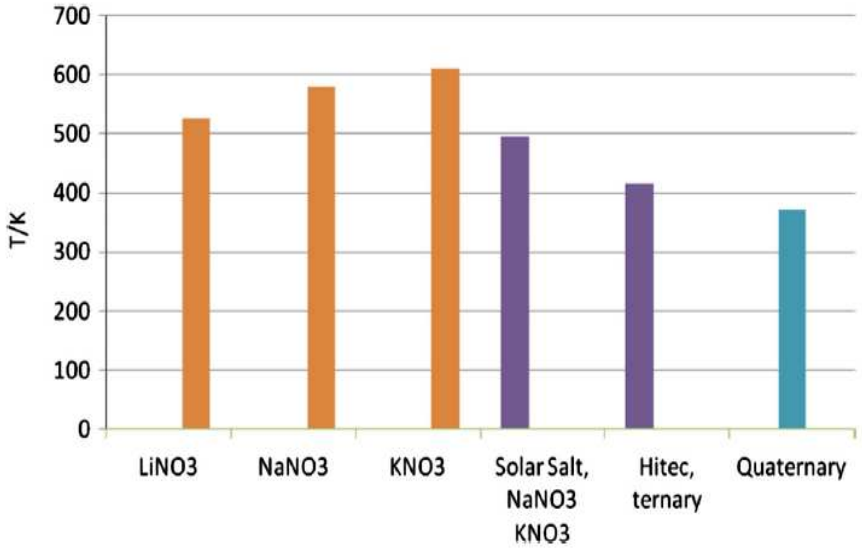

Figure 1.10: Melting point for different salt [36]

"Hitec" ($NaNO_3$ 7 % - KNO_3 53 % - $NaNO_2$ 40 %)

In order to decrease the melting point of the Solar Salt, sodium nitrite can be added, allowing operation down to 140 °C. The obtained tertiary mixture is known as "Hitec", which has been used for years in the heat-treating industry. The thermal stability is limited to 454 °C, up to 538 °C for short periods. This is due to the fact that the salt weight loss significantly increases over 500 °C. Appropriate additives may be considered to increase the stability. It presents good flow properties, similar viscosity to water and high thermal conductivity.

"Hitec XL" ($NaNO_3$ 7 % - KNO_3 45 % - $Ca(NO_3)_2$ 48 %)

The "Hitex XL" is a tertiary mixture of sodium, potassium and calcium nitrates. Compared to Hitec and Solar Salt it presents an even lower melting point (120 °C). However, the thermal stability is ensured only up to 500 °C.

Innovative mixtures

Further reduction of the melting point and substantial improvement of the thermal stability can be obtained if lithium nitrate is added to the mixture. A wide working temperature range can be achieved, ranging from 130 °C to 600 °C. The viscosity is acceptable in terms of flow properties. [34]. $LiNO_3$ can be added also to the Hitec XL, obtaining the "Sandia mix". Freezing point below 100 °C and stability over 500 °C have been tested successfully, but the corrosion resistance is not proven. The "Halotechnics ss-500" is obtained by further add of cesium nitrate, which could decrease the melting temperature to 65 °C. In all these cases, the price of the lithium salt, constantly increasing due to massive utilization in the production of batteries, reduces the potential of utilization on large scale [34]. However, it might become economically competitive by converting lithium carbonate with nitric acid [39].

Innovative studies focus on carbonates, chloride and fluoride salts [45]. Their properties can be improved by eutectic composition, in order to lower the melting points.

Nitrates and nitrites are still preferred, since they are characterized by low chemical stability, low corrosiveness and low cost, but their production might be restricted [45]. For this reason, the R&D is also investigating the use of inexpensive and naturally abundant materials, such as NaCl and KCl. Corrosion remains the main challenge and further testing is required.

1.6.4. Chosen salt and thermophysical properties

Considered advantages and disadvantages listed in the previous paragraphs and the uncertainty related to the properties of all the mixtures, Solar Salt has been selected as the most suitable heat transfer fluid for the present project. The use of molten salt in the solar field is innovative and not tested on large scale. Consequently, the technological risk may be high and the choice of the Solar Salt may limit unexpected faults. The expertise gained during its utilization in the tower technology could be beneficial for the success of the loop testing and for the development of the system.

Table 1.2: Thermphysical properties of the Solar Salt [46]

Property	Symbol	Function	Unit
Density	ρ	$2263.641 - 0.636 \cdot \mathrm{T}$	kg/m^3
Specific heat capacity	c_p	$1396 + 0.172 \cdot T$	J/kgK
Viscosity	μ	$0.0754 - 2{,}77 \cdot T + 3.49 \cdot 10^{-7} \cdot T^2 - 1.47 \cdot 10^{-10} \cdot T^3$	$Pa \cdot s$
Conductivity	k	$0.443 + 1.9 \cdot 10^{-4} \cdot (T - 273.15)$	W/mK

From an economic perspective, it is not easy to state if another salt would perform better, since there is a lack of experimental data. However, a relevant study has been performed by [37], which has compared the use of Solar Salt and Hitec. According to its result, the impact on the LCOE is barely affected by the choice of the heat transfer fluid and, for the scope of this study,

the use of the Solar Salt may be justified. The thermophysical properties are presented in Table 1.2 and they have been retrieved from [46]. T represents the temperature and it is expressed in Kelvin.

1.6.5. Compatibility and reliability of the molten salt

Once the proper heat transfer fluid has been selected, it is essential to understand its behavior with all the equipment employed in the plant. The Spanish company Abengoa Solar has performed a 5-year project (ended in 2013) to develop an R&D pathway for rapidly moving the utilization of molten salt from experimental to commercial status [41]. During the first phase, Hitec XL was identified as the best candidate but it has been consequently discarded because considered not good enough for commercial use. It was difficult to work with the thermophysical property equipment, due to its hygroscopic nature and lower thermal stability limit. Moreover, any salt mixture utilizing calcium nitrate was eliminated, due to salt decomposition at lower temperatures than expected. Once again, the choice of Solar Salt for this study seems to be reasonable. In the second phase of the project, the Solar Salt was tested with different components, with promising results in almost all the tests. The only problem was identified with the ball joints, since no design was successful during the tests at high temperature. However, as it will be described later, demonstration plants constructed after 2013 did not present any failure. NaK-based pressure sensor has been identified to be compatible with the salt, while the valves have been proven already in the tower systems. Two series of valves have been successfully tested: shut-off valves and flow control valves, whose primary concern is related to leakages. Both components performed well.

Table 1.3: Material consideration as from ASTM (American Society for Testing and Materials). "Tubes" refers to the steam generation heat exchanger, while "Plate" refers to the material used for the thermal energy storage [38]

Peak fluid temperature [°C]	**Basic material**	**ASTM designation**				
		Pipe	Fittings	Valves	Tubes	Plate
325	Carbon steel	A 106, Grade B	A234, Grade WPA	A 216, Grade WCB	A 192	A 516, Grade 70
450	Ferritic steel	A 335, Grade P22	A234, Grade WP22	A 217, Grade WP22	A 213	A 387, Grade 22
500	Ferritic steel	A 335, Grade P91	A234, Grade WP91	A 217, Grade WP91	A 213	A 387, Grade 91

The Sandia Laboratories identified the packing material for valve stems as problematic and tested numerous possibilities. An acceptable combination is represented by alternative layers of wire-reinforced graphite braid packing over a fiberglass core or Teflon washers filled with

fiberglass. In the first case, nitrate salts might slowly oxidize the graphite, requiring periodical replacement. On the other hand, Teflon has an upper temperature limit of 315 °C and valves with extended bonnets must be used on the hot side of the loops. In general, Solar salt is compatible with cost-efficient carbon steel up to 325 °C, for header pipes and solar field inlet connection line [47]. Table 1.3 is utilized as reference for the choice of the materials.

1.7. Case studies

In this section, three real case studies will be presented, in order to provide some example regarding operating strategies in MSPT plants.

1.7.1. Archimede Solar Thermal Power Plant

The first world trial for the utilization of molten salt as heat transfer fluid in a parabolic trough collector system was performed at the Archimede Solar Thermal Power Plant, located at Priolo Gargallo, in Sicily, Italy [48]. It was the first CSP plant integrated in a combined cycle power plant and its main target was the demonstration of the innovative CSP technology on industrial scale. The plant is composed by two gas turbines, each one with a nominal capacity of 380 MW_e. The CSP field has a peak power of 4.9 MW_e, producing around 9 GWh_e per year, in a site characterized by a DNI of 1936 kWh/m^2 per annum. The total reflecting surface is 30580 m^2, with 9 loops, for a total of 54 collectors of 100 meters each. Two tanks of 930 m^3 each provide 7 hours of storage. The solar-to-electricity efficiency is 15.1 %. 1 300 tons of Solar Salt are utilized as heat transfer fluid and its crystallization is avoided with the use of an electric heat trace system based on Joule and skin effect and installed in all the pipelines. The solar field is in operation since June 2011 and all the procedures, such as filling, heating, cooling and complete draining, were successfully completed. Moreover, continuous salt circulation over the entire pipeline has been obtained. The molten salt has achieved temperatures up to 540 °C, enabling steam generation at 500 °C and 100 bar.

1.7.2. Archimede MSPT Demo Plant

The second project of ASE (Archimede Solar Energy) concerned the construction of the first stand-alone Molten Salt Parabolic Trough (MSPT) demonstration plant [29]. It represents probably the most important reference for the evaluation of the technology under study. The plant is located close to the ASE manufacturing plant in Massa Martana, Italy. It consists of six parabolic linear collectors, arranged in two lines. Each collector has a collecting surface roughly equal to 600 m^2. The orientation is North-South. The Solar Salt is operated at temperatures up to 550 °C and the system is equipped with a 2750-kWh_{th} TES system, composed by two cylindrical tanks of about 25 m^3 each at fixed temperatures and variable volumes, for a total of 50 tons of salt. The system is kept at atmospheric pressure. In operation since July 2013, the system initially utilized an air cooler. Since the thermal duty of the solar field (1 900 kW) was higher than the one of the cooler (550 kW), tracking operation had to be interrupted to ensure proper cooling of the heated salt. The nominal mass flow of the molten salt in the solar field is 4 kg/s, which can be varied to meet the required outlet conditions, down to 2 kg/s. Thermocouples are placed at the inlet and outlet of the loop and in every collector,

in order to evaluate the heat losses. In the first year of operation, the system worked 5 500 hours with molten salts at temperatures higher than 250 °C and some hundred hours over 500 °C. The demonstration loop has been in operation continuously, except for the time needed for improvement and maintenance, and for the winter shutdown. All the foreseen objectives were achieved, since the plant management was successfully performed both during ordinary and extraordinary phases. No freezing problems were encountered in a location that is clearly not optimal for CSP applications, even without the use of an electric heat tracing system. Draining and filling procedures were conducted several times, without major issues. The thawing test showed that, even with diffuse freezing, it is feasible to recover the solar field without any damage to any part of the system [49]. During the second year of operation, the air cooler was substituted by a steam generator, in order to increase the number of operating hours. The steam is produced at 103 bar and 535 °C. The flow rate control demonstrated its capability to maintain the output temperature of the solar field within required boundaries. Also in this second phase, the plant has confirmed to be reliable and easy to manage and prove the feasibility of steam production at relatively high temperature and pressure. The receivers performed in lines with expected values [50].

Operation of the plant

During normal operation, the cold molten salt (290 °C) is pumped from the cold storage to the hot one through the loop, maintaining an outlet temperature of 550 °C by varying the mass flow. The flow is controlled with a variable speed pump [49]. When the solar radiation is insufficient, when the heat loss test is performed or when the hot storage is full, the assemblies are set in stow position (defocus mode). The molten salt is cooled due to heat losses and it is directly recirculated to the cold tank. During the first year of operation, the mass flow was controlled to maintain a temperature of 275 °C at the outlet of the loop [49]. However, as it can be observed in [50], during the second year, the mass flow was kept constant and equal to the nominal value. Finally, long-term stand-by mode was selected during maintenance or low-radiation season (December-March). The solar field is completely drained and 96 % of the salt is recovered into the storage tanks. During this period, the HTF is kept liquid with the use of electric heaters. The filling and draining procedures were performed successfully [49].

1.7.3. HPS2 – Évora Molten Salts Platform

The High Performance Solar 2 (HPS2) project has the aim to construct a molten salt parabolic trough demonstration loop in Évora, Portugal [36]. The project is a continuation of a former research project launched by Siemens. Different actors have contributed for this project, which involves EPC (Engineering, Procurement and Construction) partners with the co-funding of the German Ministry of the Environment, Nature Conservation and Nuclear Safety. Eskom Holdings SOC Limited provides the operating staff during the operation [51].

The plant is under construction. The solar field will be composed by four HelioTrough solar collectors, each one characterized by a length of 200 m and a width of around 7 m, while the receiver will be provided by Rioglass [52]. This information has been provided directly by the project manager. The nominal inlet temperature of the molten salt is equal to 290 °C, while the outlet one is controlled to be 550 °C. However, temperatures up to 580 °C can be achieved in

the solar receiver. Initially, the solar field was designed to consist of 6 Siemens SunField-6 solar collectors, for a total irradiated length of 600 m. Under these conditions, the nominal salt mass flow was 4.3 kg/s. With the use of the new collectors, higher mass flow will be required, due to increased size of the collecting area. However, no specific figure has been found in public documents. The system is equipped with a TES system, for a total of 56 tons of molten salt. Both tanks are designed to be able to contain the entire salt inventory. Two redundant pumps are provided to each tank, to ensure safe operation. A drainage tank located at the lowest point of the plant is present, which can contain all the molten salt of the solar field, of the piping and of the steam generation system. In this way, also in case of fault of the pump, gravity will be used to perform the procedure [36].

Once in operation, the plant will be able to produce high live steam parameters in a once-through steam generator, designer for 580 °C and 140 bar. The system generation system is designed to sustain steep start-up gradient, up to 15 K/min and it operates in real sliding pressure operation, ranging from 70 bar to 140 bar. In this way, flexible operation can be ensured, from a minimum load of 33 % to a maximum load of 120 %. The thermal duty under nominal conditions is equal to 1780 kW. The feedwater will come from a tank, which will be characterized constant temperature and pressure (270 °C and 55 bar). The constant inlet temperature is ensured by the use of an electric resistance, if necessary, and by the injection in the feedwater tank of part of the produced superheated steam [36]. The preheating of water is required to avoid salt temperature drop below 230 °C and freeze-thaw cycle, which would result in plastic deformations [53].

Expected operation of the plant

As stated before, the describe plant is still under construction. However, information referring to possible operational strategies has been reported by [54].

The operation of the plant will start in the morning, when the solar field will be heated up by the first solar irradiation, until a stationary temperature profile will be achieved at the loop outlet. In this phase, the salt will be recirculated over the cold tank. During normal operation, the mass flow of the heat transfer fluid will be controlled to maintain the desired temperature at the outlet of the solar collectors and the salt directed to hot storage tank. During shut down periods, the salt will be circulated through the field with the SCAs in stow position. During night operation, the salt will be circulated from the cold tank through the solar field back to the cold storage to avoid minimum temperatures [36]. Also in this case, the minimum mass flow of the HTF is around 2 kg/s [54].

The anti-freezing strategy makes use of the energy stored in the cold tank until the HTF reaches 270 °C. At that point, an electric-heat tracing system is used for safety reasons, with the fluid circulating with the minimum mass flow. When possible, molten salt coming from the hot tank is mixed with the cold fluid, to increase its temperature [54].

A temperature and flow gradient should be applied to increase temperature and pressure of the produced steam, up to the desired design values. Under nominal conditions, the Steam Generation System (SGS) will set the steam demand, while, during the shut-down, the mass flow of the molten salt will be reduced according to the need of the boiler [36].

2. Design of a MSPT test facility in South Africa

2.1. Plant layout

In the first section of the present report, an extensive research has been presented regarding both design and operational aspects of a parabolic trough collectors plant utilizing molten salts as HTF. In this chapter, the design of the demonstration loop will be outlined and each decision will be based and justified according to the overmentioned review.

2.1.1. Location and orientation of the plant

The MSPT technology is not proven and mature on a commercial scale. Several technological and financial risks may be associated to an investment on these systems. Furthermore, the investment cost may be initially higher than the conventional technologies, since the know-how should still be refined. It is difficult to expect that a private investor would be able to provide a cost-effective and risk-safe design under the REIPPP procurement. On the other end, Eskom can build a plant outside this procedure, since it is public-owned. Thus, the investment on the required R&D and consequent upscaling of the plant is suggested to the national electric company. Other business-related reasons will be reported in Chapter 5.

Due to their strategic nature, the Eskom power plants are considered key national points. They are characterized by high level of security and availability of land [55]. It is therefore reasonable to propose its construction inside one of these areas. This would facilitate the availability of manpower and the needed training. Additional infrastructure would not be required, reducing the initial expenditure. Finally, the transport for the delivery of the equipment and its maintenance can be coupled with other components of the existing plant.

Most of the Eskom coal-fired power plant are located around Johannesburg and this area is proposed for the construction of the plant [56]. As it can be observed in Figure 1.7, this is not the area with the optimal solar irradiation. However, the annual DNI is above 2 000 kWh/m^2/year [21]. In this study, the plant will be not optimized in economic terms, since no electricity will be produced. However, several operating hours per year must be guaranteed, in order to analyze the operation under different conditions.

A N-S orientation has been chosen for the demonstration loop, since it is the typical one for a CSP plant and it maximizes the energy gains [28].

2.1.2. Collector and receiver used

The parabolic trough collector utilized for the proposed plant is the HelioTrough collector, provided by the German company Flagsol. The receiver is the Rioglass PTR® 70-5G Advanced. They are the same collector and receiver that will be used in the HPS2 project and it has been chosen because detailed information has been received by the project manager of the plant. Their main characteristics are described in the next sections.

The HelioTrough solar collector

The HelioTrough solar collector has been designed by Flagsol GmbH. Mass reduction, improvement of the optical efficiency and cost decrease were the first targets set by this consortium [57]. The main adopted optimization measures are:

- Simplification of the collector structure to reduce the amount of work and connection materials required for the on-site assembly. Automation and manual work can be combined in different proportions, according to the boundary conditions of the project. This flexible assembly allow the supply chain for the metal structure to be done partially, or even completely, in the project country, on site [58] [10].
- The improvement of the assembly procedure has led to higher optical performance. A new-patented method for the connection of the mirrors to the steel structure realizes a three-dimensional clearance compensation, resulting in loosened tolerances of the steel structure and in perfectly aligned mirrors [58].
- The collector aperture has been increased. In this way, the number of expensive single components, such as drive units and swivel joints, has been reduced to a minimum.
- The optics has been optimized in terms of aperture angle and focal length.
- The non-interrupted mirror surface resulted in an increase of the aperture area.
- Overall, the geometry is more precise [58].

Each solar collector assembly is composed by 10 elements reaching a total length of 190 m. The aperture width is 6.77 m, while the focal length is 1.71-m long. Steel supports, located at every 4.8 m, are used to fix the heat collection element to the steel structure. The SCEs are connected to each other by using bolted joints and they can operate as a continuous beam. A hydraulic drive is used for the tracking system, located at the center pylon in the middle of the elements. The structure utilizes a torque tube design [58]. The collector is shown in Figure 2.1, while Figure 2.2 reports other dimensions of interest.

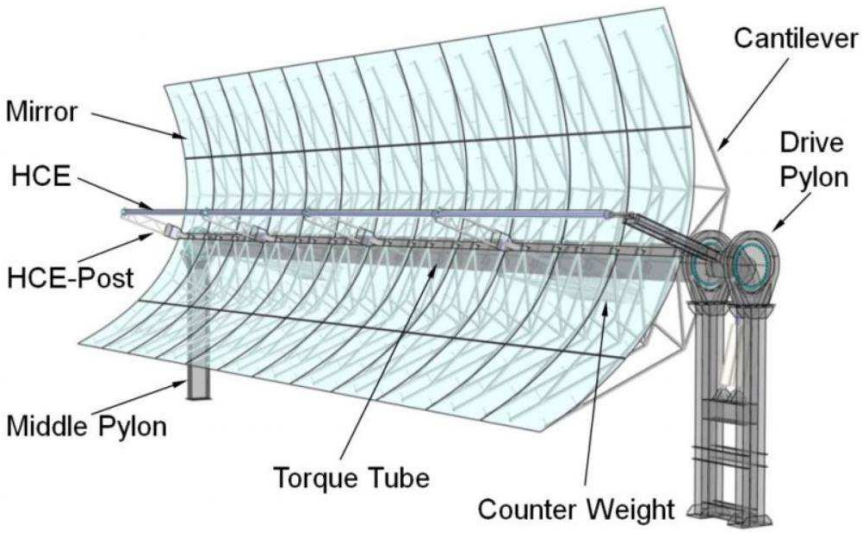

Figure 2.1: HelioTrough solar collector [53]

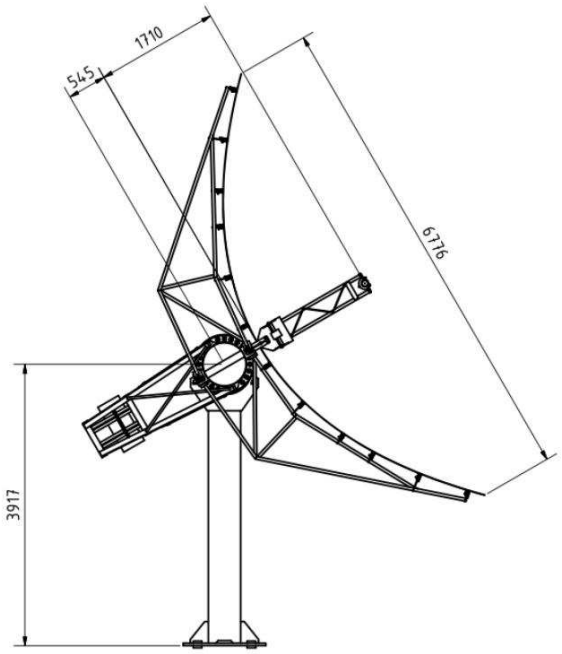

Figure 2.2: Dimensions of the HelioTrough solar collector [53]

Kotter et al. [59] report the main improvements related to the structure of the collector. The use of low torsion roller bearings increases the efficiency, due to low deformation and optimized shape of the reflector surface. Longer length of the SCA reduces the number of mirrors, heat collecting elements, steel parts, foundations, drives, swivel joints and control systems. However, higher stiffness against bending and torsion must be ensured. This resistance is provided by the torque tube design, thanks to its continuous cross-section. The torque tube is not interrupted at the end of each element or at the drive pylon and it has the same length of the assembly. The main benefits are reduced stresses on the material, reduced bending, enhanced torsional stiffness and gapless solar collector. In fact, the mirror gap has been reduced to a minimum of 30 mm, increasing the surface usage by 2.5 %. Thermal losses and space occupation are minimized, while the washing process results easier. During normal operation, the mean torsion of one half of the assembly amounts to 0.5 mrad, which is significantly lower compared to past designs. The obtained intercept factor is higher than 99.1 %.

The assembly procedure is hereafter described [59]:

1. The mirrors, resembling a perfectly shaped parabola, are placed on an accurate jig.
2. The frame of the solar collector elements is lowered on the supporting structure.
3. While the mirrors are maintained in ideal position, the pods are filled with adhesive.

All these features result in a collector that is more than 50 % larger and about 10 % more efficient compared to the previous SKALET technology, and significantly more heat can be gained by single loop [30].The peak optical efficiency is higher than 0.8, with thermal efficiencies over 70 % during nominal operation [58].

The IAM can be evaluated with formula (2.1).

$$IAM(\theta) = 1 + 1.59 \cdot 10^{-3} \cdot \theta - 9.77 \cdot 10^{-5} \cdot \theta^2 \quad (2.1)$$

where θ is the incidence angle, expressed in degrees.

The typical loop is composed by four SCAs in series, arranged in two parallel lines (Figure 2.3). The distance between two assemblies is around 2.5 m, while 22 m is the typical span of the cross-over pipe. A new cross-over system called COP-bridge is proposed to compensate adequately the thermal expansion occurring during high-temperature operation. A newly patented trussed arch pipe is utilized, which can substitute the typical joints and reduce the forces acting on the collector almost completely. No pylons required and lower pressure drops are two other major benefits of this solution [59]. The resulting test loop is represented in Figure 2.4 . All the components will be described in the next sections.

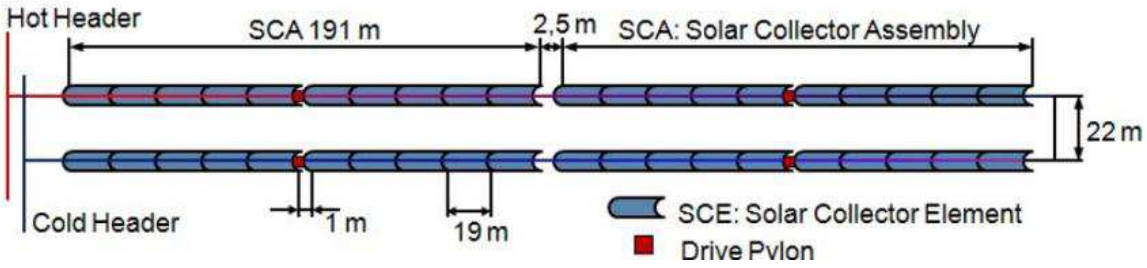

Figure 2.3: Typical HelioTrough loop [53]

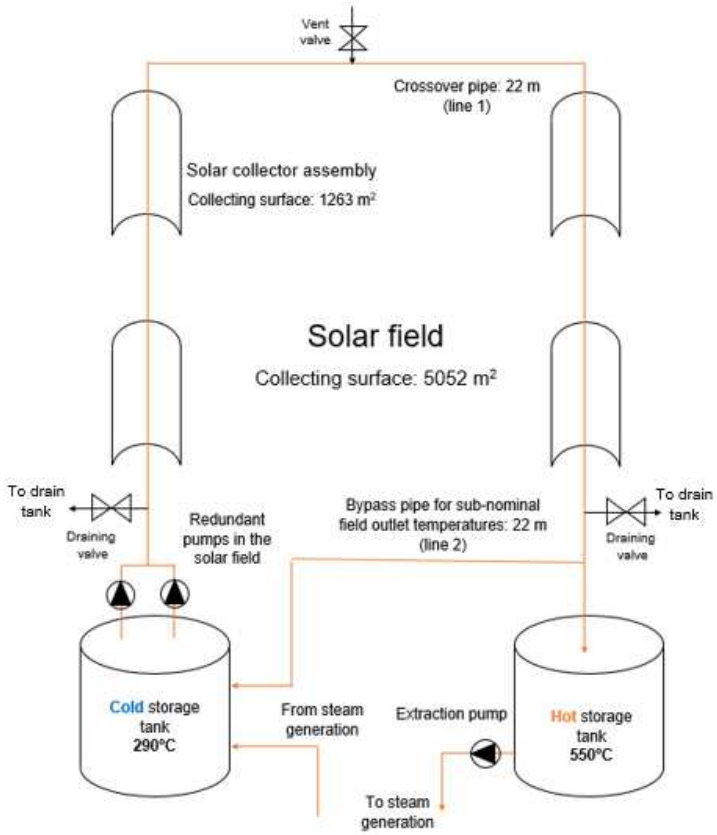

Figure 2.4: Representation of the MSPT demonstration loop

The overall solar field cost reduction compared to the state-of-the-art technology is expected to be in the order of 20 %, with the assemblies themselves and the reduction of number of components accounting for 10 % each. LCOE as low as 14 c$/kWh can be obtained [59].
The main dimensions of the collector are summarized in Table 2.1.

Table 2.1: Main dimensions of the HelioTrough collector [53]

Parameter	Symbol	Value	Unit
Focal length	f	1.71	m
Net aperture width	W	6.62	m
Rim angle	Ψ	89°	/
Concentration ratio	C_g	76	/
Number of SCE per assembly	/	10	/
Net aperture area of the SCA	A_{SCA}	1263	m^2
Gross SCA length	l_{tube}	191	m
Loop aperture area	A_{loop}	5177	m^2

The Rioglass solar receiver

The receiver that will be used in the demonstration loop is the Rioglass PTR® 70-5G Advanced. All the technical specifications here reported have been retrieved from the manual of the product [60].

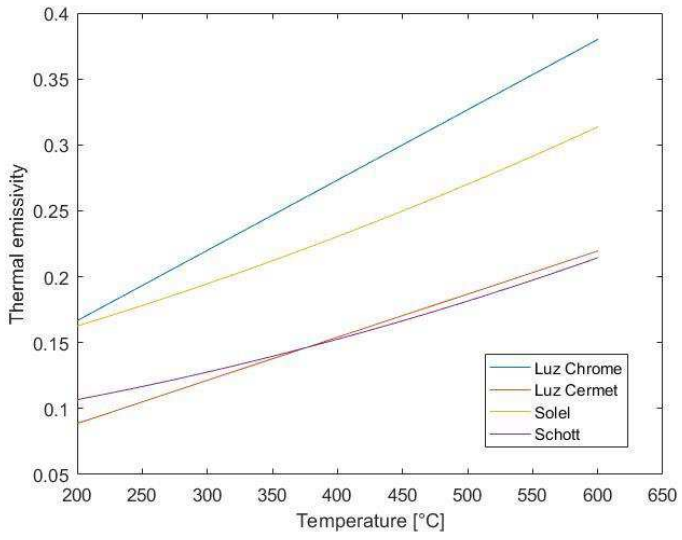

Figure 2.5: Thermal emissivity for the solar receivers used for the comparison [28]

The length of the single receiver is equal to 3.8 m at ambient temperature. The absorber has an outer diameter of 70 mm, which lies within the range recommended by [37], and a thickness of 2.2 mm. The type of steel utilized is not specified, but it is stated that the material is able to withstand high-temperature operation. The solar absorptance is equal to 0.94 and it has been considered constant with the temperature, while the thermal emissivity is lower than 0.095 at 400 °C and lower than 0.14 at 500 °C. An equation reporting the variation of the emissivity with the temperature would be required to model the system dynamically. However, such formula was not found in literature. [27] reports the emissivity for four different receivers: Luz Chrome, Luz Cermet, Solel and Schott. The trends are reported in Figure 2.5. Luz Cermet and Schott receivers seems to be characterized by properties that are closer to the ones of the chosen absorber. Due to lower emissivity at higher operating temperatures, Schott receiver has been chosen as the most representative.

The glass envelope is made of borosilicate glass and it has an outer diameter of 125 mm. Since no thickness is specified, the one of the steel pipe has been used. The solar transmittance is 0.96 and it has been assumed to be not dependent from the temperature.

The total weight of the receiver is 23 kg and it works under vacuum (pressure lower than 10^{-4} mbar). It can be operated with the standard Solar Salt, but also other tertiary mixtures can be considered. The expected operating time is around 20 000 hours, if periodic examination of the heat transfer fluid is ensured. The maximum bulk fluid temperature suggested is 550 °C and the flow should maintain a Reynolds number higher than 20 000. The maximum concentration ratio allowed is 100, which complies with the specifications of the collector reported in the previous paragraph. The emissivity of the glass is not specified and it has been assumed from [61], while the absorptivity has been take from [62]. The main properties of the receiver are reported in Table 2.2.

Table 2.2: Dimensions of the solar receiver

Parameter	Symbol	Value	Unit	Reference
Absorber outer diameter	$d_{ab,o}$	70	mm	[60]
Absorber wall thickness	t_{ab}	2.2	mm	[60]
Absorptance of the receiver	α_{ab}	0.94	/	[60]
Absorber emissivity	ε_{ab}	$2 \cdot 10^{-7} \cdot T^2 + 0.062$	/	[27]
Glass outer diameter	$d_{g,o}$	125	mm	[60]
Glass wall thickness	t_g	2.2	mm	Assumed
Absorptance of the glass	α_g	0.02	/	[62]
Glass emissivity	ε_g	0.86	/	[61]
Glass transmissivity	τ_g	0.96	/	[60]

2.2. Plant modelling and design

The size of the solar field loop has been established based on the recommendations of the manufacturer and no specific technical evaluation has been performed. In the following, the simulation of the plant behavior under a year of operation, evaluated on an hourly basis, will be presented, and it is expected to give the following outcomes:

- Size of the thermal energy storage tanks, which will be the minimum to avoid the freezing of the salt during night operation (see Section 2.6.2).
- Nominal mass flow and operating parameters of the plant under nominal conditions
- Mass flow of the heat transfer fluid during night operation, taking into account both anti-freezing protection strategy and pressure losses.
- Annual consumption of auxiliary energy, such as the electricity used by the pumps.
- Expected number of working hours.

Finally, the sizing of all the components will be defined.

2.2.1. Main assumptions for the collector modelling

The simulation of a parabolic trough collector is a common topic in the scientific literature. Tzivanidis et al. [63] state that most of the numerical studies associated to this technology are based on a one-dimensional heat transfer analysis. This approach can give results that are accurate enough compared to three-dimensional simulation tools. The same outcomes are obtained by [64], which presented a steady-state one-dimensional model, able to ensure good accuracy with experimental data. Abedini-Sanigy et al. [65] and Almasabi et al. [66] proposed detailed multi-dimensional transient models, aimed at the characterization of the performance of the collector under specific conditions. Guo & Huai [61] utilized a steady-state one-dimensional model and a genetic algorithm to optimize the solar collector parameters in terms of both energy and exergy efficiency. Finally, the System Advisor Model (SAM), created by the National Renewable Energy Laboratory (NREL), considers each solar collector assembly as an autonomous node and treats it independently [67]. The transient term is considered in the evaluation, which solves the problem by mean of linear differential equations.

The proposed simulation is based on the approach proposed by [64] and it is applied to each SCA, resulting in a zero-dimensional energy balance. According to the information gathered during the literature review, this choice seems to provide accurate results, while reducing the computational effort and time required to run the simulation. The technical manual of SAM has been also used as a valuable resource. The temperatures of the receiver and the glass have been considered uniform, as in [68].

The energy balances problem are based on the conservation equation [64]:

$$\frac{\partial(\rho \cdot c_p \cdot T)}{\partial t} + div\left[\rho\vec{v}\left(h + \frac{v^2}{2} + gz\right)\right] = div([kgrad(T)] + RT \quad (2.2)$$

t represents the time variable, $\vec{v}$ the velocity vector, h the enthalpy, g the gravitational acceleration and z the height to a reference level. In the second member, RT is the source

term. The equation is solved considering steady-state conditions, neglecting the variation of kinetic and gravitational energy, and expressing the enthalpy variation as the product of the specific heat capacity and the temperature variation.

2.2.2. Collector efficiency and solar angles

As stated beforehand, one of the expected outcomes of the simulation is the evaluation of the thermal efficiency of the solar collector.
It is defined as [28]:

(2.3) $$\eta_{th} = \frac{\dot{Q}_u}{DNI \cdot A_{SCA} \cdot cos(\theta)}$$

where $\dot{Q}_u$ is the useful heat collected by the heat transfer fluid.
This energy gain can be expressed as [28]:

(2.4) $$\dot{Q}_u = \dot{m}_{salt} \cdot c_p \cdot (T_{f,2} - T_{f,1})$$

where $\dot{m}$ is the mass flow the molten salt, while $T_{f,2}$ and $T_{f,1}$ represent the inlet and the outlet temperatures of the fluid, respectively.
The incident angle depends on temporal (day of the year and hour of the day), geographical (latitude and longitude of the location) and spatial factors (orientation of the solar field). The demonstration loop will be located in the area surrounding Johannesburg and it will be characterized by a N-S orientation. In particular, the city of Pretoria has been considered as specific site, since detailed weather data are freely available [69]. Pretoria has a latitude of 25.75 ° S and a longitude of 28.19 ° W.
θ is calculated with the following procedure [70]:

(2.5) $$\omega = (h - 12)\frac{\pi}{12}$$

(2.6) $$\delta = 23.45 \cdot \frac{180}{\pi} \cdot sin\left(\frac{360 \cdot (284 + d)}{365}\right)$$

(2.7) $$\theta_z = sin(\delta)\, sin(\varphi) + cos(\delta)\, cos(\varphi)\, cos(\omega)$$

(2.8) $$\theta = acos\left(\sqrt{cos^2(\theta_z) + cos^2(\delta) sin^2(\omega)}\right)$$

ω is the solar angle, δ is the declination angle, φ is the latitude and θ_z is the zenith angle. h is the solar hour of the day, while d represents the day on the Gregorian calendar.

2.2.3. Balance in the receiver

The balance in the absorber tube can be expressed as:

(2.9) $$\dot{Q}_{s,ab} - \dot{Q}_{cv,ab-f} - \dot{Q}_{cv,ab-g} - \dot{Q}_{rad,ab-g} - \dot{Q}_{cd,br} = 0$$

$\dot{Q}_{s,ab}$ is the energy collected by the receiver, calculated with the following equation [64]:

$$\dot{Q}_{s,ab} = DNI \cdot \eta_{opt} \cdot cos(\theta) \cdot IAM \cdot A_{SCA} \cdot \tau_g \cdot \alpha_{ab} \quad (2.10)$$

Due to the thin thickness of the receiver, the absorption can be considered a surface phenomenon [71]. η_{opt} is the optical efficiency, which is the product of various factors [64]:

$$\eta_{opt} = \eta_{end,loss} \cdot \eta_{sh} \cdot \eta_{geom,error} \cdot \rho_{m,clean} \cdot \eta_{dirt,mirror} \cdot \eta_{dirt,SCE} \cdot \eta_{other} \quad (2.11)$$

$\eta_{end,loss}$ represents the end spillage losses. During hours in which the solar irradiation is not perfectly perpendicular to the collecting surface, part of the reflected radiation does not reach the receiver [67]. It can be calculated as shown in Equation (2.12).

$$\eta_{end,loss} = 1 - \frac{L_f \cdot tan(\theta)}{l_{tube}} + \eta_{end,gain} \quad (2.12)$$

$$\eta_{end,gain} = \frac{L_f \cdot tan(\theta) + l_{gap}}{l_{tube}} \quad (2.13)$$

$$L_f = \sqrt{\frac{\left[4f^2 + \left(\frac{W}{2}\right)^2\right]^2}{f^2}} \cdot \frac{12f^2 + \left(\frac{W}{2}\right)^2}{12 \cdot \left(4f^2 + \left(\frac{W}{2}\right)^2\right)} \quad (2.14)$$

$\eta_{end,gain}$ takes into account that part of the reflected radiation by one collector can incident the adjacent one. In the southern hemisphere, this contribution is equal to zero for the assemblies that are the northernmost of loop. l_{gap} is the distance between two SCA, as pictured in Figure 2.3. Finally, L_f is the average surface-to-focus path length.

The term η_{sh} quantifies the losses related to the mutual shadowing of the two loop rows [67]:

$$\eta_{sh} = \frac{l_{spacing}}{W} \cdot \left|\frac{cos(\theta_z)}{cos(\theta)}\right| \quad (2.15)$$

Table 2.3: Coefficients for the calculation of the optical efficiency [65]

Coefficient	Value
$\eta_{geom,error}$	0.98
$\rho_{m,clean}$	0.935
$\eta_{dirt,mirror}$	0.9
$\eta_{dirt,SCE}$	$(1 + \eta_{dirt,mirror})/2$
η_{other}	0.96

$l_{spacing}$ is the distance between the two collector lines.

$\eta_{geom,error}$ considers the non-perfect parabolic shape. $\rho_{m,clear}$ is the reflectivity of the clean mirrors, while $\eta_{dirt,mirror}$ and $\eta_{dirt,SCE}$ quantifies the effect of the dirt accumulated on the reflectors and on the absorber, respectively. All possible other aspects are included in the term η_{other}. The values of these coefficients are reported in Table 2.3.

With incident angle and zenith angle equal to zero, the obtained optical efficiency is around 0.81, which is coherent with the expected value presented in section 2.1.2.

$\dot{Q}_{cv,ab-f}$ and $\dot{Q}_{cv,ab-g}$ represent the convective heat fluxes exchanged by the receiver tube with the HTF and the glass. They can be expressed as in Equation (2.16) and (2.17) [64].

$$\dot{Q}_{cv,ab-f} = \alpha_{ab-f} \cdot \pi \cdot l_{tube} \cdot d_{ab,in} \cdot \left(T_{ab} - T_f\right) \quad (2.16)$$

$$\dot{Q}_{cv,ab-g} = \alpha_{ab-g} \cdot \pi \cdot l_{tube} \cdot d_{ab,out} \cdot \left(T_{ab} - T_g\right) \quad (2.17)$$

α_{ab-f} and α_{ab-g} are the convective heat transfer coefficients with the fluid and the glass cover. T_{ab} and T_g are the temperatures of the receiver and of the glass, while T_f is the bulk temperature of the fluid in the assembly, evaluated as arithmetic average between inlet and outlet. The subscripts in and out indicate the inner and outer diameter.

$\dot{Q}_{rad,g}$ is the radiation heat transfer between the glass and the absorber [67]:

$$\dot{Q}_{rad,ab-g} = \frac{\sigma_b (T_{ab}^4 - T_g^4)}{\frac{1-\varepsilon_g}{\varepsilon_g \cdot \pi \cdot l_{tube} \cdot d_{g,in}} + \frac{1}{\pi \cdot l_{tube} \cdot d_{ab,out}} + \frac{1-\varepsilon_{ab}}{\varepsilon_{ab} \cdot \pi \cdot l_{tube} \cdot d_{ab,out}}} \quad (2.18)$$

where σ_b represents the Stefan-Botzmann constant, equal to 5.67· 10^{-8} W/m^{2}K^4.

Finally, $\dot{Q}_{cd,br}$ represents the conduction heat transfer through the supporting brackets [64]:

$$\dot{Q}_{cd,br} = \sqrt{\alpha_{br-am} \cdot U_b \cdot k_b \cdot A_b} \cdot (T_{br,0} - T_{am}) \, tanh\left(\sqrt{\frac{\alpha_{br-am} \cdot U_b}{k_b \cdot A_b}} \cdot f\right) \quad (2.19)$$

U_b and A_b are the perimeter and the section of the brackets. They are equal to 20.32 cm and 1.6129 cm^2 [67]. The brackets are made of carbon steel and they have a thermal conductivity (k_b) equal to 48 W/mK. $T_{br,0}$ is the effective bracket base temperature, calculated as the receiver temperature minus 10 °C.

2.2.4. Balance in the glass cover

An energy balance can be similarly performed for the glass cover:

$$\dot{Q}_{s,g} - \dot{Q}_{cv,g-am} + \dot{Q}_{cv,ab-g} + \dot{Q}_{rad,ab-g} - \dot{Q}_{rad,g-am} = 0 \quad (2.20)$$

An analogous expression to the one presented in the previous section can be utilized to calculate the heat absorbed by the glass cover, as shown in Equation (2.21) [64].

(2.21) $$\dot{Q}_{s,ab} = DNI \cdot \eta_{opt} \cdot cos(\theta) \cdot IAM \cdot A_{SCA} \cdot \alpha_g$$

The glass cover exchanges heat also with the external environment by convection and radiation. For the calculation of the radiative heat transfer, the glass tube is considered to be a small convex gray object in large black-body cavity, the sky [64]:

(2.22) $$\dot{Q}_{cv,g-am} = \alpha_{g-am} \cdot \pi \cdot l_{tube} \cdot d_{g,out} \cdot \left(T_g - T_{am}\right)$$

(2.23) $$\dot{Q}_{rad,g-am} = \sigma \cdot \pi \cdot l_{tube} \cdot d_{g,out} \cdot \varepsilon_g \cdot \left(T_g^4 - T_{sky}^4\right)$$

T_{am} is the air temperature, while T_{sky} is the equivalent sky temperatures, assumed to be 8 °C lower than the ambient one.

2.2.5. Balance for the heat transfer fluid

The energy collected by the receiver tube is transferred to the HTF [64]:

(2.24) $$\dot{Q}_u = \dot{m}_{salt} \cdot c_p \cdot \left(T_{f,2} - T_{f,1}\right) = \alpha_{ab-f} \cdot \pi \cdot l_{tube} \cdot d_{ab,in} \cdot \left(T_{ab} - \frac{T_{f,2}+T_{f,1}}{2}\right)$$

2.2.6. Calculation of the heat transfer coefficients

The evaluation of the convective heat transfer coefficients is based on the empirical correlations provided by [64]. They utilize the following non-dimensional parameters:

- $Re = \frac{\rho \cdot v \cdot d}{\mu}$, which is the Reynolds number.
- $Pr = \frac{\mu \cdot c_p}{k}$, which is known as the Prandtl number.
- $Gr = \frac{g \cdot \beta \cdot \rho^2 \cdot \Delta T \cdot d^3}{\mu^2}$, the Grashof number. β is the coefficient of volumetric thermal expansion, while ΔT is the temperature difference between the undisturbed fluid and the solid surface.
- $\mathrm{Ra} = Pr \cdot Gr$, which represents the Rayleigh number.
- $Nu = \frac{\alpha \cdot d}{k}$, the Nusselt number

Convective heat transfer coefficient between the absorber and the HTF

For the convective heat transfer between the molten salt and the absorber tube, the following correlation can be employed:

(2.25) $$Nu = \frac{f/8 \cdot (Re - 1000) \cdot Pr}{1 + 12.7\sqrt{f/8} \cdot \left(Pr^{\frac{2}{3}} - 1\right)} \cdot \left(\frac{Pr}{Pr_w}\right)^{0.11}$$

All the non-dimensional numbers refer to the properties of the fluid. They are evaluated at the

average temperature in the assembly, except Pr_w, which utilizes the absorber temperature. f is the friction coefficient, calculated as:

(2.26) $$f = (1.82\, log_{10}\, Re - 1.64)^{-2}$$

Convective heat transfer coefficient between the absorber tube and the glass cover

The exchange between the absorber and the glass is limited due to the presence of vacuum in the annulus and it occurs due to free-molecular heat transfer.
The heat transfer coefficient can be calculated as suggested by [64] and shown in Equation (2.27).

(2.27) $$\alpha_{ab-g} = \frac{k_{std}}{\frac{d_{ab,out}}{2} \cdot ln\left(\frac{d_{g,in}}{d_{ab,out}}\right) + b_{r-g} \cdot c \cdot \left(\frac{d_{ab,out}}{d_{g,in}} + 1\right)}$$

$$b_{r-g} = \frac{(2-\vartheta)(9\gamma - 5)}{2\vartheta(\gamma + 1)}$$

$$c = \frac{2.31 \cdot 10^{-20} T_{ab-g}}{Pr \cdot {d_m}^2}$$

k_{std} is the conductivity of the gas in the annulus, evaluated at standard conditions. ϑ represents the accommodation coefficient, fixed to one, while γ is the ratio between the specific heats of the gas. d_m is the molecular diameter of the gas. *Pr* is evaluated at T_{ab-g}, the average temperature between the receiver and the cover. For the project under study, air is considered as annulus gas, with γ equal to 1.39 and d_m equal to 3.53· 10^{-8} cm.

Convective heat transfer to the external ambient

The heat transfer with the external environment can be characterized by natural of forced convection, depending on the wind velocity.
If there is wind, the Nusselt number is evaluated as:

(2.28) $$Nu = C \cdot Re^m \cdot Pr^n \cdot \left(\frac{Pr}{Pr_w}\right)^{0.25}$$

n is equal to 0.37 for Prandtl number equal or lower than 10, while it is 0.36 in the other cases. The values of C and m depends on the Reynolds number and they are reported in Annex I. Re and Pr are evaluated at the air temperature. The correlations for the calculation of air properties are shown in Annex II.
Pr_w is calculated at the temperature of the solid surface. In the case of the heat transfer between the glass and the ambient, the reference temperature is considered. On the other

hand, for the calculation of α_b, the bracket temperature T_{br} is used, evaluated as [67]:

(2.29)
$$T_{br} = 0.5 \cdot \left(\frac{(T_{br,0} + T_{am})}{2} + T_{am} \right)$$

In case of absence of air movement, the following correlation is preferred [64]:

(2.30)
$$Nu = \left\{ 0.6 + \frac{0.387 \cdot Ra^{1/6}}{\left[1 + \left(\frac{0.559}{Pr} \right)^{9/16} \right]^{8/27}} \right\}^2$$

In this case, the non-dimensional numbers are calculated at the average temperature between the undisturbed fluid and the considered sold surface.

2.2.7. Resolution procedure

For each SCA, the inlet temperature is known, while the tube and glass ones are to be evaluated. Solar radiation, wind speed and air temperatures are the boundary conditions. Due to the high non-linearity of the system to be solved, an iterative process must be performed. Initially, the outlet temperature is assumed to be equal to the inlet one, while the temperatures of the receiver tube and the glass cover are simply guessed. Temperature-dependent properties of the fluid and the solid, as well as all the heat transfer coefficients are then calculated. The energy balances presented in the previous sections are used to evaluate the updated temperatures, which are used as new guessed values. The procedure is then repeated, until the guessed and calculated values converge for both the solids and the HTF. A convergence criteria ξ equal to 10^{-4} has been utilized. The iterative process is summarized in Figure 2.6. T^* represents the guessed temperatures, while T the calculated ones.

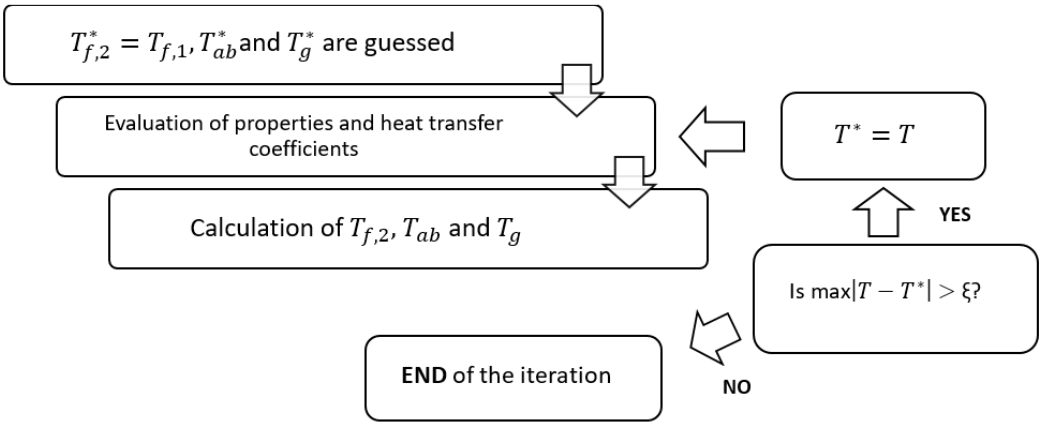

Figure 2.6: Iterative process for the calculation of the temperatures in the solar collector assembly

The described model has been tested with the experimental data reported by [72]. The results are presented in Annex III.

2.2.8. Solar field piping: sizing and heat losses considerations

Due to the small size of the demonstration loop, the extension of the solar field piping is limited. Two main branches are to be considered. The first one connects the two solar collector lines, while the second is used to recirculate the fluid through the cold storage tank. Both pipes are considered of the same length (22 m, as in Figure 2.3) and of the same material. The inner diameter is set equal to the one of the solar collector receiver, 70 mm.

The thickness of the pipe wall has been calculated according to [73], taking into consideration the maximum allowable stress the piping material can be exposed to. Utilizing Table 1.3 as reference, ferritic steel A335, has been chosen has the most suitable material for temperatures around 500 °C. In this case, the maximum allowable stress is equal to 34.5 MPa [74].

The thickness of the tube t_{pipe} can be then calculated as:

(2.31) $$t_{pipe} = \frac{d_{in,pipe} \cdot 10^5}{2 \cdot F_{max} \cdot 10^6 + 0.4 \cdot (P_{fluid} - 1) \cdot 10^5}$$

$d_{in,pipe}$ is the diameter of the pipe and F_{max} is the maximum allowable stress, expressed in MPa. P_{fluid} is the pressure of the fluid equal to 25 bar, as in [36]. A consequent thickness of 2.2 mm is obtained.

In order to minimize the thermal losses in the solar field, all the piping should be properly insulated. This aspect is even more important when molten salt is used as heat transfer fluid, due to higher operating temperatures. The thickness of the insulation layer is usually the result of a techno-economic optimization, which is out of the scope of the present analysis. For this reason, the work performed by [75] is used as guidance, which utilizes simple correlation to find the optimal thickness t_{ins}, based on material properties and maximum temperature of exposure:

(2.32) $$ln(t_{ins}) = \sum_{n=0}^{3} \varphi_n d_{out.pipe}^{-n}$$

(2.33) $$\varphi_n = A_n + \frac{B_n}{k_{ins}} + \frac{C_n}{k_{ins}^2} + \frac{D_n}{k_{ins}^3}$$

A_n, B_n, C_n and D_n are constants, whose values refer to a maximum operating temperature of the insulation around 500 °C and they are reported in Annex IV. $d_{out,pipe}$ is the outer diameter of the pipe, while k_{ins} represents the thermal conductivity of the insulation material. Mineral wool of calcium silicate can be utilized and they are both characterized by conductivity around 0.1 W/mK in the temperature range of interest. 15 cm is the required insulation thickness.

It is finally possible to evaluate the thermal losses in the solar field pipes [73]:

(2.34) $$\frac{2\pi \cdot k_{ins} \cdot \left(\frac{T_{2,f,pipe} + T_{1,f,pipe}}{2} - T_{am}\right)}{ln\left(\frac{d_{out,pipe} + 2t_{ins}}{d_{out,pipe}}\right)} \cdot l_{spacing} = \dot{m}_{salt} \cdot c_p \cdot \left(T_{2,f,pipe} - T_{1,f,pipe}\right)$$

$T_{2,f,pipe}$ and $T_{1,f,pipe}$ are the outlet and inlet pipe molten salt temperatures, respectively.

Convective resistances are ignored, since considered negligible compared to the conduction heat transfer through the insulation layer.

2.2.9. Storage system

The storage is a fundamental component of the demonstration loop. In fact, besides providing dispatchability for the test operation, it is responsible for the anti-freezing protection strategy (see Section 2.5.1). It will be sized in terms of the number of hours it could feed the steam generation system, to make it operate at nominal capacity. The hot tank is characterized by a nominal temperature of 550 °C, while the cold one operates at 290 °C, as in the Archimede Plant. Since the salt is recirculated through the cold tank, its temperature is far from being constant during the operation. The two tanks are designed to maintain always 10 % of the volume with salt. If a tank was emptied completely, the consequent introduction of fluid would create severe thermal and mechanical stresses. Each container can accommodate all the salt inventory, including the fluid of the solar field, as suggested for the plant that will be constructed in Évora. The height-to-diameter ratio is se equal to 1, like in the Archimede Power plant.

The design and materials of the storage tanks are presented by [76]. Typical tanks area steel cylindrical structure, with wall thickness equal to 4 cm. The materials that can be used are listed in Table 1.3. Typical insulation materials for the walls are mineral wool and calcium silicate, usually covered by a thin protective layer of sheet metal, such as galvanized steel. The roof of the tanks presents a thinner thickness (around 6 mm) and it is insulated with a calcium silicate board. For the floor construction, a 4 cm-steel layer can be considered, insulated by 30-40 cm of foam glass. A concrete layer is utilized to sustain the steel structure.

For the dynamic simulation of the storage tank, the structure has not been considered in detail, but an average heat loss coefficient has been used. Due to the presence of insulation, the losses are usually very low and, therefore, a more accurate model would have required substantially higher computational effort, with limited increase in the accuracy of the results. No heat transfer is assumed to occur from the top and the bottom [77].

The tank is modelled performing mass ad energy balances for each time step:

(2.35)
$$m_{end} = m_{start} + \dot{m}_{in} - \dot{m}_{out}$$

(2.36)
$$\rho c_p \frac{d(V \cdot T)}{dt} = c_p(T_{in}\dot{m}_{in} - T_s\dot{m}_{out}) - UA_{ex}(T_s - T_{am})$$

In Equation (2.35), m_{end} and m_{start} represent the mass of the molten salt before and after the time step, respectively. V is the volume of the stored salt, T_s is the temperature of the storage, U is the heat loss coefficient and A_{ex} is the lateral surface interested by the heat exchange. All the temperatures are expressed in Kelvin. The subscripts *in* and *out* define the mass that is entering or leaving the storage system. The energy balance has been discretized with an implicit scheme (parameters evaluated at the end of the time step). Solving the derivative at the first member, considering the relation between mass and volume and expressing the mass variation as in Equation (2.35), the following relation is obtained:

(2.37)
$$T_s = \frac{c_p \cdot \dot{m}_{in} \cdot T_{in} + \frac{c_p \cdot m_{end} \cdot T_{s,0}}{\Delta t} + U \cdot A_{ex} \cdot T_{am}}{c_p \cdot \dot{m}_{in} + \frac{c_p \cdot m_{end}}{\Delta t} + U \cdot A_{ex}}$$

$T_{s,0}$ is the temperature of the stored salt at the beginning of the time step, while Δt is the length of the time step, equal to 3 600 s.

The heat loss coefficient utilized is the one obtained from the evaluation of the performance of the Solar Two project, utilizes the solar tower technology and it operates between the same temperatures as the plant under study [78]. It can be calculated as:

(2.38)
$$U = 1000 \cdot \frac{0.00017 \cdot (T_s - 273.15) + 0.012}{(T_s - T_{amb})}$$

The heat loss coefficient is expressed in W/m^{2}K.

Since all the parameters are calculated with the temperature at the end of the time step, which is the unknown of the problem, T_s is initially guessed and then calculated iteratively, with a procedure similar to the one reported in Figure 2.6.

2.2.10. The steam generation system

One of the main aims of the demonstration loop is to prove the feasibility of steam production from the MSPT technology. Shell-and-tube heat exchangers are proposed and the choice will be justified in the next paragraph.

Shell-and-tube heat exchangers: advantages and design considerations

Shell-and-tube heat exchangers have been chosen for the present work because they represent a proven technology and they are a very common choice in the CSP power plants. Helical coil heat exchangers can be a valid alternative if higher performance is required. However, a higher capital cost should be expected and they have not been considered for this reason. Moreover, shell-and-tube heat exchangers are characterized by easier design procedures, which can be extensively found in literature [53].

The shell-and-tube heat exchangers are composed by a bundle of tube enclosed in a cylindrical shell. The ends of the tubes are fitted into tube sheets, which separated the shell-side and the tube-side fluids. Different shell and tube passes can be considered for the design, with conflicting outcomes regarding heat transfer efficiency and pressure losses. The mechanical design features, fabrication, materials of construction and testing are covered by the standards provided by TEMA (Tubular Exchangers Manufacturers Association) [79].

The main advantages related to their utilization are [79] [80]:

- Large surface area enclosed in a limited volume.
- Good mechanical layout and appropriate shape for pressure operation.
- Use of well-established fabrication techniques.
- Possibility to use a wide range of materials.

- Easy cleaning.
- Use of well-established design procedures.
- High versatility.

The only drawbacks concern the heavy structure and the considerable capital expenditure [53]. The materials are chosen to resist to corrosion at elevated temperature and for compatibility with the utilized fluids (see Table 1.3). One of the main design considerations is the choice of the allocation of the fluids in the shell- and tube-side. Important guidance is given by [53] and [79]. The high-pressure stream (steam) should be placed in the tube side, since a high-pressure shell would be too costly.

Main definitions

The main geometrical parameters that characterize a general heat exchanger are shown in Figure 2.7 and their description is based on [80]. The baffle cut is the ratio between the baffle window height and the shell diameter, while the baffle spacing is the distance between two header plates, used to hold the tube bundle. The maximum spacing depends on how much support the tubes require and it lies in the range 40-60 % of the shell diameter. The number of tubes depends on the fluid flow rates and on the available pressure drop. Furthermore, low velocities can have adverse effects on the fouling, while high fluid speeds can increase the rate of erosion beyond unacceptable limits. The number of tubes is lower for longer tubes, which also reduce the technical complication of the header plate. The length is limited to 6 m, due to cleaning reasons. Long tubes are also usually associated to fatigue strength during high operating temperatures and cyclic thermal loads. the design should take into consideration the thermal expansion of the tubes. The diameter of the tube is chosen to ensure high heat transfer coefficients, while facilitating the cleaning process. A 19 mm-diameter is the smallest allowed, as a trade-off of the mentioned aspects. The tube bundle can be arranged according to a square or an equilateral triangle. Triangular pitch (30° layout) is better in terms of heat transfer and surface-to-length ratio. It is also preferred when there is high pressure difference between the fluids in the shell- and in the tube- side and it is therefore chosen for the present study. The pitch ratio is the ratio between the pitch of the tube arrangement and the external diameter of the tubes. Smaller ratios ensure enhanced heat transfer capability and structure compactness, while larger values ease the cleaning. Pitch ratios below 1.25 are usually discouraged.

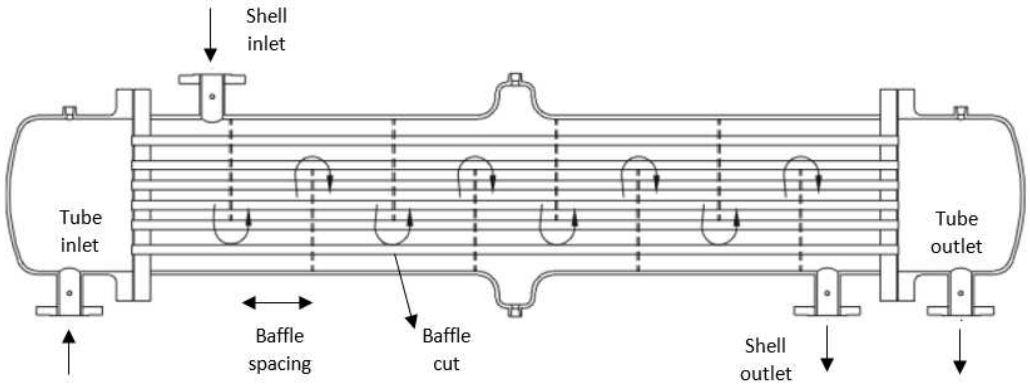

Figure 2.7: Representation of a shell-and-tube heat exchanger. Adapted from [84]

The term “tube pass” is used when the fluid flows all the way across the heat exchanger. Many passes result in an increase of the tube-side velocities, with consequent more effective heat transfer. However, higher pressure drops are present, due to additional turns. Standard design considers 1 or an even number of tube passes. An odd number is uncommon and may results in mechanical and thermal problems during both fabrication and operation.

Heat exchanger sizing

The heat exchanger must be defined in term of exchanging area. Two heat exchangers will be considered: a one-shell, one-pass heat exchanger for the evaporation and a four-passes, one-shell heat exchanger for the superheating. This choice will be justified by the obtained results. The procedure utilized for the sizing of the heat exchangers is the one proposed by [80]. Where not otherwise stated, this is the main source utilized in this section. In the commercial CSP plants, the solar field output at nominal conditions is higher than the thermal duty of the steam generator to increase the number of operating hours. In this case, no oversizing is considered.

The heat exchanger area, evaluated at the outer tube diameter $A_{hex,o}$ can be calculated as:

(2.39)
$$A_{hex,o} = \frac{\dot{Q}}{U_o \cdot \Delta T_{ml,t}}$$

$\dot{Q}$ is the thermal power exchanged by the heat exchanger under nominal operation, U_o is the overall heat transfer coefficient evaluated at the outer diameter of the tube and ΔT_{ml} is the true mean temperature difference, calculated as shown by Equation (2.40).

(2.40)
$$\Delta T_{ml,t} = \Delta T_{ml} \cdot F$$

F is the temperature correction factor that takes into consideration that the heat flows are not exactly in counter-current, while ΔT_{ml} is the logarithmic mean temperature.

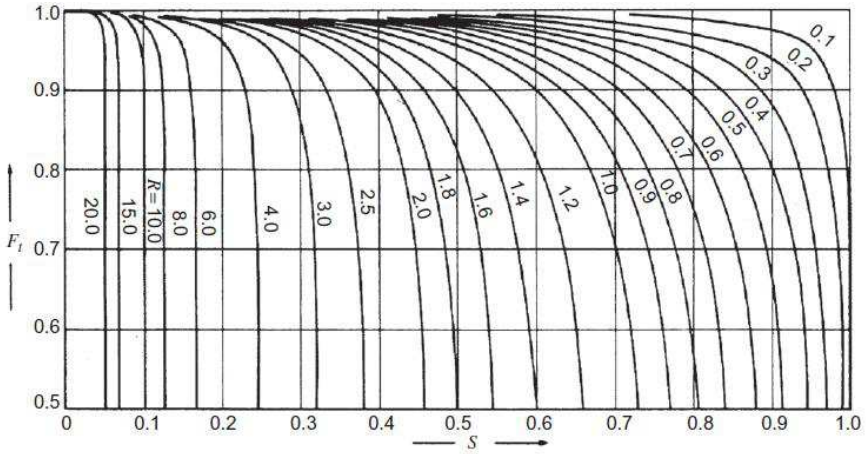

Figure 2.8: Temperature correction factor as function of S and R [81]

For the evaporator, *F* has been set equal to 1, while for the superheater the graph shown in

Figure 2.8 has been used. Initially, a single-shell pass was considered, but no intercept was found in the related graph, utilizing the nominal values presented afterwards. The correction factor is calculated as function of two additional parameters, *R* and *S* [79]:

(2.41) $$R = \frac{T_{shell,in} - T_{shell,out}}{T_{tube,out} - T_{tube,in}}$$

(2.42) $$S = \frac{T_{tube,out} - T_{tube,in}}{T_{shell,in} - T_{tube,in}}$$

The heat exchanger surface can be also expressed as function of the geometrical properties:

(2.43) $$A_{hex,o} = \pi \cdot d_{o,tube} \cdot N_t \cdot L_t$$

where $d_{o,tube}$ is the external diameter of the tubes, N_t is the number of tubes seen in the cross-section of the shell (it means that if four passes are considered, the actual number of tubes is calculated by dividing N_t by four) and L_t is the length of the tubes in each pass.
The number of tubes is evaluated as in Equation (2.44).

(2.44) $$N_t = (CTP) \cdot \frac{\pi \cdot D_s}{4A_1}$$

CTP is the tube count constant, equal to 0.93 for one tube pass and to 0.90 for four tube passes. D_s is the diameter of the shell, while the parameter A_1 can be calculated as:

(2.45) $$A_1 = CL \cdot P_t^{\,2}$$

CL is the tube layout constant, equal to 0.87 for the 30° equilateral triangular pitch arrangement. P_t is the tube pitch. Equations (2.43), (2.44) and (2.45) can be utilized for the explicit evaluation of the required shell diameter:

(2.46) $$D_s = 0.637 \cdot \sqrt{\frac{CL}{CTP}} \cdot \left[\frac{A_{hex,o} \cdot \left(\frac{P_t}{d_{o,tube}}\right)^2 \cdot d_{o,tube}}{L_t} \right]^{1/2}$$

In the present study, the pitch ratio has been set equal to 1.25, as suggested by TEMA [81].
For the evaluation of the required surface, the overall heat transfer coefficient has to be determined. Neglecting the fouling, it can be expressed according to the following equation:

(2.47) $$U_o = \frac{1}{\frac{1}{\alpha_{shell}} \cdot \frac{d_{o,tube}}{d_{in,tube}} + \frac{1}{\alpha_{tube}} + \frac{d_{o,tube}}{k_{wall} \cdot ln\left(\frac{d_{o,tube}}{d_{i,tube}}\right)}}$$

α_{shell} and α_{tube} are the convective heat transfer coefficient on the shell- and tube-side, respectively. k_{wall} is the thermal conductivity of the tube wall, while $d_{i,tube}$ represents its inner

diameter. The outer diameter is set equal to 19 mm, with a wall thickness of 2 mm, as suggested by [79]. The suggested materials for the tube walls are ferritic steel A 387, Grade 91 as reported in Table 1.3 or 304 stainless steel can be used, as in [82]. The thermal conductivity is around 21 W/mK in the temperature range of interest [74].

The heat exchanger sizing must consider also the pressure drops that the fluids undergo through the steam generator, since the design parameters have usually contrasting effect on pressure losses and heat transfer effectiveness.

The convective heat transfer coefficient on the shell-side has been evaluated with the Kern's method [79]. Firstly, the area for the cross-flow A_s is calculated:

(2.48) $$A_s = \frac{(P_t - d_{o,tube}) \cdot D_s \cdot L_b}{P_t}$$

Secondly, the shell-side mass velocity G_s and linear velocity u_s can be calculated:

(2.49) $$G_s = \frac{\dot{m}_{salt}}{A_s}$$

(2.50) $$u_s = \frac{G_s}{\rho}$$

The equivalent hydraulic diameter can be then evaluated for the triangular arrangement:

(2.51) $$d_e = \frac{1.10}{d_{o,tube}} \cdot \left({P_t}^2 - 0.917 \cdot {d_{o,tube}}^2 \right)$$

The Reynolds number can be calculate utilizing the equivalent diameter and the linear velocity. The Nusselt number is evaluated as:

(2.52) $$Nu = j_h \cdot Re \cdot Pr^{0.33} \cdot \left(\frac{\mu}{\mu_w} \right)^{0.14}$$

All the properties are evaluated at the average temperature of the salt in the heat exchanger, while μ_w is calculated at the all temperature. j_h is the Colburn j-factor, calculated as:

(2.53) $$j_h = a_1 \cdot \left(\frac{1.33}{\frac{P_t}{d_{o,tube}}} \right)^{a} \cdot Re^{a_2}$$

$$a = \frac{a_3}{1 + 0.14 \cdot Re^{a_4}}$$

The pressure drop is calculated with the following equation:

(2.54) $$\Delta p = 8 j_f \cdot \frac{D_s}{d_e} \cdot \frac{L_{tube}}{L_b} \cdot \rho \cdot v_s^2 \cdot \left(\frac{\mu}{\mu_w} \right)^{0.14}$$

(2.55) $$j_f = b_1 \cdot \left(\frac{1.33}{P_t}\right)^b \cdot Re^{b_2}$$

$$b = \frac{b_3}{1 + 0.14 \cdot Re^{b_4}}$$

j_f is the friction factor. The values of the constants a_1, a_2.. *and* b_1, b_2... etc. are function of the Reynolds number and they are listed in Appendix V.

On the tube-side, the mass flow should be divided into the different tubes:

(2.56) $$\dot{m}_{w,tube} = \dot{m}_{water} \cdot \frac{N_p}{N_t}$$

$\dot{m}_{w,tube}$ is the mass flow of water/steam in a single tube, while $\dot{m}_{water}$ is the total mass flow. N_p is the number of tube passes considered.

Even if the economizer and the evaporator have been considered in the same heat exchanger, different correlations should be used for the heat transfer coefficients. The thermodynamic properties of water have been evaluated utilizing the free software XSteam [83].

For the water in liquid form, the correlation utilized has been taken from [79]. It is shown by Equation (2.57).

(2.57) $$\alpha_{tube} = 4200 \cdot (1.35 + 0.02 \cdot (T - 273.15)) \cdot \frac{v^{0.8}}{{d_{i,tube}}^{0.2}}$$

The average velocity and temperature are considered.

When the water undergoes a phase-change, it is not possible to utilize a single correlation to characterize the whole process. Thus, ten different heat transfer coefficients for steam qualities ranging from 0.05 to 0.95 have been calculated. Finally, an average value has been used as representative of the evaporation. This approach could lead to a rough estimation, since the heat transfer coefficient should be weighted on the tube length needed to pass from a steam quality to another. However, as it will be better shown afterwards, this methodology has resulted in reasonable overall heat transfer coefficient and it has been considered accurate enough for the present study. The subscripts *f* and *g* refer to the properties of the saturated liquid and steam, respectively, while *w* refers to the wall temperature. In the other cases, average properties are used. The correlation utilized has been provided by [84].

(2.58) $$Nu = \frac{0.00061 \cdot (S+F) \cdot Re_f \cdot Fa^{0.11} \cdot Pr^{0.4}}{ln(B)}$$

$$S = 142.5 \cdot Bo^{0.9} \cdot M^{0.55} \cdot \left(\frac{\rho_f}{\rho_g}\right)^{0.33}$$

$$Bo = \frac{\dot{q} \cdot A_{cross,tube}}{h_g - h_f}$$

$$F = \bar{x} \cdot \left(\frac{\bar{x}}{1-\bar{x}}\right)^{0.9} \cdot \left(\frac{\rho_f}{\rho_g}\right)^{0.35}$$

$$Re_f = \frac{(1-\bar{x}) \cdot \rho \cdot v \cdot d_{i,tube}}{\mu_f}$$

$$Fa = \frac{(\rho_f - \rho_g) \cdot \sigma}{(v \cdot \rho)^2 \cdot d_{i,tube}}$$

$$B = 1.02 \frac{\mu_f}{\mu_w}$$

The length of the is divided into 10 segments, each one characterized by an average steam quality $\bar{x}$, which progressively and uniformly increases from 0.05 to 0.95. The specific heat flux $\dot{q}$ is considered constant in each segment. *M* is the molar mass of water (18 .01 kg/kmol), σ is the surface tension, $A_{cross,tube}$ is the cross-sectional area of the tube and *h* is the enthalpy.

Finally, the Nusselt number for the superheated steam convective heat transfer coefficient is calculated as follows:

(2.59)
$$Nu = \frac{C/2 \cdot Re \cdot Pr}{1.07 + 12.7 \cdot \left(\frac{f}{2}\right)^{0.5} \cdot \left(Pr^{\frac{2}{3}} - 1\right)}$$

(2.60)
$$f = (1.58 \cdot ln(Re) - 3.28)^{-2}$$

f is the friction factor.

The pressure losses are calculated in three different ways, for the economizer, the evaporator and the superheater. In the economizer, two different correlations are utilized for the friction factors, depending on the Reynolds number:

(2.61)
$$f = \frac{16}{Re} \quad for\ Re < 2000$$

(2.62)
$$f = 0.046 \cdot Re^{-0.2} \quad for\ Re > 2000$$

In the superheater, the calculation of the friction factor has been already reported. In the zones where the fluid presents a single-phase, the pressure drop can be estimated as:

(2.63)
$$\Delta p = 4 \cdot N_p \cdot \left(f \cdot L_t \cdot \frac{1}{d_{i,tube}} + 1\right) \cdot \frac{\rho}{2} \cdot v^2$$

For the evaluation of the pressure losses in the evaporation zone, the Lockart and Martinelli method has been used [85]. It considers the three phenomena: gravity (static pressure losses), acceleration (momentum pressure losses) and friction. The static pressure losses for a vertical tube are expressed in Equation (2.64).

(2.64) $$\Delta p_{static} = \rho_H \cdot g \cdot \frac{L_{t,eva}}{10}$$

$$\rho_H = \rho_f \cdot (1 - e_H) + \rho_g \cdot e_H$$

$$e_H = \frac{1}{1 + \frac{\rho_g}{\rho_f} \cdot \frac{1 - \bar{x}}{\bar{x}}}$$

$L_{t,eva}$ is the part of the tube interested by the phase change, while e_H represents the void fraction for homogeneous flow.

The momentum pressure losses are calculated as:

(2.65) $$\left(\frac{\partial p}{\partial z}\right)_{momentum} = \frac{\frac{\partial \dot{m}_{steam}}{\partial \rho_H}}{dz}$$

z is the coordinate representing the dimension along the length of the heat exchanger. Since the evaporator is divided into sections characterized by constant steam quality, these losses can be neglected.

Finally, the losses related to friction are calculated with the same correlation presented from economizer and superheater. The friction coefficient is expressed by Equation (2.66) [85].

(2.66) $$f = \frac{0.079}{Re^{0.25}}$$

The viscosity utilized for the calculation of the Reynolds number is the average of the viscosities of the saturated steam and water, weighted on the steam quality of the considered tube section. Once again, the accuracy of the calculation in the two-phase zone is lower, since more assumptions and simplifications have been used.

The calculation of the surface area required and of the overall heat transfer coefficient is not straight forward, since the geometrical dimensions are needed for the calculation of the coefficient itself. For this reason, an iterative process is required:

1. The shell diameter is initially guessed, and imposed equal to one fifth of the tube length.
2. The tube number and the real mean temperature are evaluated.
3. The tube wall temperature is guessed and set equal to the average between the inlet and the outlet conditions of the shell-side fluid.
4. The convective heat transfer coefficients are calculated.
5. The overall heat transfer coefficient is evaluated
6. The required exchange area is calculated, as well as the shell diameter and the number of tubes.
7. The tube wall temperature is calculated with the following heat balance:

$$U \cdot (T_{shell} - T_{tube}) = \alpha_{shell} \cdot (T_{shell} - T_{wall})$$

T_{shell} is the average temperature of the shell-side fluid, T_{tube} the one of the tube-side fluid, while T_{wall} is the temperature of the tube wall.

8. The calculated values are used as the guessed ones and the procedure is repeated till convergence, starting from point 3.

In the case of the evaporator, additional complications are introduced by the fact that the tube length dedicated to bringing the water to the boiling point and the one needed to complete the evaporation process are not known a-priori. Besides the iterative process previously described, a second one is needed and constructed over the first. The length of the tube required by the economizer and the evaporator is initially subdivided according to the heat flux that each part must exchanger. Consequently, points 1-8 are applied for the two parts, separately. The guessed values are then updated and the procedure is repeated until convergence. The overall heat transfer coefficient for the whole heat exchanger is calculated as the average of the single coefficients, weighted on the required heat exchanger area.

The calculation has been performed various times for different tube lengths and baffle spacings, in order to obtain acceptable heat transfer effectiveness and limited pressure drops. The results of the sizing will be shown in the section 2.4.

Dynamic behavior of the steam generator

The dynamic behavior of the steam generation system has been modelled to resemble the once-through boiler that will be operating in the demonstration plant located in Évora [36]. In order to ensure fast ramping and steep start-ups, the steam generator will operate under sliding pressure mode. This means that the evaporation pressure adapts to the load fraction and the steam mass flow changes proportionally. Once-through design is usually preferred, since the possibility of continuous recirculation is limited by the wide variation in fluid specific volume. However, recirculation pumps are usually provided to the system to protect the operation of the steam generator at low loads, when the departure from nucleate boiling may cause high tube temperatures. Sliding pressure operation involves the presence of a two-phase liquid over most of the load range and multiple passes might become difficult to manage. This aspect justifies the employment of a single pass heat exchanger for the evaporator [86].

The variation of the pressure with the load is defined by a characteristic curve for the steam generator. This information was not available and, therefore, the pressure was assumed to vary linearly from the minimum to the maximum load:

(2.67)

$$\frac{p_{eva}-p_{eva,min}}{p_{eva,max}-p_{eva,min}} = \frac{1-\frac{\dot{Q}_{min}}{\dot{Q}_N}}{\frac{\dot{Q}_{max}}{\dot{Q}_N}-\frac{\dot{Q}_{min}}{\dot{Q}_N}}$$

The subscripts *min* and *max* refer to the minimum and maximum load, which are assumed to be 33 % and 120 %, respectively, as in [36]. $\dot{Q}_N$ is the nominal heat flux.

The steam mass flow is then calculated as:

(2.68)

$$\dot{m}_{steam} = \dot{m}_{steam,N} \cdot \frac{\dot{Q}}{\dot{Q}_N}$$

Once the evaporation pressure and the steam mass flow rate have been determined, it is possible to calculate the thermodynamic properties of both the shell-side and the tube-side fluids performing a simple energy balance in each heat exchanger:

$$\dot{m}_{steam} \cdot \left(h_{steam,2} - h_{steam,1}\right) = \dot{m}_{salt} \cdot c_p \cdot \left(T_{salt,1} - T_{salt,2}\right) \quad (2.69)$$

1 and *2* indicate the condition of the fluid at the inlet and at the outlet.

The steam generation system considered in the current study is assumed to be able to vary the load almost instantaneously. In fact, compared to the state-of-the-art boiler, a once-through sliding-pressure generator is more flexible. However, particular attention has been put on the start-up, since the load increased is limited to 15 K/min [36]. For this reason, in the morning, the boiler will start at the minimum load and it will increase its power output with the time. The mass flow of the molten salt will be adapted accordingly. The energy required to maintain the inlet temperature equal to the minimum load level during the night has been neglected, since it would require a detailed evaluation of the heat losses in each component of the power block, which is out of the scope of the present study. The outlet temperature of the molten salt is assumed constant and equal to 290 °C.

2.2.11. Steam loop layout

The layout of the steam cycle has been modelled as the simplified version of the one of the demonstration loop in Portugal, whose design has been directly given by the project manager. In this case, no recirculation after the evaporator is directly considered, since it does not affect the plant during normal operation. The same can be said for the make-up water tank, the drain tank and the control valves. The steam cycle is represented in Figure 2.9.

The superheated steam undergoes a first expansion (from evaporation pressure to 65 bar) and then a portion is injected in the feedwater tank, in order to maintain an adequate inlet temperature of the water. The remaining part expands through a second expansion valve and it is then cooled by an air condenser. The saturated liquid is collected in the condensate tank, partly re-circulated and mixed with the fluid coming from the valve. The fraction *f* is calculated under design conditions and maintained constant during part-load operation. This aspect results in the need of additional heat to provide an ensure water temperature of 270 °C, which is provided by an auxiliary electrical resistance. Two pumps are present in the circuit. The first one brings the saturated water from condensation pressure (5 bar the design point) to 55 bar. The second one is required to extract the fluid from the feedwater tank and enhance its pressure till the one dictated by the boiler. The fractions y_1 and y_2 have been taken from the Évora plant, and they are equal to 1.33 and 0.25, respectively.

Expansion valves

The demonstration loop will serve to prove the feasibility of steam production, but no electricity will be produced. Thus, a turbine will not be provided. The superheated steam will be expanded through two expansion valves, undergoing a iso-enthalpic transformation.

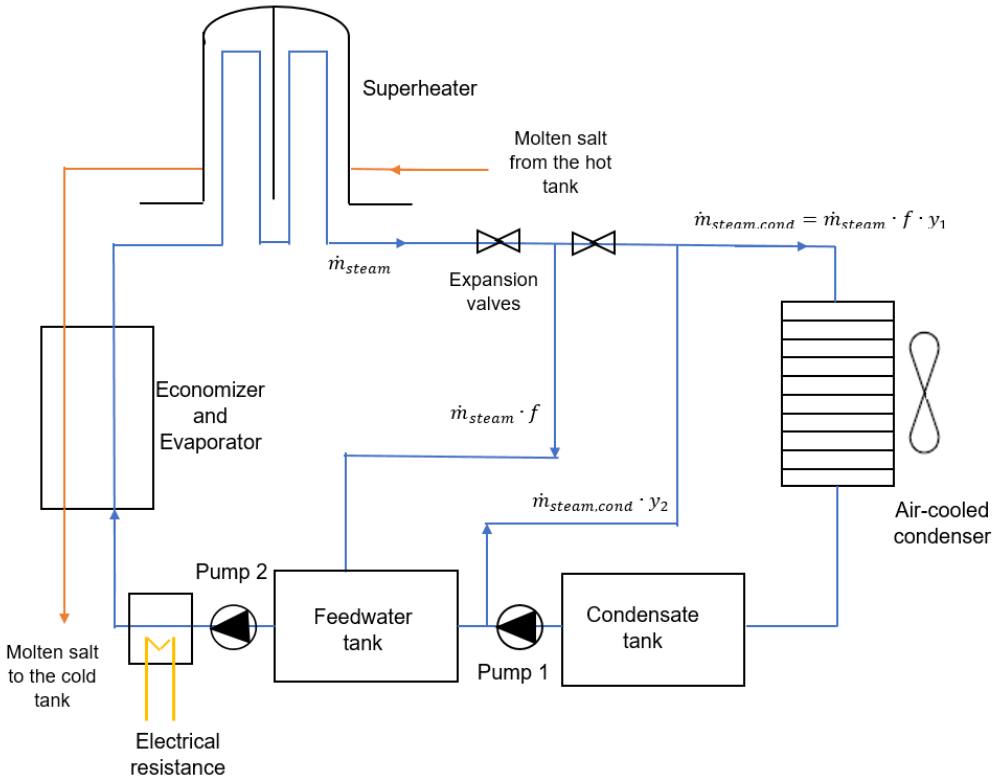

Figure 2.9: Steam loop layout

Condenser

In order to minimize the water consumption in the plant, dry-cooling is proposed. The performance of an air-cooled condenser is influenced by the external weather conditions, since the air temperature has an impact on the possible condensing pressure. The model used by the SAM software has been utilized [67].

The nominal air mass flow $\dot{m}_{air,N}$ is evaluated as:

(2.70)
$$\dot{m}_{air,N} = \frac{\dot{Q}_{rej}}{c_{p,air} \cdot (T_{ITD,des} - \Delta T_{out})}$$

$\dot{Q}_{rej}$ is the heat rejected by the condenser, $T_{ITD,des}$ is the initial steam-to-ambient temperature difference, while ΔT_{out} is the temperature difference at the hot side of the condenser, equal to 3 °C. The condenser nominal pressure is 5 bar [36]. Consequently, $T_{ITD,des}$ is evaluated as the temperature difference between the condensing temperature and the environment temperature of design, set equal to 25 °C. The air mass flow can adapt to the load variation.

The heat rejected by the air condenser is calculated as follows:

(2.71)
$$\dot{Q}_{rej} = \dot{m}_{steam,cond} \cdot (h_{cond,1} - h_{cond,2})$$

$\dot{m}_{steam,cond}$ is the mass flow of steam passing through the condenser, which is assumed to

leave as saturated liquid.
The main parasitic consumption of the condenser is related to the electricity used by the fan to compress outside air and use it too cool the steam. The temperature of the air after isentropic compression $T_{fan,out,is}$ is:

$$T_{fan,out,is} = T_{amb} \cdot r^{\frac{R}{c_{p,air}}} \quad (2.72)$$

r is the condenser air pressure ration, equal to 1.0028, while *R* is the ratio between the universal gas constant and the molar mass of air.
Considering 0.8 as isentropic efficiency $\eta_{fan,is}$ of the fans, the real outlet temperature can be calculated as:

$$T_{fan,out} = T_{fan,in} + \frac{T_{fan,out,is} - T_{fan,in}}{\eta_{fan,is}} \quad (2.73)$$

Finally, the consumption of the fans can be evaluated, considering a mechanical efficiency $\eta_{fan,mech}$ equal to 0.9:

$$\dot{W}_{fan} = \frac{\dot{m}_{air} \cdot c_{p,air} \cdot (T_{fan,out} - T_{fan,in})}{\eta_{fan,mech}} \quad (2.74)$$

Pumps

The consumption of the pumps is modelled according to [67]. The pressures in the steam-loop are known and the enthalpy are calculated considering an isentropic compression and then applying the isentropic efficiency, equal to 0.7.

$$h_{pump,out} = h_{pump,in} + \frac{h_{pumo,out,is} - h_{pump,in}}{\eta_{pump,is}} \quad (2.75)$$

As in the previous section, the electric consumption is evaluated:

$$\dot{W}_{pump} = \frac{\dot{m}_{steam} \cdot (h_{pump,out} - h_{pump,in})}{\eta_{pump,mech}} \quad (2.76)$$

“Pump 2” is needed also to cover the pressure losses in the steam generator Δp_{SG} and its consumption is calculated as in Equation (2.77).

$$\dot{W}_{pump} = \frac{\Delta p_{SG} \cdot \dot{m}_{steam}}{\rho_w \cdot \eta_{pump,mech}} \quad (2.77)$$

$\eta_{pump,mech}$ represents the mechanical efficiency of the pump, equal to 0.75, while ρ_w is the average density of the water/steam through the heat exchangers. The same equation is used to calculate the consumption of the pump on the salt-side.

Mixer (feedwater tank) and electrical resistance

The feedwater tank is the last component of the steam cycle. It is used to mix a fraction of the superheated steam with the steam coming from the condenser, in order to increase its temperature and limit the issues related to molten salt freezing. Under design operation, the portion of superheated steam entering the tank f_{steam} is the one able to ensure nominal conditions at the inlet of the boiler:

(2.78) $$f_{steam} = \frac{h_{feed,boiler} - h_{mix,in}}{h_{steam,SH} - h_{mix,in}}$$

$h_{feed,boiler}$ is the enthalpy of the feedwater entering the boiler, $h_{mix,in}$ is the one of the cooled steam coming from the condenser and $h_{steam,SH}$ is the one of the superheated steam.

If the thermodynamic properties of the water at the outlet of the mixer does not fulfill the temperature requirements, an electrical resistance is utilized, whose electric consumption is estimated as:

(2.79) $$\dot{W}_{el,res} = \dot{m}_{steam,boiler} \cdot \left(h_{feed,boiler} - h_{mix,out}\right)$$

$\dot{m}_{steam,boiler}$ is the steam mass flow entering the steam generation system, which depends on the load fraction.

2.3. Solar field layout and operation strategy

A simplified representation of the designed solar field has been reported in Figure 2.4, in order to summarize all the component previously described. If the sketch is combined with Figure 2.9, an overall view of the demonstration plant is obtained. Two pumps are considered in the solar field, in order to provide redundancy. This aspect is particularly important, due to the anti-freezing strategy adopted. As described in section 2.5.1, the circulation of the molten salt must be ensured during night operation to avoid low fluid temperature. In the unlike case both pumps failed, the loop is drained by air entering the vent valve, as described in section 2.5.2.

The operational strategy of common CSP power plants is based on the electricity demand and on the role that the plant has on its provision (peak or base-load power plant). On the contrary, the designed plant will not produce electricity and thus any strategy can be considered valid, as long as it can demonstrate reliable steam production. Consequently, a simple approach has been chosen: the storage system is initially fully charged and then the steam is produced with the stored energy. In some days, the energy coming from the solar field could not be enough to fill the hot tank and the storage system is emptied at the sunset.

The molten salt mass flow utilized for the steam production $\dot{m}_{salt,SG}$ is the minimum between the nominal mass flow (calculated as in the next section) and the available salt mass stored in the hot tank:

(2.80) $$\dot{m}_{salt,SG} = min \begin{cases} \dot{m}_{salt,N} \\ \frac{m_{hot}}{\Delta t} + \dot{m}_{salt,hot,IN} \end{cases}$$

$\dot{m}_{salt,N}$ represents the nominal mass flow, m_{hot} is the mass of the molten salt stored in the hot tank, while $\dot{m}_{salt,hot,IN}$ is the salt mass flow entering the hot tank. As previously described, the minimum load allowed in the steam generation system is 33 %.

In order to ensure proper outlet temperature of the solar field, a variable-speed pump should be used. The first parameters to be set are the minimum and maximum velocities that the heat transfer fluid can have in the receiver tube. According to [49], the minimum allowable mass flow is 2 kg/s. Considering an inlet design temperature of 290 °C and the geometrical specifications of the utilized receiver, this results in a minimum velocity of 0.3 m/s. The upper limit (v_{max}) has been taken from [87], which suggests 1.2 m/s. However, the availability of mass stored in the cold tank should be taken into account. The maximum possible velocity of the molten salt in the solar field during the considered time step, $v_{max,SF}$, is the minimum between the physical limit and the quantity available:

(2.81)
$$v_{max,SF} = min\left\{ \begin{matrix} v_{max} \\ \frac{m_{cold}}{\Delta t \cdot \rho_{cold} \cdot A_{cross,section}} \end{matrix} \right.$$

Where m_{cold} is the salt mass stored in the cold tank, ρ_{cold} is the density of the fluid stored in the cold tank and $A_{cross,section}$ is the cross-sectional area of the receiver tube.

The inlet velocity of the solar field, v_{SF} is adapted to the incident radiation, in order to meet an outlet temperature of 550 °C, utilizing the following equation:

(2.82)
$$v_{SF} = v_{SF}^{*} \cdot \left(1 - \frac{T_{SF,out,N} - T_{SF,out}}{T_{SF,out,N}}\right)$$

$T_{SF,out,N}$ is the nominal temperature at the solar field outlet, while $T_{SF,out}$ is the temperature obtained with the guessed inlet velocity v_{SF}^{*}.

If the outlet temperature is lower than the nominal one, even when the minimum inlet velocity is utilized, two different approaches are used, depending on the presence of solar radiation. During the day, if the DNI is higher than zero, the velocity is set equal to the lower limit. On the other hand, during night operation, the mass flow that can ensure anti-freezing protection and minimum pressure losses is used, as explained in section 2.6.2. In both cases, the HTF is re-circulated through the cold storage tank ("line 2" Figure 2.3). When the solar radiation is very high, the inlet velocity is increased up to the upper limit. If the outlet temperature is still higher than the nominal one, partial defocus of the collectors is applied. In this case, the mass flow can enter the hot tank, storing energy useful for the steam production.

2.3.1. Pressure losses in the solar field

The calculation of the pressure losses is important to estimate the parasitic consumption in the system. On the salt side, distributed and localized pressure drops in the solar field are considered, as in [73]. Losses due to velocity increase have not been considered. On the steam side, the two pumps are needed to increase the pressure of the water from condensation to evaporation pressure and to cover the losses in the steam generator, while friction losses in the water circuit have been neglected.

The pressure losses in the solar field take into consideration both fluid friction and the presence of valves, elbows, ball joints and branch connections (Weldolets).

Table 2.4: Components interested by localized losses. Adapted from [73] *and* [74]

Component	Symbol	Number per loop (n)	Value
Control valve	$k_{valve,c}$	1	2.5
Gate valve	$k_{valve,g}$	2	0.19
Weldolet	k_w	2	1.8
Ball joints	k_j	$2 \cdot n_{SCA}$	4.73
Elbows	k_{el}	$(10 + m)$	0.9

The pressure drops are calculated as:

(2.83) $$\Delta p = f \cdot \rho \cdot \frac{v_{av}^2}{2} \cdot \frac{\pi \cdot d_{ab,in} \cdot L_{tot}}{A_{cross,section}}$$

v_{av} represents the average velocity of the HTF in the solar field, while the friction factor has been evaluated as in section 2.2.6.

L_{tot} is the total length interested by the pressure losses. It is the sum of the total piping length, L_{distr}, and of the equivalent length of the localized losses, L_{loc}. L_{distr} is evaluated as:

(2.84) $$L_{distr} = n_{SCA} \cdot l_{tube} + \frac{N_{sca}}{2} \cdot l_{gap} + m \cdot l_{spacing}$$

N_{SCA} is the number of solar collector assemblies, while *m* is a coefficient equal to 1, when the molten salt enters the hot storage tank, or 2, when the fluid is recirculated to the cold tank.

The localized losses are calculated as:

(2.85) $$L_{loc} = k_{loc} \cdot \frac{d_{ab,in}}{2 \cdot f}$$

k_{loc} is the localized loss coefficient, calculated as the sum of the contributions of all the components present in the solar loop:

(2.86) $$k_{loc} = \sum k_i \cdot n_i$$

k_i is the coefficient of the *i*-th component of the loop, which is present n_i times. The values of *k* for each component are shown in Table 2.4.

2.4. Sizing of the system and nominal conditions

The sizing of the system should be performed under nominal conditions. Usually, the design point is chosen in summer, when the production is at the maximum. In this way, the risk to oversize the storage system to minimize the energy waste is limited. Moreover, the solar field is oversize, in order to maximize the electricity production [28].

In this case, a different approach has been used:

- The system is sized considering a solar irradiation of 800 W/m^2 and cosine losses equal to 0.9. These parameters are representative of the average autumn equinox at noon (see section 2.6.1). The aim of the demonstration plant is not to sell electricity, and sizing the system at optimal conditions would limit too much the operating hours. For these reasons, the utilized values can be considered a reasonable trade-off.
- The air temperature at design conditions is 25 °C, with wind velocity set to zero.
- The thermal output of the solar field is equal to the thermal duty of the steam generator.
- The heat exchangers are sized at nominal conditions.

Applying the methodology presented, a nominal mass flow of 5 kg/s is obtained, resulting an inlet design velocity of 0.78 m/s. This value lies within the range presented in section 2.3. The thermal output is 2 MW_{th}, while the pressure losses in the solar field amount to 7 bar. The Archimede power plant produces steam at 102 bar, while the loop located in Portugal will operate with pressures up to 140 bar. Considering an inlet temperature of the feedwater of 270 °C and a temperature of the live steam equal to 535 °C (approach point of 15 °C), an evaporation pressure of 100 bar has been considered the most suitable, since it results in a pinch point of around 4.5 °C at 100 % load. 70 bar and 109 bar are the maximum and minimum allowed pressures, respectively, according the sliding pressure operation previously described. The mass flow of steam is 0.88 kg/s.

The efficiency of the solar field is equal to 55 %, with the SCAs with molten salt at lower temperature performing better. Overall, efficiencies of the single collectors range from 45 % to 65 %. The values of the main design parameters are summarized in Table 2.5.

It is then possible to proceed with the sizing of the heat exchangers. The results obtained have been compared with the study performed on the boiler utilized in the Solar Two project [82] and with the study performed by [88]. The overall heat transfer coefficient seems to be precise, while the pressure losses are slightly different. On the shell-side, they are higher, probably due to the choice of two shell passes in the superheater. On the tube-side, they are lower, especially in the economizer-evaporator. This could be due to the small water mass flow and the use of a single pass. However, in all the cases, the obtained results are of the same order of magnitude, underlining how the utilized methodology, even if characterized by several assumptions, can be considered consistent. The results are reported in Table 2.6.

Table 2.5: Design parameters under nominal conditions

Parameter	Value
Molten salt mass flow	5 kg/s
Design inlet velocity	0.78 m/s
Inlet/outlet solar field temperature	290/550 °C
Solar field thermal output	2 MW_{th}
Solar field pressure losses	7 bar
Steam generator duty	2 MW_{th}
Steam mass flow	0.88 kg/s
Nominall steam pressure	100 bar
Minimum/maximum steam pressure	70/109 bar
Nominal water/steam inlet/outlet temperature	270/535 °C
Pinch/approach point	4.5/15 °C

Table 2.6: Results of the heat exchanger sizing

Parameters	Economizer-Evaporator	Superheater
Shell diameter D_s	277 mm	158 mm
Tube inner diameter/thickness	19/2 mm	19/2 mm
Tube length L_t	6 m	6 m
Passes N_p	1	4
Baffle spacing L_b	0.5· D_s	0.7· D_s
Shell number	1	1
Tube number N_t	72	22
Overall heat transfer coefficient U	1482 W/m^2K	1212 W/m^2K
Area required $A_{hex,o}$	31 m^2	9.5 m^2
Shell-side/tube-side pressure drop	403/140 kPa	

2.5. Plant operation

The designed demonstration loop utilizes a mature and proven technology, such as the parabolic trough collectors, with an innovative heat transfer fluid, the molten salt. Furthermore, no commercial applications are currently in operation. For these reasons, the operation of the plant relies both on suggestions found in literature and on the expertise gained in demonstrations plants. As highlighted many times, considerable care must be put to avoid the freezing of the salt in the loop [39]. Different options will be presented and discussed, and, finally, the one chosen for the current evaluation will be tested.

2.5.1. Freeze protection strategies

As it has been recalled several times, the main issues related to the utilization of molten salts as HTF is their high melting point. However, there is no collective agreement about the minimum temperature of utilization. Donnola et al. [89] state that temperatures around 200 °C can be reached during the circulation of the HTF without critical events, relying on the kinetic energy of the fluid. Other authors set 260 °C as limit for the molten salt, in order to maintain a safe margin over the crystallization temperature, or rather the temperature of which all the substance is in liquid phase, equal to 240 °C [90] [91]. In the present study, more importance will be put on the data provided by the Archimede plant, since they come from the experience gained in a real system. A lower limit will be considered for the circulating fluid, while the salt present into the storage tanks will be kept at higher temperatures.

Three main strategies can be considered to maintain the temperature of the fluid above reasonable limits:

- Continuous electrical heating during night or use of an auxiliary heater.
- Complete draining of all the salt during night, morning preheating and refill of the piping before starting the operation.
- Recirculation of the fluid through the cold tank.

These three strategies will be described and compared in the following paragraphs.

Electrical heating and auxiliary heater

An electrical heat trace system can be considered to avoid freezing during night operation, with a mineral insulated cable used to heat all the piping. This is the only known type of heat trace cable able to withstand temperatures over 250 °C and it represents the most expensive option, requiring energy consumption [41] [28]. Alternatively, an auxiliary heater, usually fossil-fuel based can be considered when the temperature falls below a certain threshold [38]. Both possibilities use a substantial amount of power reducing the overall efficiency of the process [53]. Many authors agree that these strategies would be too costly to make the utilization of molten salt economically competitive and, therefore, alternatives should be considered [47].

Night draining and morning preheating

According to [47], the complete draining of the fluid during night would be the best option to avoid the fluid to reach its melting point. All the salt is drained during the evening by gravity and compressed air. The fluid is evacuated and consequently collected in an underground drainage tank. This tank is located at the lowest point of the plant. The salt is then pumped in the cold tank, to store energy for the next day. The tube walls are kept hot by a thermal fluid heat tracing system, which utilizes heat from the thermal storage tanks. A thin piping system is installed between the thermal insulation and the inner steel pipe (see Figure 2.10). Special aluminum adapters between the tracing pipes and the main pipe ensure an effective heat transfer. The mass flow on the inlet salt is controlled by mixing fluid from the hot and cold tank, reaching temperatures in the range 290°C-560 °C. The cooled salt leaves the heat tracing system at about 50 °C above the freezing temperature and it then sent to the drainage tank.

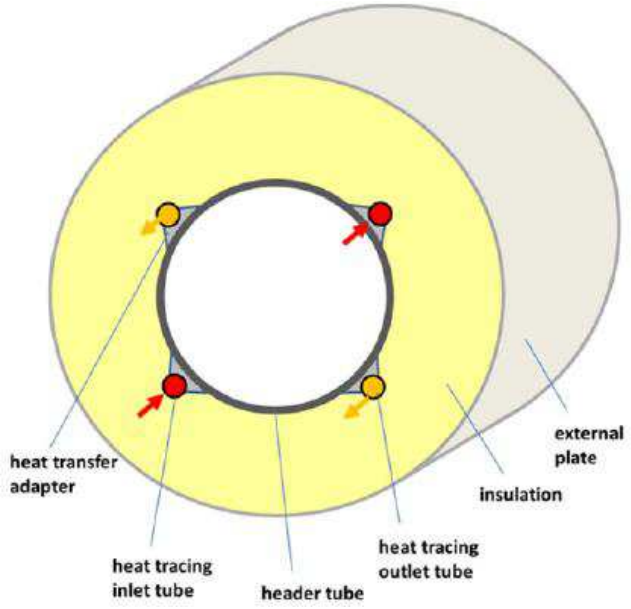

Figure 2.10: Thermal fluid heat tracing system [47]

In the morning, inlets and outlets of the solar field are preheated by air, utilizing the heat from the hot tube walls of the header lines and from the first solar radiation. During the preheating, the heat tracing system must be operated with an elevated mass flow and higher inlet temperatures to increase air temperature sufficiently. Since the heat transfer coefficient is low and the solar irradiation is highly ununiform, the collectors must be partly defocused to avoid critical thermal gradients and sever mechanical stresses. The preheating of the absorber walls to 240 °C takes less than an hour. Once the wall temperature in the whole circuit is higher than the melting point of the salt, the solar field is filled by pumping the fluid from the cold tank to the absorbed tubes. The entering salt moves out the air, which is released in the atmosphere. About then minutes are needed to fill the solar field. Normal operation can then begin.

An air blower and an airline are necessary to move the fluid from the pipes. No electrical heat tracing or impedance heaters (see section 2.5.3) must be installed in the solar field. Compared to the electric night heating, considerable cost reduction can be achieved (about 5 %).

Night circulation through the cold storage tank

The HTF can be circulated through the solar field during the whole night, keeping the piping warm and avoiding critical temperature gradients during the start-up [47]. The salt passes through the cold storage tank and the stored heat is used to keep the temperature of the fluid above reasonable limits. The main drawback of this strategy is that cold tank might need to be heated up at the beginning of morning operation, with consumption of solar energy [38].

Chosen strategy: advantages and main challenges

The strategy chosen for the plant to be designed is the third one, which utilizes the heat stored in the cold tank to maintain the temperature of the molten salt above its melting point. This strategy presents several advantages:

- No electric heat tracing system is needed, with beneficial impact on the investment.
- No losses of salt. In fact, during drainage, not all the HTF can be recovered [38].
- No continuous night heating should be provided, reducing the ongoing costs.
- No auxiliary heater needed and consequent no consumption of auxiliary energy. Safe night operation can be ensured by adapting storage size and fluid mass flow.
- Overall, the capital expenditure related to freeze protection is nearly equal to zero, since no additional component is needed for night operation.

The strategy should be tested for different storage sizes, while the night mass flow should be optimized, considering a trade-off between pressure losses and temperature aspects. The annual simulation will be used to validate the proposed strategy. In the next sections, other aspects related to the adopted plant operation will be described.

2.5.2. Draining

The drainage of the solar field can be necessary, for instance in cases of maintenance or emergency. In the present analysis, a drainage tank is considered for the operation [47]. In a large-scale application, the loops are drained one by one, progressively. The resistance heating system in the piping (see section 2.5.3) is activated and electric power is delivered to the heat collection elements to maintain a minimum temperature of 200 °C. The isolation valves are closed, while the vent valve located at half loop position is opened and a flow of air entering the loop pushes the salt inside the collecting tank [92]. Void spaces should be carefully avoided everywhere in the loop, in order to limit the danger of plastic deformation [38].

The detailed procedure to be followed for the draining of a single loop is described by [92]. The collectors are defocused and kept vertical, which is the best position for draining. The input and output valves of the loop (V1X and V2X) are closed, in order to bottle the HTF inside, and the circulating pump is stopped. After, the draining valves (V1X_DR and V2X_DR) are opened, together with the vent valve (V4X), and the molten salt is drained (see Figure 2.11). The collectors should be slightly inclined, to facilitate the draining and to ensure it in cases of air-blower faults. They can be adapted to the natural slope of the ground or artificially tilted by 0.1 % modifying the foundation heights. The solar field pipes are also arranged to have a slight

slope towards the drainage tank. If 0.3 bar are applied at the highest point of the field, five minutes are required to empty a 300-m long pipe. A 70-diameter pipe, filled with Solar Salt at 290 °C would roughly take one hour to cool down to 240 °C, considering average thermal losses in the order of 150 W/m. Therefore, the drainage is considered uncritical. The required time can be reduced by applying higher pressure difference [47]. The temperature of the fluid must be monitored at any time. The total drain lasts less than one hour, with the collectors with higher temperatures requiring less time, due to lower content (lower density of the fluid in the same volume).

While the drainage of a single loop is a routine maintenance, the whole plant is drained only in case of major faults or severe maintenance. The procedure present similar aspects to the one described above, with the collectors kept in vertical position and the circulation pump stopped. In this case, the inlet and outlet valves are kept fully open and two main draining valves located at the distribution line are utilized to discharge the whole HTF to the service tank [92].

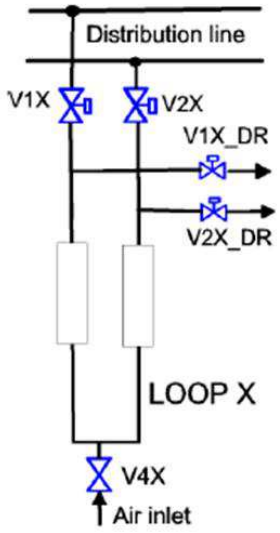

Figure 2.11: Representation of the drained loop with required valves [92]

2.5.3. Preheating methods

Preheating of the pipes is always needed before the molten salts is reintroduced in the system, in order to avoid thermal shocks. Furthermore, it could be necessary for thawing frozen salt following a severe failure in the salt circulation equipment.

Three main possibilities can be considered [38]. The first one is an impedance system, which utilizes an electric current passing directly through the heat collection element. This method has been successfully used in pipe heating systems in the last 30 years and it represents a mature, proven and reliable possibility. Additionally, a 5.4 kW_e impedance heating system has been tested with success on a 16-meters section of nitrate salt piping at the Sandia National Laboratories. The main advantages related to the impedance preheating are uniform heating around the pipe circumference, possibility to achieve power densities up to 350 W/m, with consequent short preheat time, and the absence of heating element inside the heat collection

element, which does not alter both flow characteristics. No penetrations through the wall are required, minimizing the risk of leakages. The main problems are related to the low electric resistance of the stainless steel, which requires high currents to obtain considerable power levels. This aspect results in large transformers, cables and switchgear. In the field piping, the impedance heating seems to be unpractical, due to thicker wall and mass per meter. The second option is represented by a resistance heating system, which uses a resistance heating cable placed inside the receiver tube. The cable consists of an Inconel tube with a diameter of 9.5 mm, two Nichrome heating wires inside the tube and mineral insulation. This method has been utilized in the 10 MW_e Solar Two solar tower project. Compared to the impedance system, the heating is less uniform, since it depends on conduction and radiation. Furthermore, power densities cannot overcome 165 W/m, to prevent the corrosion of the Inconel tube. The third possibility has been presented in the section 2.5.1.

For the demonstration loop under study, impedance heating is suggested for the receiver tubes, while the electric resistance system is proposed for the piping. In this way, uniform heating is ensured when possible and the time required is reduced to a minimum. The pre-heating with HTF has been discarded, since not tested yet.

If no daily draining is considered during normal operation, Kearney et al. [38] foresees around 15 fills of the solar field during the lifetime of the plant, since they will be related only to un-forecasted issues. For this reason, the capital investment in a permanent transformer and associated supply wiring are not justified and the use of a portable engine-generators and transformers is suggested. A 300-kW engine generator would be started on a maintenance truck and, once all the piping will have reached the necessary temperatures, the isolation valves will be opened and the salt would flow in the loop. The procedure will be repeated for each assembly [38].

2.6. Yearly results

The presented methodology has been adapted for the sized system, in order to simulate the behavior of the plant during one year of operation, with a time step of one hour. The simulation has been run in Matlab and the main goals are the sizing of the thermal energy storage, the evaluation of the best mass flow during night operation, the estimation of the parasitic consumption and the potential production of steam.

2.6.1. Weather data utilized

The definition of the Typical Meteorological Year (TMY) is the first essential step for the creation of a robust model. The weather data utilized have been taken from [69], which reported hourly values for different years. The weather station considered is located in Pretoria and it presents continuous data gathering with no long interruptions for 2015 and 2016. Consequently, the values used are the average of these two years. In the case of lack of data in a day, the average of the values characterizing the following and the previous day have been used. The 29th of February has been neglected. The accuracy of the values cannot be considered high enough for a techno-economic study, but they have been considered a good starting point for an initial evaluation.

2.6.2. Anti-freezing results and night operation

The protection strategy adopted to avoid freezing of the molten salt is the re-circulation of the heat transfer fluid through the cold storage tank. The temperature limit for the salt in the loop is lower than the one inside the storage tank, where the presence of cold spots is of primary concern.

The analysis is divided into two distinct parts:

1. Initially, the simulation is run for different storage sizes, utilizing the nominal mass flow during night operation. The minimum storage volume needed is then found.
2. Since the utilization of the nominal mass flow during night operation would increase the pressure losses, different mass flows are tested for the selected storage system. The optimal mass flow would ensure freeze-protection with minimum pressure losses.

In Figure 2.12, the minimum temperatures for the cold storage tank and the solar field outlet are reported for different storage sizes. The trends are compared to different limits: the crystallization temperature, especially important for the storage tank, the melting temperature, which should be carefully avoided in any cases, and the reference temperature reported by [90]. It is important to underline that, during normal operation, temperatures below the limit set by [90] have been reached in the Archimede plant, without any freezing issues. Therefore, this temperature is reported only for the sake of comparison. A storage size of 3 hours (6 MWh_{th}) seems to be enough to avoid solidification of the heat transfer fluid during an entire year of operation. Both cold tank and solar field outlet temperatures are always above the crystallization point, ensuring the presence of a single-phase. The choice of the storage size if further justified when Figure 2.13 and Figure 2.14 are analyzed. They report the temperature distributions for hours of storage ranging from 2 to 6 hours. The y-axis states the number of hours in the year during which the temperature is lower than the one reported in the x-axis.

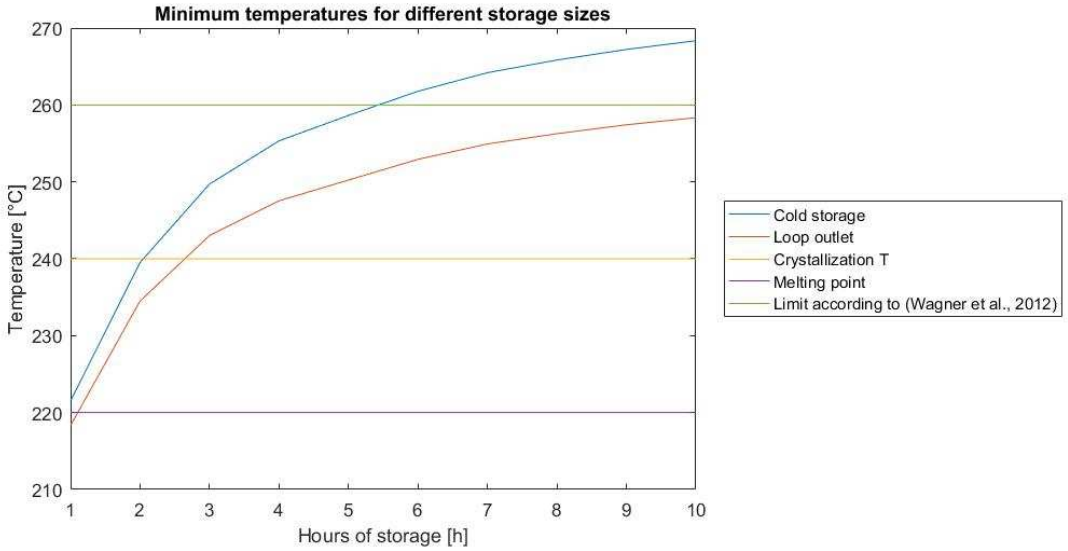

Figure 2.12: Minimum cold storage tank and solar field outlet temperatures for different storage sizes

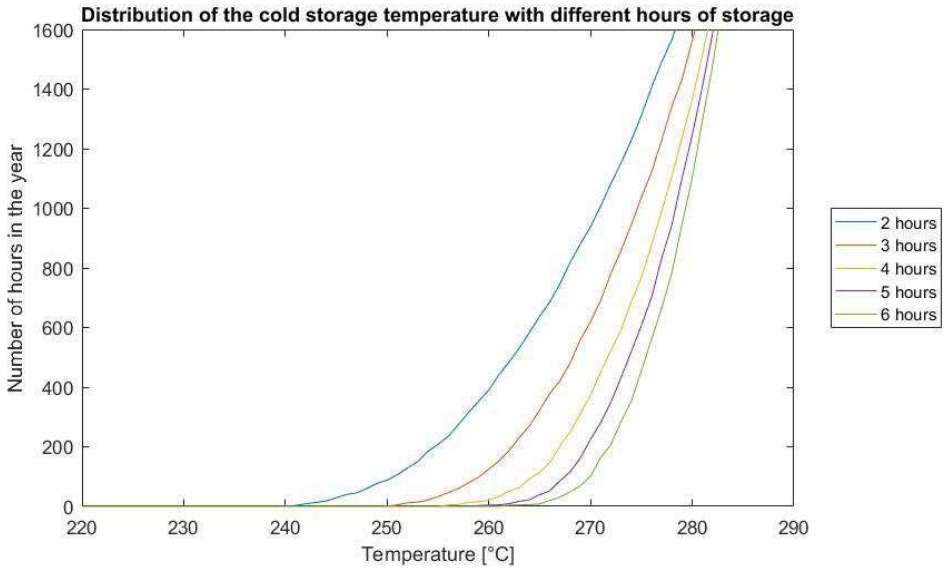

Figure 2.13: Distribution of the cold storage temperature for different storage sizes

The temperature of the cold storage is always above 250 °C and below 260 °C for less than 200 hours per year. The HTF at the outlet of the solar field presents slightly lower temperatures, due to higher losses in the loop. However, the temperature of the molten salt is below 260 °C for not more than 500 hours. It is essential to highlight that, in this scenario, no external auxiliary energy is needed. Additionally, the hot tank is assumed to be empty at the end of each day. This places the analysis on the safe side, since part of the energy stored in the hot tank could be used [54]. Furthermore, immersed heaters are usually included in the design of the storage system to protect the tanks from possible cold spots at the wall boundaries.

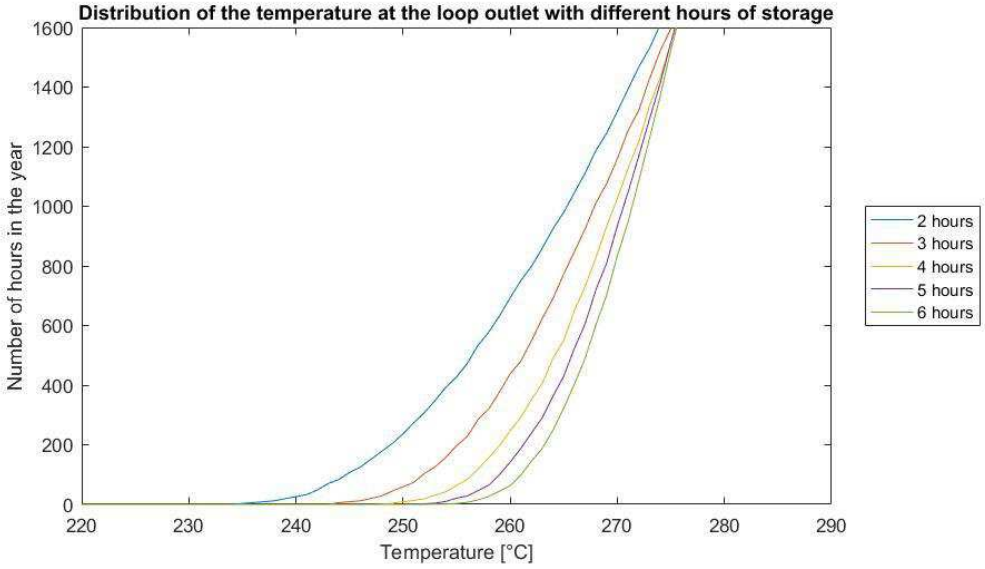

Figure 2.14: Distribution of the solar field outlet temperature for different storage sizes

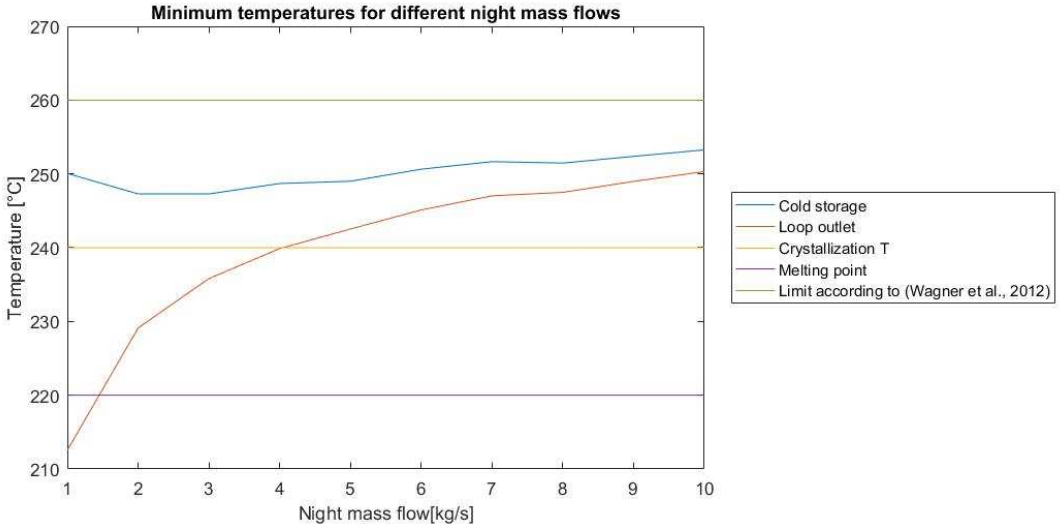

Figure 2.15: Minimum cold storage and solar field outlet temperatures for night mass flows

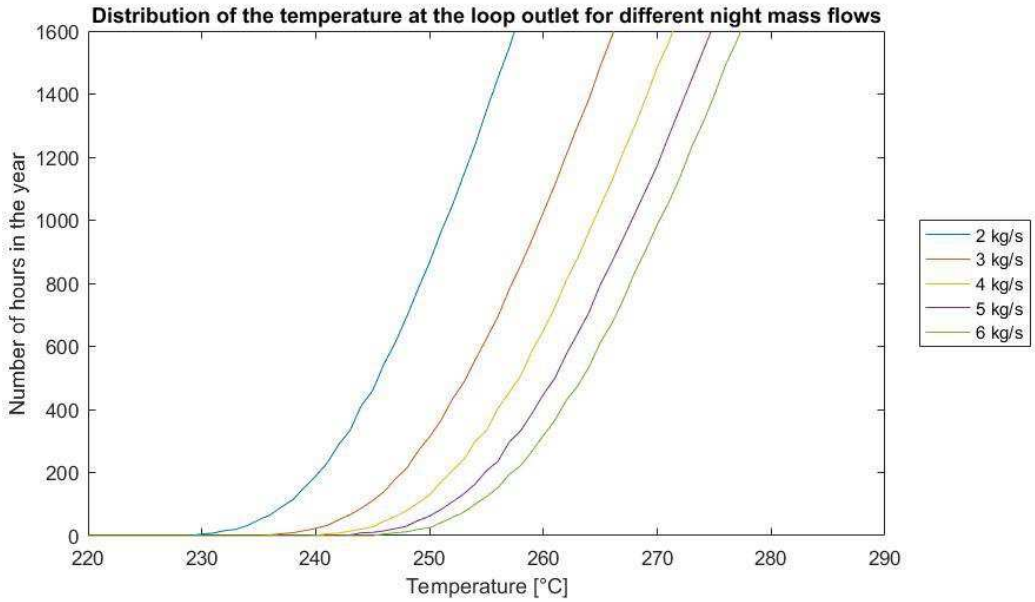

Figure 2.16: Distribution of the solar field outlet temperature for different night mass flows

The mass flow utilized in Figure 2.12 is the nominal one (5 kg/s). Higher mass flows reduce the losses in the solar field and have a small influence on the temperature of the cold tank, which is not reported for this reason. If 4 kg/s is used, the HTF is still above the crystallization temperature (see Figure 2.15). The pressure losses are reduce compared to the previous case, due to lower velocity in the solar field piping. Consequently, 4 kg/s can be chosen for night operation.

Taking into account the procedure presented in the section 2.2.9, the main characteristics of the storage system are shown in Table 2.7. The molten salt inventory includes the usable fluid, the amount of salt always stored in the tanks and the HTF in the solar field.

ETSEIB

Table 2.7: Sizing of the storage system

Parameter	Value
Hours of storage	3
Cold/hot tank nominal temperature	290/550 °C
Total volume (per tank)	36 m^3
Diameter/height	3.6/3.6 m
Molten salt inventory	66 tons

The drainage tank should be able to collect the HTF contained in the solar field. A 2.8 m^3 tank can be used, with a 10 % margin always ensured to avoid the container to be completely full.

2.6.3. Expected operation of the plant

The dynamic behavior of the plat relies on its ability to adapt the mass flow in the solar field to meet the required outlet temperature. In order to highlight this capability, the operation of the plant during a typical sunny day will be presented. After having analyzed the weather data, the 21st of January 2016 has been chosen. The results are reported from the 22:00 of the day before, in order to show the behavior during night operation. A time step equal to one minute has been considered, to increase the accuracy. The weather data have been taken from [69].

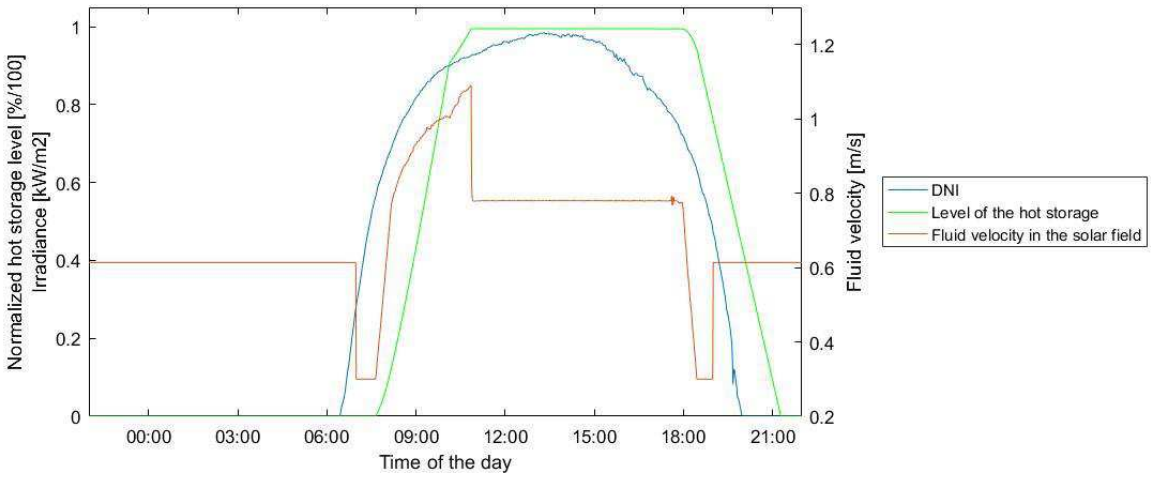

Figure 2.17: DNI, inlet fluid velocity and level of the hot storage tank during a typical sunny day

The main parameters to be analyzed are the inlet velocity of the HTF in the solar field and the loop outlet temperature. In Figure 2.17, the fluid velocity is reported with the DNI and the level of the hot storage tank. During the night, the velocity corresponds to a mass flow of 4 kg/s. When the first solar radiation starts heating the solar field, the variable-speed pump decreases the velocity to its minimum value, increasing the outlet temperature of the HTF. With increasing

DNI, the mass flow is regulated accordingly. Once the level of the hot storage tank has reached its maximum, the steam generator starts producing and the maximum amount of salt that could enter the storage system is the nominal flow, as represented by the horizontal orange line in the middle of the day. Defocusing is applied to maintain the outlet temperature within reasonable limits. The behavior of the plant during sunset is specular to the one during sunrise.

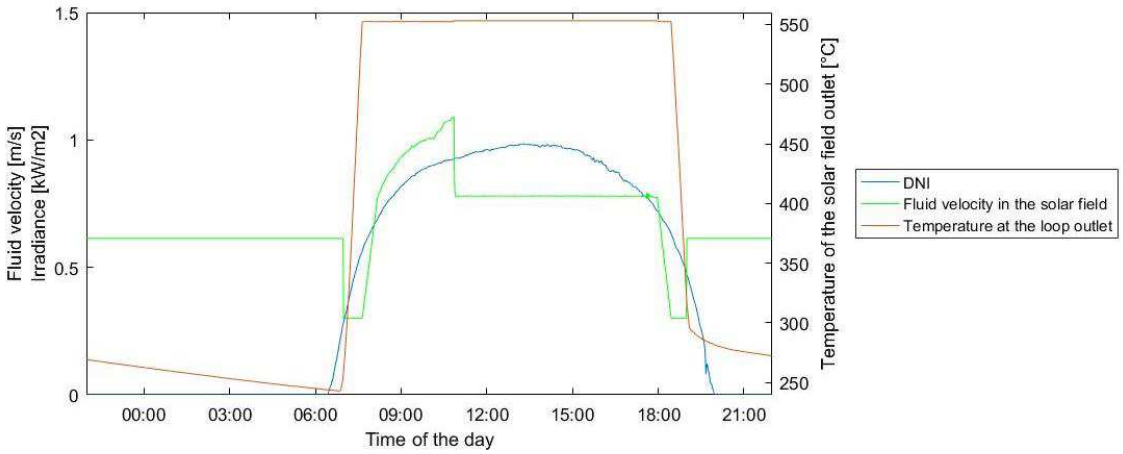

Figure 2.18: DNI, inlet fluid velocity and outlet loop temperature during a typical sunny day

The ability of the system to maintain high outlet temperatures is shown in Figure 2.18, where their trend can be compared with the one of the fluid velocity. It is also clear how, at the end of the day, switching to freeze-protection mode substantially reduces the temperature decrease.

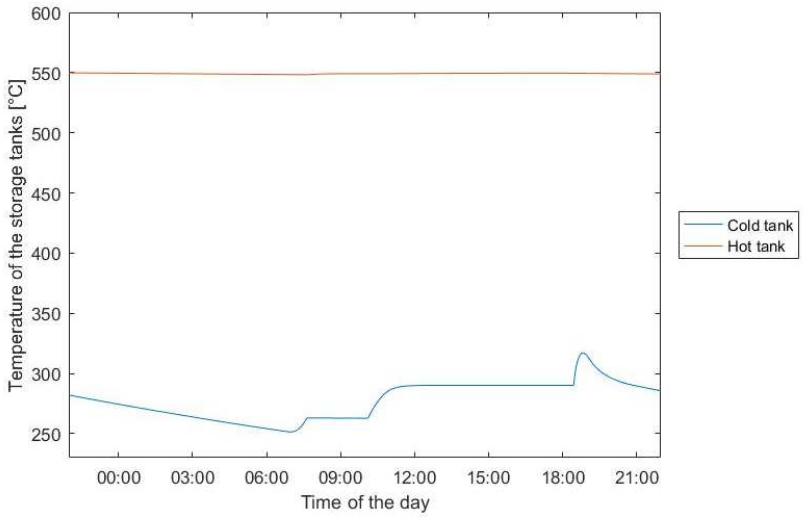

Figure 2.19: Temperature of the storage tanks during a typical sunny day

In Figure 2.19, it is possible to observe the trend of the temperature of the storage tanks. Due to limited losses, the temperature of the hot tank is nearly constant throughout the day. On the other end, the one of the cold tank initially decreases during the night. In the morning, before reaching nominal conditions, the re-circulated HTF increases the temperature of the storage. When the plant operates normally, the insulation can maintain the stored energy effectively.

ETSEIB

Finally, the temperatures of the cold storage tank and the loop outlet can be compared, for the night preceding the chosen day (Figure 2.20). The simulation is started with full cold tank at nominal temperature (290 °C). The recirculation of the fluid slowly consumes the energy stored in the cold tank. Consequently, the inlet temperature decreases. However, temperatures above safe limits are maintained till the morning, with no use of auxiliary energy.

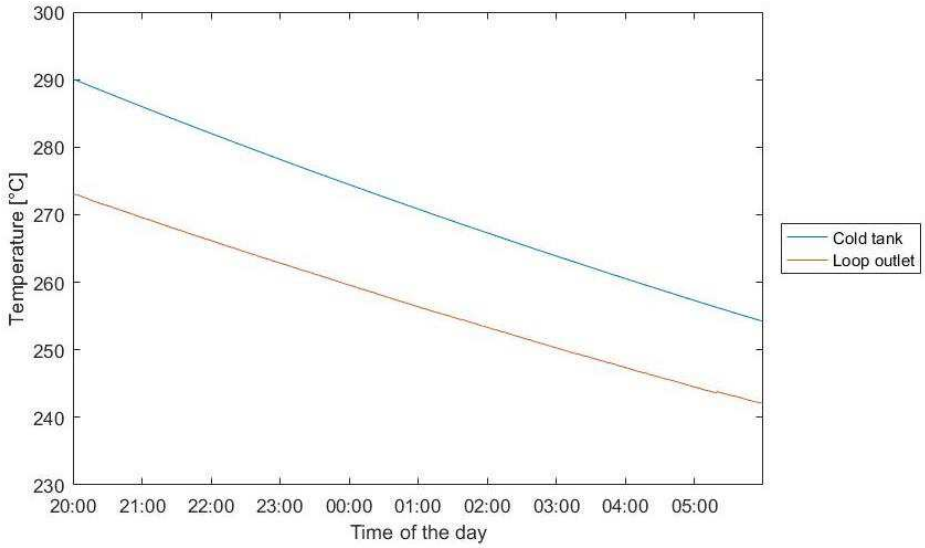

Figure 2.20: Temperature of the loop outlet and the cold storage tank for the day under study

2.6.4. Plant performance and parasitic consumption

The results of the annual simulation are not only useful for the evaluation of the required storage size and night mass flows, but also to estimate the equivalent number of hours of operation at full load and the parasite consumption. As previously stated, the strategy of the plant is very easy: the hot storage tank is initially fully charged, and then discharged to produce steam. During real operation, the strategy could be adapted to allow the required testing.

The designed plant will be able to operate around 2304 hours per year (25 % of the time) at rated power, producing 4.6 GWh_{th} of high-pressure live steam. It means that, on average, there will be six hours per day to test the steam generation. This result seems to be reasonable and satisfactory for a test facility. The temperature of the molten salt at the solar field outlet will be 3084 hours higher than 500 °C, 3644 hours above 400 °C and 4921 hours over 300 °C. As explained in the section 2.6.2, the fluid will always be above 240 °C.

The parasitic losses have been calculated as reported in section 2.2. They amount to 78.5 MWh, and the single contributions are shown in Table 2.8. It is important to underline that the energy required at the start-up and the pressure losses in the steam -loop have been neglected and to observe that, since the plant will mostly operate at nominal conditions, the consumption of the electrical resistance is limited. The fan consumption for the air-cooled condenser is based on a nominal thermal duty of 2 MW_{th}: since the expansion of the steam through the valve is isentropic, the condenser should reject all the produced power. The highest consumption related to this component is 5.2 kW. The nominal capacity of the circulation pumps on the steam-side are calculated to cover the highest value during the annual

simulation, 10 kW. On the salt side, the pumps will consume up to 14 kW. The maximum power delivered by the electrical resistance is 21.5 kW. In order to have a term of comparison for the obtained parasitic losses, the concept of "equivalent production" should be introduced. It means that the nominal thermal capacity of the plant (2 MW_{th}) and the annual thermal energy produced (4.6 GW_{th}) can be converted in equivalent electricity, utilizing an efficiency of 40 % [38]. In other word, the equivalent production is the amount of electricity that the designed plant would produce if equipped with a turbine and a generator. An equivalent plant operating with a turbine would produce 1843 MWh. Consequently, the parasitic losses would be around 4.2 % of the electricity produced, which represent a good standard value.

Table 2.8: Parasitic losses during one year of operation

	Contributions	Electricity consumed
Steam-side	Fan consumption	11584 kWh/year
	Pump 1	22889 kWh/year
	Pump 2	22643 kWh/year
	Electrical resistance	309 kWh/year
Salt-side	Pressure losses (solar field and steam generator)	3203 kWh/year

2.6.5. Environmental impact

The environmental impact of the demonstration loop is limited, since no fossil fuel are consumed in the operation. Moreover, land occupation and water consumption are contained, due to the small size of the system. These aspects are still presented in order to provide and overall and comprehensive view of the project. Furthermore, the consumption of auxiliary electricity should be considered as indirect emitter of GHG. Common solar plants are considered to be carbon-saving systems, since they usually replace highly pollutant conventional generation. However, this is not the case for the designed demo loop, since no electricity is produced and the generated steam is not utilized in any application.

Since an air-cooled condenser is utilized, the water consumption is minimized and mainly used for cleaning purposes. A more detailed description of the water needs of a MSPT plants will be highlighted the Chapter 3. For the present evaluation, a value of 250 m^3/GWh_e can be used, resulting in around 456 m^3 per annum [4]. Sau et al. [93] evaluate the land use as the total reflecting area multiplied by 3.3. For the design plant, this would result in 16672 m^2. The characteristic emission factor of the South African electricity production is equal to around 900 g/kWh_e of equivalent carbon dioxide, which is a typical for electric systems characterized by massive use of coal resources [94]. Since the electricity consumption amounts to 78.5 MWh, 70.38 tons of equivalent CO_2 are emitted annually for the operation of the plant. The environmental benefits related to a large-scale implementation will be presented in Chapter 4.

3. Economic evaluation

3.1. The cost of the demonstration loop

In the first part of the report, the design of the demonstration plant based on the MSPT technology has been outlined. The scope of the present section is to evaluate the capital and running expenditures related to the construction and operation of the plant. This study will be useful both to verify the chosen design parameters and to provide an initial estimation of the economic aspects of the proposed technology for the main stakeholder involved, Eskom. The economic analysis of a demonstration plant is not a common topic, increasing the uncertainty and the need of assumptions. However, the result can be considered at least in the order of magnitude of a real-case scenario and valuable from the perspective of a pre-feasibility study. In the next section, the methodology utilized will be presented and justified.

3.2. Methodology and assumptions

The main difficulty related to the cost evaluation of the designed demonstration plant is the lack of a steam turbine, with consequent no electricity production. In fact, most of the costs present in literature are reported per kW_e. The equivalent production described in the previous section can be utilized also in this case. A similar approach has been used to convert costs coming from different technologies. For instance, if a cost is reported for the common parabolic-trough technology, an efficiency of 37 % has been used to express it in equivalent thermal power [38]. The tower power technology has the same efficiency (40 %) and, therefore, no conversion was used.

The costs have been converted in Rand (the South African currency), with the most updated conversion factors. Since most of the equipment will be imported, the fact that components bought in distinct locations may have a different price, have been neglected [14]. The transportation cost can be compensated by the purchase of part of the equipment locally (mainly generic equipment, see Chapter 5). The investment cost can be divided into direct, including the effective acquisition of the equipment, and indirect, related to contingency, Engineering Procurement and Construction (EPC) and project and land management.

3.3. Direct cost

The direct costs (DC) related to purchase of the needed equipment will be presented separately for the solar field and the power block. Site improvement and heat transfer fluid expenditure will be also taken into account, while the cost of the land will not be considered, since the demonstration plant will be built inside one of the Eskom's properties.

3.3.1. Solar field cost

The main cost related to the solar field is the one for the solar collectors. It has not been possible to retrieve the cost of the HelioTrough collector in literature. The cost of the UltimateTrough collector has been used for the present evaluation. In fact, the two collectors present several common peculiarities. Firstly, they are both characterized by increased dimensions compared to the state-of-the-art and they are both composed by ten solar collector elements. Secondly, they aim at an overall cost reduction for the erection of the solar field of about 20 % [95]. Finally, also the Ultimate Trough can be operated with molten salts. The cost of the collector has been then set equal to 178 $/m^2, as in [96]. The same source has used for the cost related to site improvement and HTF system, which are expressed in terms of total occupied area. The first one includes the initial sediment control procedure and consequent earthwork to ensure nearly zero slope. This expenditure may be limited in this case, since the used land is already inside Eskom's properties. The HTF system considers all the auxiliary components needed for the solar field operation, such as pumps, expansion system, control and piping, insulation and fitting. The presence of redundant pumps is not explicitly considered, but the simplified control system, due to limited size of the plant, could compensate this cost. The values provided by [96] has been decreased by 10 %, since the utilization of the HelioTrough collector is expected to generate this reduction for these cost components [30].

*Table 3.1: Cost of the solar field. * indicates the components whose costs have been reduced by 10 %*

Component	Specific Cost	Cost in Euro	Cost in Rand	Reference
Collector	178 $/m^2	802,662 €	11,582,417 R	[96]
Site improvement	30 $/m^2	401,782 €*	5,797,716 R*	[96]
HTF system	70 $/m^2	937,492 €*	13,528,003 R*	[96]
Land	0	0	0	Assumed
Storage	240 R/kWh$_{th}$	7,140 €	103,023 R	[24]
Drainage tank	150 €/m^3	386 €	5,563 R	[93]
Salt	0.8 €/kg	52,566 €	758,533 R	[93]
Total solar field		2,202,027 €	31,775,254 R	

The cost of the storage system has been taken from [24] and it refers to the central tower technology, ensuring the same operating temperatures. The drainage tank is an essential component of the solar field, since it allows proper procedure during maintenance of faults. Since its duty is not to store energy, the cost is expressed in R/m^3. Finally, the cost of the heat transfer fluid has been set equal to 11.2 R/kg [93] .The currency exchange rates are 12.88 R/$ and 14.43 R/€ [97]. The results are shown in Table 3.1.

3.3.2. Power block cost

For the power block, the cost has been evaluated directly for the main components, such as heat exchangers, pumps and the air-cooled condenser. The remaining equipment, including valves, mixer, condensate tank and electrical resistance, has been estimated from average values. The procedure can be summarized as follows:

1. Calculation of the costs of heat exchangers, pumps and condenser.
2. Conversion of the nominal thermal output of the plant in equivalent electric.
3. Calculation of the average cost for a power block, based on the electric power output. It refers to a tower power plant with dry cooling [96].
4. Calculation of the cost of equivalent turbine and generator [26].
5. Calculation of the cost of the power block based on the thermal output, as difference of the equivalent electric cost and the expenditure for turbine and generator.
6. Evaluation of the overall cost of the remaining components, subtracting the values calculated at point 1 from the cost estimated at point 5.

Table 3.2: Cost of the power block

Component	Cost function	Cost in Euro	Cost in Rand	Reference
Economizer-Evaporator	28,000+54·$A_{ex,o}{}^{1.2}$ $	27,962 €	403,489 R	[98]
Superheater	28,000+54·$A_{ex,o}{}^{1.2}$ $	25,711 €	371,005 R	[98]
Pump 1	16,800·$\left(\frac{P_e}{200}\right)^{0.67}$ $	2,014 €	29,076 R	[26]
Pump 2	16,800·$\left(\frac{P_e}{200}\right)^{0.67}$ $	2,015 €	29,076 R	[26]
Condenser	597·$\dot{Q}_{rej}{}^{0.68}$ $	93,611 €	1,350,799 R	[26]
Equivalent power block	1190 $/kW$_e$	/	/	[96]
Equivalent turbine	31,093·$P_e{}^{0.41}$ $	430,110 €	6,206,480 R	[26]
Equivalent generator	2,447·$P_e{}^{0.49}$ $	57,782 €	833,804 R	[26]
Mixer, condensate tank, mixer, resistance, BOP	/	187,920 €	2,038,031 R	Assumed
Total power block		361,848 €	5,221,476 R	

The Balance Of Plant (BOP) includes all the supporting components needed for the operation

of the plant. According to [96], it is composed by water treatment system, compressed air system (for mirror cleaning), fire protection, sanitary drains and auxiliary steam.

This approach could lead to a rough estimation of the cost of secondary components. However, it is important to remind that the steam cycle has been designed based on the plant that will be constructed in Portugal. A specific layout for the present plant could be outlined. Consequently, the only components that are fundamental are the ones whose cost has been directly evaluated. The results of the economic analysis for the power block are reported in Table 3.2, together with the utilized cost functions and sources. P_e represent the electric power associated to the component, expressed in kW. The heat rejected by the air condenser is also expressed in kW, while the surface of the heat exchangers is reported in m^2.

The total direct costs are equal to 36,996,730 R (2,563,875 €).

3.3.3. Indirect costs

The indirect costs (IC) are not directly related to the construction or operation of the plant, but they are necessary during the preliminary phase of the project. Contingency addresses unforeseen elements of cost and it is estimated as 10 % of the total direct costs. The Engineering, Procurement and Construction (EPC) is an important part of the indirect expenditure, being 15 % of the DC. The construction costs take also into account insurance expenditure, which are essential for high technological-risk project. Finally, all the other IC, such as project and land management, are calculated as the 3.5 % of the total direct cost [96].

The total indirect cost amount to 10,544,068 R (730,705 €).

3.3.4. Total investment cost

The total investment cost of the plant is 47,540,797 R (3,294,580 €). Considering the equivalent electric output, its specific cost is 59,426 R/kW_e, or rather 4117 €/kW_e. This value lies close to the lower limit of the range outlined in section 1.2.6. This can be due to various reasons:

- The plant under study does not present turbine and generator. If these components are considered, the specific cost rises to 4728 \$/kW_e.
- The use of HelioTrough collectors reduces the cost related to the solar field.
- The steam cycle is simplified compared to a common CSP plant.
- The size of the storage system is small compared to large base-load applications.
- No land cost has been considered.

It is important to underline that no direct cost is related to the freeze-protection strategy.

3.3.5. Running costs

An annual expenditure is related to the operation of the plant and it includes operation and maintenance (O&M). In the present evaluation, fixed and variable O&M costs will be


considered:

- Fixed O&M: it includes cost for the administration of the plant. The labor cost represents the main contribution. Even if the average South African wages are usually lower than in Europe or in the US, EY & enolcon gmbh [10] underline how the workforce is mainly low-skilled and it requires more time to accomplish the same task. For this reason, the overall cost is similar. The value provided by [99] can be then used. The annual fixed O&M expenditure is 333.6 R/kW_e.
- Variable O&M: It is mainly composed by maintenance and repair, water utilization and auxiliary electricity consumption. The first component is the most difficult to be analyzed, since the utilized technology is innovative and can results in enhanced maintenance requirements. Turchi [99] reports a value of 8.7 \$/MWh_e (111.6 R/MWh_e) for conventional PT plants. To consider additional expenditure, the value has been increased by 10 %. The water cost can be estimated as 10 R/m^3 [100]. Since Eskom is addressed for the current project, the cost of electricity is the production cost for the electric utility. According to [101], it is equal to 0.61 R/kWh.

The various components of the O&M cost are reported in Table 16.

Table 3.3: O&M expenditure

Cost component	Cost [R]	Cost [€]
Fixed O&M	266,880 R/year	18,495 €/year
Maintenance and repair	223,679 R/year	15,501 €/year
Water cost	4,050 R/year	281 €/year
Electricity cost	47,885 R/year	3,318 €/year
Total	542,543 R/year	37,598 €/year

The total expenditure for O&M is 543,728 R/year (37,680 €/year), around 1.1 % of the total investment cost. This value is coherent with the study performed by [99], but lower than the one proposed by [93], which considers the use of molten salt specifically and obtains a value of 2 %. This can be due to the low cost of the auxiliary electricity utilized by the plant. Annual costs between 1% and 2% can be expected.

The LCOE of the plant has not been directly calculated, since the produced steam will not be sold and loop will be build or test purposes only. Moreover, the lifetime of the plant is more difficult to assess. The cost of electricity will be reported for the upscaled system.

4. Proposed upscaling for a 100-MWe plant

The design and the simulation of the demonstration plant have shown the potential of the MSPT technology, in term of freeze-protection strategy and reliable steam production. The operation of the loop would prove this capability in a real-case scenario, underlining possible improvements and enhancing the know-how. After the completion of the test period, the plant should be upscaled and equipped with the components needed for the electricity production. It will be designed to cover the base load, demonstrating how the solar power can compete with the coal production. A brief proposal for the plant upscaling will be presented. No detailed evaluation will be performed, but the outcomes obtained from the previous evaluation will be integrated with studies found in literature. [102] is the source of reference, since it presented a study concerning the sizing of the solar field for the MSPT technology, employing the same freeze-protection strategy. Other important aspects, such as location, cooling technique and environmental impact will be presented to provide an initial input for future specific studies.

4.1. Choice of the location

For a multi-MW plant, the maximization of the electricity production should be the aim. Land availability, distance from the electricity network and water availability should be taken into consideration. The South-Wester region of Africa is considered to have one of the best direct normal irradiation worldwide and five out of nine provinces of South Africa present a daily irradiation over 7 kWh/m^2 [103] [8].

The main aspects to be considered for the choice of the location are [103]:

- Annual direct normal irradiation.
- Distance from the transmission grid. The generated power should be evacuated at high voltage and the distance from the grid should be kept to a minimum, in order to limit the need of infrastructure upgrade and consequent high capital costs.
- Distance from load centers and accessibility, essential to facilitate the delivery of components.
- Slope of the ground: it should be lower than 7 % for south-facing plants, but some studies limit it to 1 % [21].
- Land availability and property.
- Water availability. Dry cooling will be proposed, entailing a limited need of water. However, mirror cleaning still represents an essential maintenance procedure.
- Environmental aspects, such as preservation of the most threatened vegetation.

As presented in section 1.3.2, the best site in terms of DNI is represented by the Northern Cape, especially the city of Upington. This province is also characterized by vast and sparsely populated areas. It has also the lowest population and rainfall in South Africa (100-520 mm per year) [17]. However, it might be far from transmission line, load centers and access to

water [103] [16]. Furthermore, it is essential to consider that all the already constructed CSP plants are located in the Northern Cape. Grouping would result in an under- or over- production due to influence of weather conditions and it should be avoided, if possible [12]. In Figure 4.1, the work performed by [103] is presented. It considers all the overmentioned aspects and it outlines the most suitable locations. For the upscale plant, the area between the Northern and Eastern Cape is proposed, in order to intensify the power production in the central area of the country. The site is characterized by a DNI well-above the 2 000-kWh/m^2/year threshold, it is close to the HV transmission lines and not far from water sources. Since Eskom is addressed for the construction of the plant, even if the capacity factor may be higher elsewhere, the stabilization of the production can have important benefits for the electric utility, such as reduced balancing expenditure and grid infrastructure improvements.

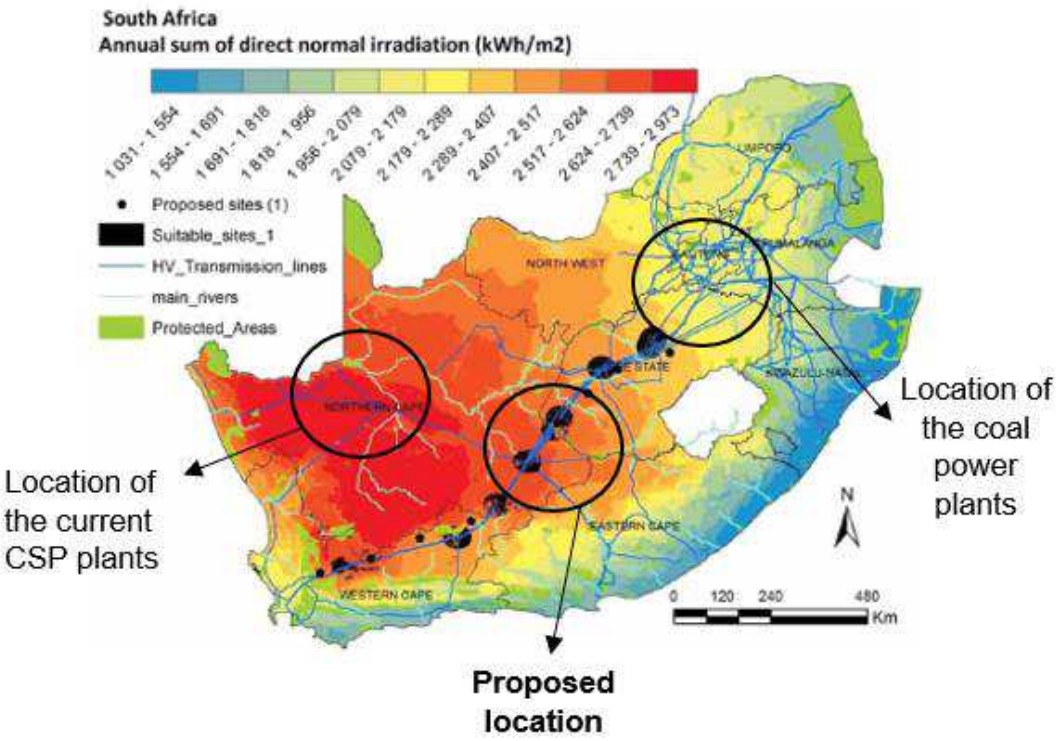

Figure 4.1: Chosen site for the plant. Adapted from [104]. Locations of the plants from [22] and [57].

4.2. Operation, size and layout of the proposed plant

The first parameter to be defined is the nominal electric output of the plant. The current maximum capacity for a CSP system in South Africa is 100 MW_e, which can be chosen as initial reference value [22].

A CSP power plant can operate in two different operation modes, covering either the base- or the peak-demand. In the first case, the system would produce at one system output level all year. It would enhance the flexibility of the production and it would compete with the coal production, but with reduced risks associated with fuel cost. In the second case, the CSP would

avoid expensive pollutant generation from OCGT [12]. In the present case, the first option is chosen, as described in section 1.3.3. This choice can be justified by the fact that, even if very expensive, the oil turbines operate for a very limited number of hours per year, providing a small contribution for the electricity production (see Figure 1.6). Moreover, the challenging GHG reduction targets set by the South African government could be met only if the dependency from the coal resource is substantially reduced.

By oversizing the solar field and pulling the excess heat to thermal storage component, turbine can operate at fairly constant output. The solar multiple (SM) is defined as the number of time the solar field is oversized, compared to the nominal thermal duty of the steam generator [5]. It means that, generally, the thermal output of the field is higher than the power required by the power block, in order to increase the number of operating hours during sub-optimal radiation levels. The size of the plant in terms of SM and hours of storage is usually a result of detailed techno-economic optimization, which is out of the scope of the present study. Tolksdorf & Dinter [102] studied the performance of a 100-MWe MSPT base-load power plant located in Upington, Northern Cape. The main goal was the sizing of the system to minimize the LCOE. A SM of 3, with a TES of 15 hours was found to be the optimal design point. The number of annual equivalent working hours was not explicitly reported but, considering the layout and the solar resource, capacity factor of at least 75 % (657 GWh) can be expected [104]. The resulting electricity cost of 11.1 c$/kWh (9.9 c€/kWh, 1.43 R/kWh). The radiation of the location studied in that report is characterized by a DNI about 7 % higher. Consequently, the LCOE can be 7 % lower than for the upscaled plant of the current analysis [1]. Further optimization might reduce this difference.

In [102], the design irradiation is equal to 900 W/m^2, with incident angle set equal to zero. In order to ensure consistency in the analysis, the design point of a single loop has been calculated with a similar procedure as presented in section 2.4, but with these new values. A nominal mass flow of 7 kg/s per loop is obtained, for a total of 2.8 MW_{th} as nominal thermal output of each loop, consisting of 4 HelioTrough solar collectors and utilizing 290 °C and 550 °C as nominal inlet and outlet fluid temperatures, respectively. Considering an average power block efficiency of 40 %, the thermal duty of the boiler would be 250 MW_{th}. It means that, under nominal conditions, roughly 90 loops would be required. If a SM of 3 is applied, 270 loops are obtained, for a total of $1.3 \cdot 10^6$ m^2 of reflecting surface. In [102], the Ultimate Trough collector is used. Since it is characterized by a higher surface per SCA, it presents 192 loops. However, the resulting overall mirror area is similar ($1.4 \cdot 10^6$ m^2).

As for the demonstration plant, a N-S orientation is the most suitable, since it ensures the maximization of the energy gains throughout the year. The way the different rows are connected is very important to control pressure drops. Moreover, the hot outlet piping should be shorter that the inlet, in order to minimize the thermal losses [28]. In large power plants, the center-feed configuration is used, with the power block located at the center of the solar field. This configuration keeps the length of the piping to a minimum, with no pipe running the length of the collector row. Easier access to the loop for routine maintenance is an additional benefit [28]. Considering this configuration, two different sub-layouts can be chosen [73]:

- In the “H” layout, the solar field is divided into four sections. The headers with the cold and hot fluid run in the E-W direction.


- In the “I” layout, the field is divide into two header-pair sections.

Alternatives, such as 1/2 H and 3/2 H configurations can be considered. All the possibilities are shown in Figure 4.2.

When HelioTrough collectors are utilized, Riffelmann et al. [30] suggests the utilization of the H-design for a 175 MW_e plant. Due to the smaller size of the proposed system, the I-configuration could be the optimal one. Furthermore, it would facilitate the drainage process. Finally, the LCOE calculated by [102] is based on this configuration, which is therefore proposed for the upscaled plant.

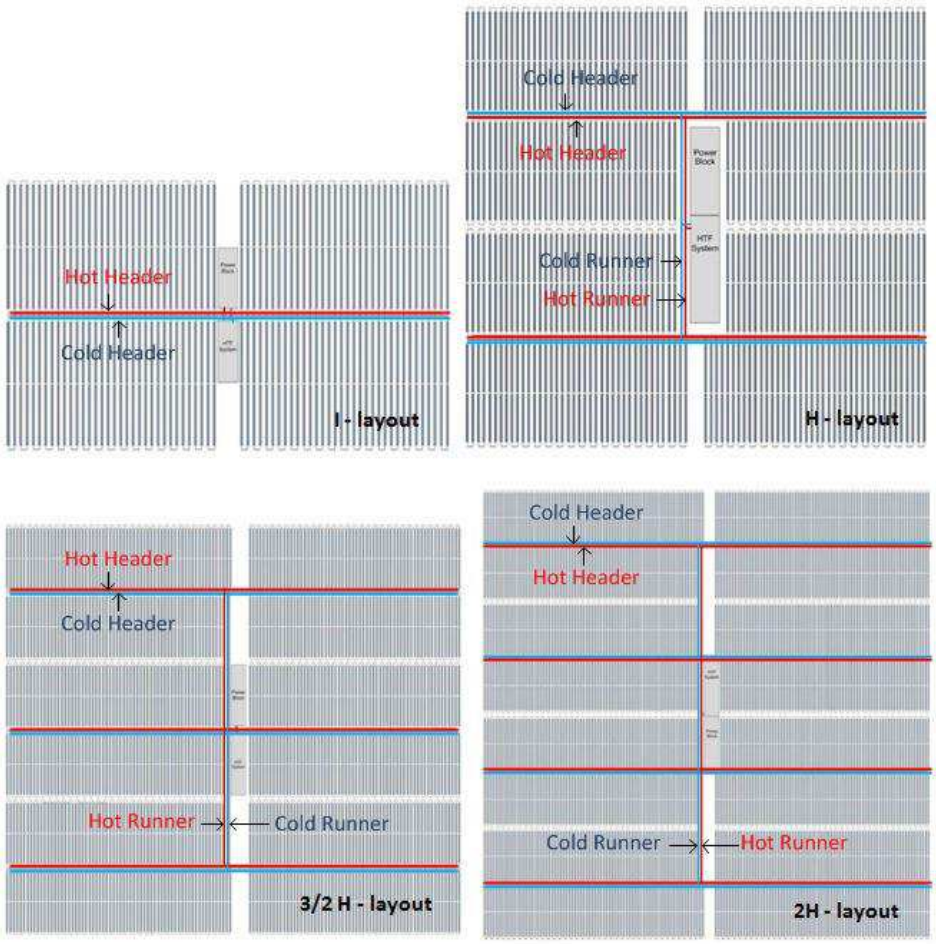

Figure 4.2: Possible solar field layouts [105]

4.3. Check freeze-protection strategy

The most innovative aspect of the proposed demonstration plant is the utilization is the freeze-protection strategy making use of the energy stored in the cold TES tank, with no further utilization of auxiliary electricity (see sections 2.5.1 and 2.6.2). The evaluation of the storage size and the night salt mass flow have been determined based on the allowed temperature

limits. On the contrary, the size of the upscaled plant presented in the previous section is based on an economic approach. Thus, the effectiveness of the strategy should be tested in this case. The cooling of the HTF in the loops is the same as in the designed plant, since each loop operates autonomously. The 6-MWh storage of the demonstration loop can provide freeze-protection for a mass flow of 4 kg/s. The minimum temperature reached by the storage is around 250 °C. Considering an average specific heat capacity of the salt equal to 1 500 J/kgK and the mass stored in the tank, it results in energy losses equal to 0.9 MWh_{th} (15 %). In the upscaled plant, the total mass flow entering the storage system during night operation would be 1 080 kg/s (4 kg/s multiplied the number of loops). A 15-h storage for a 100-MW_e plant equals 3 750 MWh_{th}. In this case, the ratio between amount of salt that is cooled in the solar field and the one stored in the cold tank, which is only subjected to moderate heat losses, is lower. Consequently, the upscaled plant is expected to perform better than the demonstration loop in terms of freeze-protection strategy, even if additional heat losses, due to longer piping, might arise. Due to higher inlet temperatures for the fluid during the night, lower mass flows can be considered, in order to further reduce the pressure losses.

4.4. Cooling techniques and environmental impact

The condenser is the component of the component of the power block responsible for the rejection the heat to the environment, enabling the cycle to be repeated. Different alternatives, characterized by different water and geographical requirements can be considered. Wet-cooling can be used, with water utilized for the absorption of the released heat. Either open or closed loop can be employed. In the first case, the system makes use of considerable quantities of water from rivers or other reservoirs, returning the heated water to the sources. Increased temperature of the water basin is a major environmental concern. In a closed loop, lower withdraw of water from the source is necessary, but the efficiency is 0.8-1.4 % lower. In the case of a dry-cooling system, the water needed by the power block is minimal, since it involves only the operative fluid operations. Blowdown represents the main portion of this consumption. It is the periodic removal of corrosion products and sludge, which can form over time, and it is used to control the chemical composition of water [53]. Dry cooling is more expensive to build (+2 %) and characterized by lower efficiencies in hot days than wet cooling. In fact, the condensing pressure is related to the ambient temperature, as shown in section 2.2.11. The work performed by the steam through the turbine can be therefore limited, with adverse implications on the overall system efficiency, up to 10 % in the case of North Africa [100]. Overall, the water use is reduced by 50-85 %, but the power output can decrease by 3 % [5].

Hybrid cooling combines air-cooled system with evaporating water spray on the hot surfaces of the condenser or into the hot ambient inlet air to increase the cooling rate. It is designed to reduce efficiency losses, with a trade-off regarding water usage. However, it is generally more expensive than the other two possibilities [100].

In the CSP plants, water consumption is a primary consideration [5]. In arid and desert area, water is a rare resource, which should be mainly used for agriculture. Moreover, growing population, economic development and climate change consequences, such as rising

temperatures, can further decrease water availability. Overall, the water demand constraints the large-scale development of wet-cooled CSP in these regions [100]. For wet-cooled systems, the water consumption is around 3.27 m^3/MWh, while only 0.25 m^3/MWh for dry-cooled ones, of which 0.075-0.12 m^3 are for mirror cleaning, that can significantly vary according to local ground and wind conditions [44] [103] [4]. This consumption is even lower than common wet-cooled coal-fired plants, which employ around 2 m^3 of water per MWh generated [9]. Finally, Fluri [103] underlines how a "multi-GW roll-out of CSP in South Africa will only be feasible if dry or other water-wise cooling methods are utilized". For these reasons, dry-cooling is suggested for the upscaled system, minimizing the related social and environmental impact. Treating wastewater and desalinating seawater can be viable solutions for meeting the water requirements, even for dry cooling [100].

When placed in the world's arid and semi-desert regions, land requirements would be a very small square in a very large area. The land use can be estimated as 3.3 times the total reflecting surface [93]. The upscaled plant will necessitate 4.3 km^2 and it will consume roughly 164,250 m^3 of water annually. Since a detailed design of the plant is not the scope of the analysis, an economic evaluation would be too inaccurate. In this sense, the work presented by [102], and previously described in terms of LCOE, can be used as a reference.

For the quantification of the carbon emission related to the operation of the plant, the same methodology presented in section 2.6.5 can be used. As previously stated, the expected capacity factor of the upscaled plat would be around 75%, producing 657 GWh_e per annum. The parasitic consumption can be estimated in the order of 5%, slightly higher than the demonstration plant, due to high number of loops. It is a typical value for common CSP plants, such as the Gemasolar one, in Spain [7]. Overall, a 100-MW_e CSP plant based on the MSPT technology providing base-load would avoid the emission of 561.7 kt of greenhouse gases every year. Additional emissions should be considered on a lifecycle perspective, due to manufacturing, transport and maintenance of the components. However, if a large-scale penetration of the technology is achieved, all the additional electricity consumed would come from a less-polluting energy mix. Other benefits would be related to a lower land preservation, due to less need of excavation and mining, lower land occupied by the dumps needed for the combustion products and lower emission of other harmful pollutants, such as particulate and nitrogen and sulfur oxides.

The development of a highly efficient solar-based system would be the first essential step for South Africa towards a decarbonized and sustainable energy sector.

4.5. Comparison with a state-of-the-art plant

In the previous sections, the layout of an upscaled MSPT plant has been briefly outlined. The use of molten salt as HTF introduces innovative features compared to the state-of-the-art (which is shown in Figure 1.1), which are worth to be outlined.

The thermal oils are characterized by an upper temperature limit of 400 °C. Considering an inlet temperature of 290 °C, the maximum temperature increase would be around 100 °C, 2.6 times lower than in the case employing MS. The average specific heat capacity of the oil is around 1.2 time higher than the one of the salt (2200 J/kgK, compared to 1800 J/kgK).

Considering these two aspects, thermal oils should have a mass flow that is around 2 times higher to ensure the same energy gain. This would have adverse implications regarding pressure losses and consumption of circulating pumps. As an alternative, a bigger solar field could be considered. However, it is important to consider that operation at lower temperatures entails lower heat losses and, consequently, higher thermal efficiency of the solar receivers.

In order to store the same amount of energy, a TES system for a parabolic trough plant utilizing thermal oil would be 2.6 times bigger (up to 2.75, if temperatures of the salt to 275 °C are allowed). This aspect would have an impact both on the investment cost and on the land occupation of the plant. Furthermore, the storage system would be indirect, requiring additional heat exchanger between the oil and the molten salt, used as storage medium. This would reduce the storage efficiency of the system. Since MS are usually characterized by enhanced heat transfer properties, the heat exchangers needed for the steam production would have a larger surface area for the state-of-the-art plant. More pumps would be required, due to the presence of additional fluid circuits.

On the water-side, the main difference would be the inlet temperature of the steam entering the turbine. A reduced temperature would entail lower efficiencies. Consequently, larger solar fields would be required to obtain the same electric power output.

Finally, the use of oil is related to many operational issues. The freezing problem is less severe, but it still has to be avoided during long shut-down periods. Kearney et al. [38] report the strategy employed in the SEGS plant. A gas-based auxiliary heater is utilized to maintain the fluid temperature above 150 °C. No recirculation though the cold tank may be considered and the use of the stored energy would reduce the production potential of the plant. Moreover, in the case draining was needed, the high vapor pressure of the oil would complicate the storage of the fluid. The toxicity and flammability of the thermal oils are two other important characteristics. The fire protection system would be fundamental and a fluid spillage would have serious environmental consequences.

Overall, a state-of-the-art plant would be characterized by higher capital investment and consequent higher LCOE, as reported in section 1.6.1.

5. Business potential

The CSP systems are at a transition point in their development [106]. The industry is undergoing a serious and continuous development, becoming very attractive from a business standpoint [1]. EY & enolcon gmbh [10] define it as a "young and dynamic market". Furthermore, a general increase in the electricity demand expands the potential of the CSP technology, since most of the growth is expected in the countries characterized by high solar irradiation. South Africa is well positioned to supply good and services regionally. Even if limited to the areas around the "sun belt", CSP might evolve into a real and scalable alternative to conventional power generation at competitive levels [1] [107]. It represents the only RE option able to provide both base- and peak-load, generating sustainable and dispatchable electricity, thanks to flexible power block arrangement and large thermal energy storage systems.

It is essential to underline the main socio-economic implications of a large-scale roll-out of such an innovative technology. Moreover, the choice to address Eskom for the initial construction and testing should be further justified. In this chapter, all these aspects will be analyzed, including the keys for a sustainable development of the industry in South Africa with related macroeconomic benefits.

5.1. R&D and innovation: a business opportunity for Eskom

As stated several times throughout the report, Eskom should take the lead for the required R&D and testing of the demonstration plant. The advantages related to the MSPT technology and the necessity to increase the production from flexible RES sources for the public utility have been already described.

Public support is still required to unlock CSP investment in South Africa, since alternatives are usually characterized by lower technical and economic risk [107]. This aspect is especially true for the use of molten salt as HTF, since no commercial applications are yet present. The REIPPP procurement, described in section 1.3.1, is structured as a series of independent transactions between the national Department of Energy (DoE) and various IPPs. It encourages maximum competition to provide secure RE at lowest possible price and promote local economic development. Special attention should be put on the communities living close the plants. Broad-base black economic empowerment (BBEEE) is of primary importance. The target for the local content in CSP construction is 60 %, with 40 % set as minimum threshold [108]. The REIPP is not suitable for the development of the MSPT technology for the following reasons:

- Technology development is risky and expensive. It would be difficult to get an industrial company to become and Original Equipment Manufacturer (OEM), given the massive development expenditures required [108]
- The construction of the upscaled plant may be characterized by high technological risk, which could threat private investors.

- As a state-owned regulated entity Eskom has access to a diverse set of financing resources and required political support [107]
- Eskom's PPP (public-private partnership) enables strategic sourcing tied to a selected technology.
- The REIPP seems to have a lack of ambitious targets [1].

The presence of private investors would be needed, since availability of concessional financing and public balance sheet financing is limited [108]. So far, it was not clear is either private or public sector was the best mover to foster the CSP development [1]. An effective partnership would facilitate a faster development of the technology, with a fair distribution of the associated risk. Eskom is currently developing its first CSP plant (Eskom CSP project), based on the tower power technology. It will be located in Upington and characterized by 100 MW of nominal capacity, with 500 GWh of expected production. Feasibility studies started already in the late '90s, early designs were discussed in 2003, while environmental approval was received in 2007. After being put in hold due to global recession, the project received low-cost debt lending support from International Financial Institutions (IFIs). The Government of South Africa developed the Clean Technology Fund (CTF) Investment Plan, allocating 250 million $ to the Eskom project. Private actors will not contribute to the financial requirement, which amount to around 1 billion $, but they will provide technology design and advisor services, engaging both in the construction and maintenance phases. Without the political support and concessional lending from international financial institutions, Eskom was unlikely to develop Eskom CSP [107]. The plant will be procured by a technology provider and then transferred to Eskom, with an agreement which includes specific training of the Eskom staff. The electric utility own and operates the plant post-construction, sharing the risks associated to the technology with the private partners [108]. The public-private partnership can be a win-win situations for all the actors involved: the industrial partners can have a safer investment, coping with possible failures and policy changes, while the public utility can maintain affordable electricity prices [107]. This reduced risk resulted in a larger pool of competitors in the case of the Eskom tender than for the most recent round of the REIPPPP. Outsourcing element of the project development would also mitigate high-risk events, while the continuous training would help Eskom to get the proper expertise for future projects [108]. Successful examples are represented by Morocco, which employs the PPP approach in the early-state technology and industry development, and by China, which has been able to create a globally competitive RE manufacturing sector [108].

The R&D potential related to the MSPT technology is massive and it represents an important opportunity for Eskom. In order to benefit from this research, it should focus on new area, rather than on more established ones. Furthermore, the R&D incubation by large companies may be very helpful for the fast development of the technology: Eskom can foster technological improvement and gain central position in the African industrial landscape at the same time [10]. The initial scale-down of the project can contribute to reduce uncertainties and to increase the confidence in the system, maximizing the value of the technology [109]. Eskom proved to be able to adapt its procedures to the specific of innovative technologies and it is therefore the best candidate for the initial development of the system [107].

The procurement of a frontier renewable system creates additional challenges, but also opportunities on large-scale. It is essential to achieve a critical mass, able to place the country

in a central position for the design, manufacturing and construction of the plant. The replication possibility of CSP plants in Southern African region is huge, with a potential of 40 GW in South Africa and up to 120 GW considering also Botswana and Namibia [107]. Fostering the demand with central leadership would be beneficial for the stimulation of the manufacturing sector [1]. All these aspects will be presented, considering both short- and long-term scenarios.

5.2. Innovative CSP projects: a new industrial frontier for the manufacturing sector

South Africa's manufacturing sector has become a main source of concern to policymakers. After the global recession of the period 2008-2009, other economic sectors have recovered, but the growth in manufacturing has been slower, due to lack of local good demand. It is the only sector which has continued shedding jobs since the third quarter of 2010, with a contribution of the total employment which dropped from 14 % in 2008 to 12 % in 2012. Moreover, South Africa's share of world manufactured exports dropped from 0.33 % in 1995 to 0.29 % in 2013. Main reason is the inadequate export on low- and medium-skilled goods, compared to the Asian producers [108]. Consequently, South Africa must compete in knowledge and in technology-intensive goods. However, in the recent years, the country has not properly developed its industrial sector. It has lower R&D resource allocations than all the other BRICS (Brazil, Russia, India, China, South Africa) countries, but India, and it is lagging regarding number of patents registered. Green innovation, meant as the creation and commercialization of frontier technologies, is a pillar of economic growth for these countries. Bio-fuels in Brazil and PV in China are just two of the main examples. An emerging economy can become market leader and design center of excellence in an innovative technology, if an adequate development path is outlined [108]. CSP components can be distinguished between basic (civil work, assembly, electronically equipment, power block) and specialized (solar field, glass production, mirror, support structure, receiver, HTF and storage system) [10]. The main industrial opportunities (40-50 % of the plant value) are in the design and manufacturing of key components: addressing these aspects will contribute to a substantial increase of the GDP, of which manufacturing currently accounts for 13 %. The process can be enabled by the development of own design or, as it will be shown, by initial partnership with international actors (licensing agreements or joint ventures). Precision engineering has legal protection, which can enhance the resilience of the South African industry against the lower foreign costs [108].

An effective development of the MSPT technology would make South Africa a first mover, placing the country in a position of advantage in the Southern Africa environment. In the next paragraphs, the possible industries than can be involved in the process will be reported, in order to highlight the current and future potential of local involvement.

5.3. Involvement of the local industry sector

South Africa is currently integrated into several global value chains, becoming a specialist assembly hub. The availability of local minerals and the well-developed automotive sector can

serve as a platform for developing the CSP industry [108]. Other local industrial actors can be involved for the realization of different components, as described by [10]:

- Glass manufacturing: glass is one of the most specialist logistics areas in CSP. Local glass companies produce glass for building and automotive industries. PFG Building Glass in the only local company able to manufacture low-iron float glass and silver flat mirrors. However, it does not have the ability to produce bent mirrors. The high iron content of the raw materials found in South Africa may require additional costs. For the PT plants constructed in South Africa, the production of mirrors has been outsourced. Without an international partner, two years would be required to achieve the proper expertise. A transitional phase, during which glass is supplied partly from a local and rom an international player, is therefore required. The establishment of dedicated factories can be an option only if adequate economy of scale is ensured.
- Support structure: steel can be produced locally by Arcelor-Mittal or Evraz Highveld Steel, which represent roughly 80-90 % of the local market. Since South Africa is mineral-rich, cost of steel is comparable and competitive with international suppliers. Currently, overcapacity is present, due to low demand. Steel producers can be thus successfully involved during the construction phase.
- Construction: the construction industry is well-established in South Africa. Main local companies are present, such as Muray&Roberts, Group 5, Aveng Group, Basil Read, Crowie and WBHO. CSP can be a good business opportunity for them, since it requires more civil work than other RE systems. The assembly can be easily internalized but, at least initially, it requires international supervision.
- Piping: piping systems are mainly supplied to mining, petrochemical, construction and energy sectors. Spiral welded pipes, which are needed in PT fields, are currently manufactured by local companies for transportation for water. However, the design is slightly different and the demand is already high, making difficult to create the needed incentive to shift towards the CSP applications.
- Pumps: they are mainly used in the gas and mine industries. Only one local supplier can provide pumps to handle molten salt and it is an agency of a German company.
- Tracking device: Reurech is a South African defense company, which supplies tracking devices to other industries. It did not qualify for the use in CSP so far, but it equipped some concentrated PV plants.
- Receivers: there is basically no local capability to supply high performance solar receivers, since the global market is controlled by few actors. Moreover, the production would be difficult to localize, due to intellectual property rights. This is the best example to underline how global collaborations is essential. However, the local company John Thompson has shown interest for an initial development [108].
- Molten salt: for the HTF, only logistics can be considered for local involvement, since the main suppliers are based in Chile. Use of innovative mixtures could be considered to increase the exploitation of locally available resources.
- Power block: similarities exist between the components needs in CSP power blocks and in coal-fired power plants. However, providers of turbines and boilers, such as

Hitachi, does not focus on the small capacities characterizing solar thermal power plants. For this reason, specific production should be established.

- Heat exchangers: the volume required would be too low to justify a new local production facility, but logistics and after sale support can be provided locally.

The potential to achieve high local content level, up to 60 %, is clear. An effective time-scale should be outline, in order to allocate resources and to design business strategies, both in the short- and long-term.

5.4. Value chain in the short- and long-period

International cooperation should be a first fundamental step for the development of the MSPT technology in South Africa. Strategic supplier partnerships are central to success in developing innovative industries in emerging economies [108]. International players can provide the adequate knowledge and know-how to address all the phases of the project development, from engineering to construction and operation management [10]. Moreover, banks can be initially reluctant to fund project with high financial risk, if the involved players have no track of past successful projects. Germany and USA are global technology-intensive leaders, which could be initially involved. Both the collector and the receiver proposed for the demonstration plant come from a German supplier.

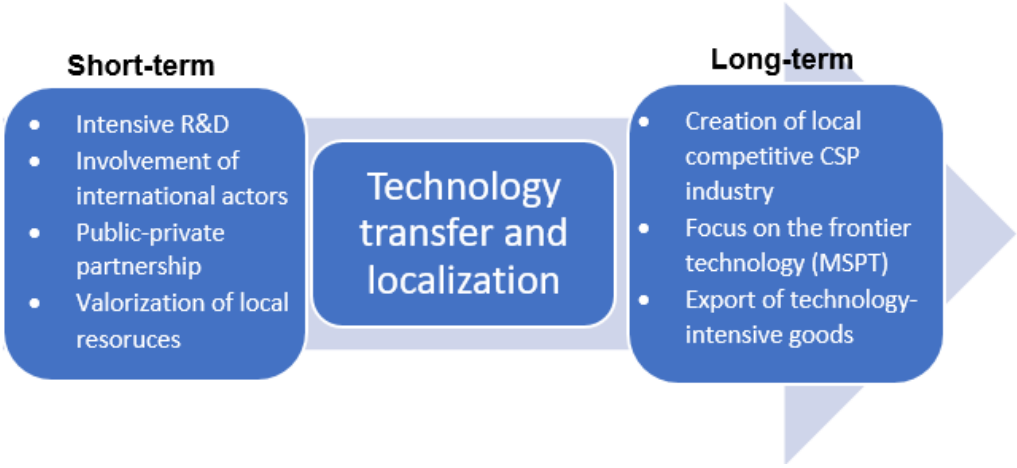

Figure 5.1: Proposed timeline forf a competitive CSP industry based on MSPT technology

This choice can be justified by the fact that German technology companies have a prominent market position at all stages of the value chain. Schott, Flabeg and Solar MIllenium are amoung the leading CSP suppliers [110]. When international partners are considered, adequate foreign exchange rate risk mitigation is essential [108]. Key components and research topics should be identified for joint national agreements, and partnerships with foreign universities and institutions can be beneficial in this sense [108]. International co-invention has been a central driver for the increasing number of registered patents in China and India [10]. After having developed technologies in partnerships with foreign actors and having learnt the

best practice, the research should immediately move towards the technology frontier [108]. High local content can be achieved by training with internationally experienced employees [10]. In the short term, focus on R&D, international partnerships and strong local integration should be the main targets [10]. In the long-run, the establishment of a competitive South African CSP industry and the achievement of local contents up to 60 % should be pursued. The best components for initial localization are the ones that are used in different CSP projects and in different industries [10]. The creation of a manufacturing cluster would ensure socio-economic benefits for a sustainable development [1]. Currently, only storage material and receiver manufacturing are completely beyond country's capabilities. However, the need of critical mass is required to justify the local production of some components, such as bent mirrors. The IDC glass facility constructed in Upington is an example of industrialization resulting from specific projects. It combines international knowledge from Rioglass and PFG to silver the mirrors locally [10]. A large-scale implementation of this model would be successful only if the IRP would include further CSP capacity in the power allocation. In fact, the PPP from Eskom can initially stimulate the demand and the needed research but, without a high number of private actors involved, a fleet procurement could result in limited industrial impact [108]. It is essential to ensure a pipeline of projects, avoiding the peak of demand usually created by the REIPPP process. The creation of skills would be easier and more effective, and industrial suppliers would be subjected to a more sustainable order [10]. The creation of a competitive local industry would be the result in the long term, with macro-economic benefits that will be highlighted afterwards. A summary of the proposed timeline is shown in Figure 5.1.

5.4.1. Strengths and weaknesses of the South African value chain

The realization of a competitive CSP industry needs to valorize the main strengths and try to cope with the main weaknesses of the local value chain. South Africa presents both a strong industrial background, which can actively contribute to the emerging technologies, and important R&D capabilities [1]. The ability to produce standardized components can make the country compete on an international level immediately, especially regarding basic products. It showed also good adaptation to the changing industrial landscape, by fostering the development of cooling systems and thermal energy storage. Mature manufacturing sectors, such as automotive and defense, have expressed interest in expanding their capabilities to the CSP. The possibility to transfer skills from international partners, combined with the local expertise in developing and building large energy projects, can be the turning key for an effective industrial development. Finally, 100 % of the O&M requirements can be handled locally [10].

The main concerns are related to the competitivity of the local labor, on the cost of local resources and on the cost of the local transport. In fact, even is labor rates are lower than in Europe of in the US, the labor time is higher, due to lower-skilled personnel. This issue can be solved by providing continuous training, as previously stated. Raw materials in South Africa may be more expensive than abroad and this aspect should be taken into consideration if high level of local content at a minimum cost are required [10]. Finally, the local transport can be higher than international shipping. It is therefore clear that the development of CSP industry should be integrated with an overall infrastructure improvement. The economic growth related

to a mass roll-out can be used to sustain the sector itself. From a policy perspective, the uncertainty regarding future CSP allocation is fundamental. A demand able to support the development of domestic manufacturing capabilities is central [1].

5.5. Macro socio-economic benefits

A competitive CSP industry would have a positive impact on the socio-economic development of the country. Job creation and GDP increase potential are the main positive outcomes under this perspective. The South African Department of Energy announced 1 800 jobs during construction and 120 jobs during the operational phase of the first three CSP plants [10]. No specific studies to estimate job creation potential for the MSPT technology were found in literature. However, full-time equivalent job ratios for the PT technology can be utilized for an initial estimation [10]. Direct job creation is expected during construction and operation of the plant, which represent the biggest job creator (even if limited in time) [108]. Indirect jobs can arise from increasing demand in the supply chain, while induced jobs, related to the effects such as consumption of good and service on working sites, should be also considered. Manufacturing would create 4 direct jobs per MW installed, while construction and assembly would contribute to 20 jobs/MW. O&M can generate 0.8 direct jobs per MW. Learning curve could rapidly allow the South African companies to increase the ability to capture the benefits from the last component. Each direct job would create 0.9 indirect jobs and 0.25 induced jobs. On the other hand, each indirect job would create 0.25 induced jobs. The reported values refer to the expected 25-years lifetime of the project [10]. According to the estimation of [108], 6 030 full-time jobs can be created for a 200 MW plant, while 13 380 jobs can be generated if 300 MW are constructed locally and components for the construction of a 300-MW plant in the neighbor countries are exported.

Direct economic effects are related to the construction of the plant, while indirect effects are from demand in the supply chain. Induced effects can arise for higher consumption due to increased wealth. All these aspects can contribute to a growth of the GDP. Under the export scenario previously described, the Gross Domestic Product would grow by 100 billion R (2.5 %) [108].

The creation of CSP industry based on a frontier technology would be beneficial under all the aspects for South Africa. The current study demonstrated that it would place the country in a favorable position to be globally competitive and leader in the exports for specific systems. Furthermore, job creation and economic growth are the main local benefits. The importance the proposed project goes beyond the merely energy aspects. The CSP technology is likely to be the only technology able to effectively involve the local population, in a process of innovation towards a more sustainable future.

6. Summary, conclusions and future research

In the present work, the design CSP demo Molten Salt Parabolic Trough (MSPT) plant has been proposed. The system couples the most mature, proven and bankable CSP technology with the use of an innovative HTF. State-of-the-art parabolic trough collectors usually utilize thermal oils, whose upper operating temperature is limited by chemical stability reasons. The use of MS would also facilitate the integration of large thermal energy storage systems, able to ensure continuous production, also during low-irradiation periods. South Africa represents an almost unique place in the world regarding direct normal irradiation. Currently, most of the electricity production is covered by polluting and less flexible coal power plants. In order to achieve the ambitious emission reduction targets, the country should get rid of the conventional production technology. CSP represents the only sustainable option, providing firm and dispatchable energy. Furthermore, a large-scale implementation of the technology would have substantial benefits for the overall electric grid: the flexibility

Due to technological risk and need of R&D, the national public utility, Eskom, has been addressed for the realization of the plant. It could be constructed within one of its properties, which are characterized by land and workforce availability. Most of Eskom's plants are around Johannesburg and Pretoria has been chosen as reference, due to weather data availability.

The most innovative aspect of the technology is the use of molten salt as HTF. Its usage would increase the temperature of the produced steam, with consequent enhancement of the power block efficiency. No additional heat exchanger would be required, reducing the capital investment. Moreover, MS are neither toxic nor flammable. The higher heat capacity and the higher operating temperature (up to 600 °C) would increase the storage capability. The most important consequence is the reduction of the LCOE, down to 11 c$/kWh. The main challenge is related to the high melting point of the salt, which lies in the range 120-220 °C, depending on the mixture. An appropriate freeze-protection strategy should be outlined. Solar Salt has been designated as the most suitable salt, due to past usage in the power tower technology.

The proposed demonstration plant will be composed by a single loop. HelioTrough collectors, equipped with Rioglass solar receiver, have been selected, due to higher performance compared to past designs and availability of data. Four collectors will be used in each loop, for a total of 5177 m^2 of reflecting surface. The sizing and the performance of the plant has been based on an annual simulation, utilizing one hour as time step. The model utilized a zero-dimensional stead-state approach. A 70-mm steel pipe, with a wall thickness of 2 mm and insulation thickness of 15 cm has been selected for the solar field piping: this arrangement can provide mechanical strength and reduce thermal losses. The storage system will operate between 290 °C and 550 °C. No electricity will be produced, but the steam will be cooled down by an air condenser. The steam generation system and the steam cycle layout has been designed like the demonstration loop that will be constructed in Évora, Portugal. Two shell-and-tube heat exchangers will be utilized to generate high-pressure live steam. They are characterized by high overall heat transfer coefficient, while the pressure losses are maintained to a minimum. The boiler will operate under sliding pressure mode to ensure fast ramping. It will adapt the evaporation pressure according to the load fraction, from 33% to 120%. With 800 W/m^2 and cosine losses equal to 0.9 as design point, a nominal mass flow of

5 kg/s is obtained. The nominal thermal output of the solar loop will be 2 MW_{th}, which has been set as thermal duty of the steam generator. The pressure losses in the solar field are 7 bar. The nominal evaporation pressure is 100 bar, since it can ensure an appropriate pinch point.

The recirculation of the HTF through the cold tank during night operation has been chosen as the best anti-freeze protection strategy, since it does not require auxiliary electricity or specific components. The size of the storage system has been set as the minimum able to maintain the salt temperature always above reasonable limits. With a 3-h storage and a night mass flow of 4 kg/s, temperatures always over the crystallization point can be achieved. The temperatures at the loop outlet are slightly lower, but the fluid can rely on its kinetic energy. In the case of failure of the pumps, the HTF can be drained with the use of an air-compressor or simply by gravity. Vent and draining valves should be provided to the loop. The refill of the plant should be anticipated by an initial preheating, which relies on inductive heating for the receiver and on resistance heating for the solar field piping.

The simulation of the plant proved its ability to adapt the salt mass flow according to the solar condition to ensure high outlet temperatures. The plant will operate for around 2 300 equivalent hours, producing 4.6 GWh_{th} of steam. The parasitic electric consumption is 78.5 MWh. The demonstration plant will consume 456 m^3 of water and it will occupy 16 672 m^2, being responsible of 70.38 tons of equivalent CO_2 emitted per year, due to use of auxiliary electricity.

The costs related to the construction and operation of the demonstration loop have been estimated. The first ones include both direct (purchase of the equipment) and indirect (mainly contingency and project management) expenditures and they amount to 47,540,797 R (3,294,580 €). O&M consider fixed, such as labor, and variable, mainly for electricity and water usage, costs. Running costs have been estimated as 542,543 R (37,598 €) per year (around 1.1% of the initial investment).

An upscaling of the designed demonstration loop up to 100 MW_e has been proposed for future realization. It will be located in the central area of the country, since it is characterized by high solar radiation, water availability and grid accessibility. The plant will provide base-load, competing with the coal production. A solar multiple of 3 and a 15-h storage system are proposed, resulting in a capacity factor of around 75%. 270 loops will be arranged in a I-layout, which would facilitate the drainage process when needed. The nominal mass flow would be 7 kg/s. LCOE has low as 1.43 R/kWh (11.2 $/kWh) can be obtained with this design. The freeze protection strategy previously outlined has been successfully tested on the upscaled plant. The system will be equipped with an air condenser to minimize the water usage. It will need 4.2 km^2, consume 164 250 m^3 of water annually and avoid 561.7 kt of carbon emission per year.

The development of a frontier technology would create important business opportunities for Eskom. It would place the company in a central industrial position of the Southern African region, with the possibility to become an exporter of technology-intensive goods. Public-private partnership would be beneficial for risk sharing and knowledge transfer. In the long-term, all the industrial actors should be involved in the realization of a competitive sector. South Africa could create an independent CSP industry based on the MSPT technology, with important benefits for job creation and GDP contribution.

The technology under study has proven to be able to operate safely. However, some crucial point should be deeper analyzed, in order to increase the confidence with the system and to

reduce the associated technological risk:

- For the proposed freeze-protection strategy, a constant night mass flow has been considered. Further research should be performed to understand the possibility of cold spots both in the storage system and in the receiver piping. The results obtained can be varied according to the opinions of experts, but the presented methodology is still valid.
- Related to the previous point, the immersed heaters present in the storage tanks could be used to maintain a higher margin above the temperature limits.
- The freeze-protection strategy has been chosen based on a technical approach. Once the definitive layout will be defined (see previous points), an economic comparison with different approaches should be performed.
- The layout of the steam loop has been designed like the plant that will be constructed in Portugal. A tailored design should be proposed or adapted for the specific case.
- In the same way, the chosen boiler behaves as the one that will be used in Évora, but with a slightly different layout. A specific design would enhance the performance of the design, while reducing the investment cost.
- The use of innovative salt mixtures, characterized by wider operating range, might be explored.
- For the preheating of the solar field, impedance and resistance heating have been proposed. A heat tracing system based on the use of HTF circulating through micro-channels might be considered, as proposed by [47]. In this way, the utilization of auxiliary electricity would be further reduced.
- Once the demonstration loop will have demonstrated its capabilities, the upscaled plant will have to be build. A detailed techno-economic analysis should be performed to establish specific location, size of the system and steam-loop layout.
- A more detailed study regarding the freeze-protection strategy for a large-scale power plant should be considered.

The present work highlighted the potential of the MSPT technology. Technical, social, economic and business-related aspects have been considered. Main advantages have been underlined, while the related challenges have been properly addressed. CSP systems are the only option able to provide zero-emission, flexible and dispatchable electricity during the entire year, facilitating the integration of other RE, towards the decarbonization of the electricity sector. The use of molten salt as HTF open new great possibilities in terms of R&D and business potential, which would be able to create an international industrial and research hub. This represent a unique opportunity for South Africa: economic growth, local involvement and environmental preservation are keys for a successful sustainable future.

Bibliography

[1] S. Grobbelaar, P. Gauché and A. Brent, "Developing a competitive concentrating solar power industry in South Africa: Current gaps and recommended next steps," *Development Southern Africa 31,* pp. 475-493, 2014.

[2] K. Lovegrove and W. Stein, "Introduction to concentrating solar power (CSP) technology," in *Concentrating solar power technology*, New Delji, India, Woodhead Publishing, 2012, pp. 3-15.

[3] D. Barlev and P. S. R. Vidu, "Innovation in concentrated solar power," *Solar Energy Materials & Solar Cells 95,* pp. 2703-2725, 2011.

[4] F. Trieb, T. Fichter and M. Moser, "Concentrating solar power in a sustainable future electricity mix," *Integrated Research System for Sustainable Science,* pp. 47-60, 26 September 2013.

[5] NREL, "Utility-Scale Concentrating Solar Power and Photovoltaics Projects: A Technology and Market Overview," 2012.

[6] G. Morin, M. Karl, M. Mertins and M. Selig, "Molten Salt as a Heat Transfer Fluid in a Linear Fresnel Collector – Commercial Application Backed by Demonstration," *Energy Procedia, 69,* pp. 689-698, 2015.

[7] NREL, "Gemasolar Thermosolar Plant," 2017b. [Online]. Available: https://www.nrel.gov/csp/solarpaces/project_detail.cfm/projectID=40.

[8] P. Gauché, A. C. Brent and T. v. Backstrom, "Concentrating solar power: improving electricity cost and security of supply, and other economic benefits," 2014.

[9] M. H. C. W. J. A. Mathews, "Concentrating solar power: a renewable energy frontier," *Carbon Management,* pp. 293-308, 15 December 2015.

[10] EY & enolcon gmbh, "Assessment of the localization, industrialization and job creation potential of CSP infrastructure projects in South Africa – A 2030 vision for CSP," 2013.

[11] Eskom, "Electricity generation," February 2017. [Online]. Available: http://www.eskom.co.za/AboutElectricity/FactsFigures/Documents/GX0001GenPlantMixRev18.pdf.

[12] S. Pfenninger, P. Gauché, J. Lilliestam, K. Damerau and F. Wagner, "Potential for concentrating solar power to provide baseload and dispatchable power," *Nature Climate Change,* pp. 689-692, 22 June 2014.

[13] IEA, "South Africa.: Electricity and heat for 2014," 2014. [Online]. Available: https://www.iea.org/statistics/statisticssearch/report/?country=SouthAfric&product=electricityandheat.

[14] C. Silinga, P. Gauché and W. v. Niekerk, "CSP scenarios in South Africa: Benefits of CSP and the lessons learned," in *AIP Conference Proceedings 1734,*, 2016.

[15] Eskom, *Concentrating Solar Power (CSP) - FACT SHEET,* 2015.

[16] DoE - Republic of South Africa, "State of Renewable Energy in South Africa," 2015.

[17] J. Rudman, P. Gauché and K. J. Esler, "Initial review and analysis of the direct environmental impacts of the CSP in the Northern Cape, South Africa," in *AIP Conference Proceedings*, 2016.

[18] DoE - Republic of South Africa, "Integrated Resource Plan update – Assumptions, base case results and observations," 2016.

[19] SASTELA, "Status of CSP and its future in the South African energy mix," 2015.

[20] A. Fernàndez-Garcìa, E. Zarza, L. Valenzuela and M. Pérez, "Parabolic-trough solar collectors and their applications," *Renewable and Sustainable Energy Review n 14,* pp. 1695-1721, 2010.

[21] M. Schlecht and R. Meyer, "Site selection and feasibility analysis for concentrating solar power (CSP) systems," in *Concentrating solar power technology*, New Delji, India, Woodhead Publishing, 2012, pp. 91-119.

[22] NREL, "Concentrating Solar Power Projects in South Africa," 4 May 2017. [Online]. Available: https://www.nrel.gov/csp/solarpaces/by_country_detail.cfm/country=ZA.

[23] F. Dinter and L. Möller, "A review of Andasol 3 and perspective for parabolic trough CSP plants in South Africa," in *AIP Conference Proceedings 1734*, 2016.

[24] C. Silinga and P. Gauché, "Scenarios for a South African CSP peaking system in the short term," *Energy Procedia 49,* pp. 1543-1552, 2014.

[25] V. K. Jebasingh and G. M. J. Herbert, "A review of solar parabolic trough collector," *Renewable and Sustainable Energy Reviews n 54,* pp. 1085-1091, 2016.

[26] N. B. Desai and S. Bandyopadhyay, "Line-focusing concentrating solar collector-based power plants: a review," *Clean Technologyies and Environmental Policy,* pp. 9-35, 21 June 2016.

[27] O. Behar, A. Khellaf and K. Mohammedi, "A novel parabolic trough solar collector model – Validation with experimental data and comparison to Engineering Equation Solver (EES)," *Energy Conversion and Management 106,* pp. 268-281, 2015.

[28] E. Z. Moya, "Parabolic-trough concentrating solar (CSP) systems," in *Concentrating solar power technology*, New Delji, Woodhead Publishing, 2012, pp. 197-239.

[29] F. Matino and A. Maccari, "Molten salt receivers operated on parabolic trough demo plant and in laboratory conditions," *Energy procedia n 69,* pp. 481-486, 2015.

[30] K. Riffelmann, J. Kotter, P. Nava, F. Meuser, G. Weinrebe, W. Schiel, G. Kuhlmann, A. Wohlfahrt, A. Nady and R. Dracker, "HelioTrough – A new collector generation for parabolic trough power plants," 2009.

[31] K. Riffelmann, T. Richert, P. Nava and A. Schweitzer, "Ultimate Trough® – A Significant Step towards Cost-competitive CSP," *Energy Procedia, 49,* pp. 1831-1839, 2014.

[32] J. Stekli, L. Irwin and R. Pitchumani, "Technical Challenges and Opportunities for Concentrating Solar Power with Thermal Energy Storage," *Journal of Thermal Science and Engineering Applications,* June 2013.

[33] T. Bauer, N. Pfleger, N. Breidenbach, M. Eck, D. Laing and S. Kaesche, "Material aspects of Solar Salt for sensible heat storage," *Applied Energy 111,* pp. 1114-1119, 2013.

[34] K. Vignarooban, X. Xu, A. Arvay, K. Hsu and A. M. Kannan, "Heat transfer fluids for concentrating solar power systems - A review," *Applied Energy n 146,* pp. 383-396, 2015.

[35] V. M. B. Nunes, C. S. Queiròs, M. J. V. Lourenco, F. J. V. Santos and C. A. N. d. Castro, "Molten salts as engineering fluids – A review. Part I. Molten alkali nitrates," *Applied Energy 183,* pp. 603-611, 2016.

[36] C. Muller-Elvers, M. Wittmann, A. Schubert, M. Ubler, R. Ernst, S. Hillebrand and M. Saur, "Design and Construction of Molten Salt Parabolic Trough HPS Project in Evora, Portugal," 2012.

[37] T. Ruegamer, H. Kamp, T. Kuckelkorn, W. Schiel, G. Weinrebe, P. Nava, K. Riffelmann and T. Richert, "Molten salt for parabolic trough applications: system simulation and scale effects," *Energy Procedia 49,* pp. 1523-1532, 2014.

[38] D. Kearney, B. Kelly, U. Herrmann, R. Cable, J. Pacheco, R. Mahoney, H. Price, D. Blake, P. Nava and N. Potrovitza, "Engineering aspects of a molten salt heat transfer fluid in a trough solar field," *Energy 29,* pp. 861-870, 2004.

[39] R. W. Bradshaw and N. P. Siegel, "Molten nitrate salt development for thermal energy storage in parabolic trough solar power systems," *Energy Sustainability ,* pp. 1-7, 2008.

[40] T. Richert, K. Riffelmann and P. Nava, "The influence of Solar Field inlet and outlet temperature on the cost of electricity in a Molten Salt Parabolic Trough Power Plant," *Energy Procedia 69,* pp. 1143-1151, 2015.

[41] Abengoa Solar, "Development of Molten-Salt Heat Transfer Fluid Technology for Parabolic Trough Solar Power Plants," Lakewood, USA, 2013.

[42] Kearney & Associates, *Engineering Evaluation of a Molten Salt HTF in a Parabolic Trough Solar Field,* 2014.

[43] D. Kearney, B. Kelly, R. Cable, N. Potrovitza, U. Herrmann, P. Nava, R. Mahoney, J. Pacheco, D. Blake and H. Price, "Overview on use of a Molten Salt HTF in a Trough Solar Field," NREL Parabolic Trough Thermal Energy Storage Workshop, Golden, CO, United States, 2003.

[44] J. J. Burkhardt, G. A. Heath and C. S. Turchi, "Life Cycle Assessment of a Parabolic Trough Concetrating Solar Power Plant and the Impacts of Key Design Alternatives," *Evironmental Science&Technology 45,* pp. 2457-2464, 2011.

[45] K. Minnici, *Molten Salts as Heat Transfer Fluids for Solar Thermal Power Plants,* Drexel University, 2015.

[46] R. Serrano-Lopez, J. Fradera and S. Cuesta-Lopez, "Molten salt database for for energy applications," Burgos, Spain, 2013.

[47] M. Eickhoff, M. Meyer-Grunefeldt and L. Keller, "New operating strategies for molten salt in line focusing solar fields – Daily drainage and solar receiver preheating," in *AIP Conference Proceedings, 1734*, 2016.

[48] D. Consoli, "Archimede Solar Thermal Power Plant," ENEL Ingegneria e Innovazione SpA – Research T.A., Ravenna, Italy, 2012.

[49] A. Maccari, D. Bissi, G. Casubolo, F. Guerrini, L. Lucatello, G. Luna, A. Rivaben, E. Savoldi, S. Tamano and M. Zuanella, "Archimede Solar Energy molten salt parabolic trough demo plant: a step ahead towards the new frontiers of CSP," *Energy Procedia 69,* pp. 1643-1651, 2015.

[50] S. Donnola, A. Maccari, F. Matino and S. Tamano, "Archimede Solar Energy Molten Salt Parabolic Trough Demo Plant: improvements and second year of operation," 2016.

[51] Steinmüller Engineering GmbH, "Steinmüller Engineering news," 2017.

[52] Flagsol GmbH, "HelioTrough," 2013. [Online]. Available: http://www.heliotrough.com/index.html.

[53] Sandia National Laboratories, "Design Considerations for Concentrating Solar Power Tower Systems Employing Molten Salt," Albuquerque, New Mexico, USA, 2010.

[54] Eskom, "HPS2 Project - Operation Modes," 2017.

[55] dvtel, "Eskom Secures Mission-Critical Site with DVTEL Thermal and Video Analytics Solution," 2015.

[56] Eskom, "Map of Eskom power stations," 2017b. [Online]. Available: http://www.eskom.co.za/Whatweredoing/ElectricityGeneration/PowerStations/Pages/Map_Of_Eskom_Power_Stations.aspx7.

[57] N. Janotte, G. Feckler, J. Kötter, S. Decker, U. Herrmann, M. Schmitz and E. Lüpfert, "Dynamic performance evaluation of the HelioTrough collector demonstration loop – towards a new benchmark in parabolic trough qualification," *Energy Procedia, 49,* pp. 109-117, 2014.

[58] J. Kotter, K. Riffelmann, S. Decker, J. Fellmuth, A. Macke, P. Nava, G. Weinrebe, W. Schiel, A. Steindorf and R. Dracker, "One Year Experience with the Loop in a Commercial Solar Power Plant," 2010.

[59] J. Kotter, S. Decker, R. Detzler, J. Schafer, M. Schmitz and U. Herrmann, "Cost reduction of Solar Fields with HelioTrough Collector," 2012.

[60] Rioglass, "Rioglass 70mm HCE Receiver technical specifications," 2017.

[61] J. Guo and X. Huai, "Multi-parameter optimization design of parabolic trough solar receiver," *Applied Thermal Engineering, 98,* pp. 73-79, 2015.

[62] M. Wirz, "Optical and thermal modelling of a Parabolic Trough concentrator system," Bern. Switzerland, 2014.

[63] C. Tzivanidis, E. Bellos, D. Korres, K. Antonopoulos and G. Mitsopoulos, "Thermal and optical efficiency investigation of a parabolic trough collector," *Case Studies in Thermal Engineering, 6 ,* pp. 226-237, 2015.

[64] H. Liang, S. You and H. Zhang, "Comparison of different heat transfer models for parabolic trough solar collectors," *Applied Energy, 148,* pp. 105-114.

[65] M. Abedini-Sanigy, F. Ahmadi, E. Goshtasbirad and M. Yaghoubi, "Thermal Stress Analysis of Absorber Tube for a Parabolic Collector under Quasi-Steady State Condition," *Energy Procedia, 69,* pp. 3-13, 2015.

[66] A. Almasabi, A. Alobaidli and T. Zhang, "Transient Characterization of Multiple Parabolic Trough Collector Loops in a 100 MW CSP Plant for Solar Energy Harvesting," *Energy Procedia, 69,* pp. 24-33, 2015.

[67] NREL, "Technical manual for the SAM Physical Trough Model," 2011.

[68] T. E. Boukelia, M. S. Mecibah and A. Laouafi, "Performance simulation of Parabolic Trough solar collectors using two fluids (thermal oil and molten salt)," *Journal of Fundamental and Applied Sciences,* pp. 600-626, 1 May 2016.

[69] SAURAN, "UPR - GIZ University of Pretoria," 2017. [Online]. Available: http://www.sauran.net/ShowStation.aspx?station=5.

[70] W. A. K. Al-Maliki, F. Alobaid, V. Kez and B. Epple, "Modelling and dynamic simulation of a parabolic trough power plant," *Journal of Process Control 39,* pp. 123-138, 2016.

[71] A. A. Hachicha, *Numerical modelling of a parabolic trough solar collector,* Terrassa: Centre Tecnològic de Transferència de Calor - Departament de Màquines i Motors Tèrmics - Universitat Politècnica de Catalunya, 2013.

[72] A. Moss and D. A. Brosseau, "Final Test Results for the Schott HCE on a LS-2 Collector," Sandia Laboratories, Albuquerque, New Mexico, USA, 2005.

[73] NREL, "Paraboic Trough Solar System Piping Model," 2006.

[74] R. V. Padilla, "Simplified Methodology for Designing Parabolic Trough Solar Power Plants," University of South Florida, 2011.

[75] A. Bahadori and H. B. Vuthaluru, "A simple correlation for estimation of economic thickness of thermal insulation for process piping and equipment," *Applied Thermal Engineering, 30,* pp. 254-259, 2010.

[76] F. Zaversky, J. García-Barberena, M. Sánchez and D. Astrain, "Transient molten salt two-tank thermal storage modeling for CSP performance simulations," *Solar Energ, 93,* pp. 294-311, 2013.

[77] K. M. Powell and T. F. Edgar, "Modeling and control of a solar thermal power plant with thermal energy storage," *Chemical Engineering Science, 71,* pp. 138-145, 2012.

[78] U. Hermann, B. Kelly and H. Price, "Two-tank molten salt for parabolic trough solar power plants," *Energy, 29,* pp. 883-893, 2004.

[79] G. Towler and R. Sinnott, "Chapter 19 - Heat-Transfer Equipment," in *Chemical Engineering Design: Principles, Practice and Economics of Plant and Process Design*, Elsevier, 2013, pp. 1047-1205.

[80] R. K. Shah and D. Sekulic, Fundamentals of Heat Exchanger Design, John Wiley & Sons , 2003.

[81] V. Ariu, Heat exchanger analysis for innovative molten salt fast reactors, Villingen, Germany: Paul Scherrer Institut, 2014.

[82] W. A. Allman, D. C. Smith and C. R. Kakarala, "The Design and Testing of a Molten Salt Steam Generator for Solar Application," ASME, 1988.

[83] XSteam, "X Steam - Properties for water and steam," 2017. [Online]. Available: http://xsteam.sourceforge.net/.

[84] X. Fang, Z. Zhou and H. Wang, "Heat transfer correlation for saturated flow boiling of water," *Applied Engineering, 76,* pp. 147-156, 2015.

[85] J. R. Thome, "Laboratory of Heat and Mass transfer," 2015. [Online]. Available: htttp://ltcm.epfl.ch.

[86] B. P. Vitalis and P. J. Hunt, "Constant and Sliding Pressure Options for New Supercritical Plants," Las Vegas, Nevada, 2005.

[87] M. Wagner, *Modeling Parabolic trough Systems,* 2014.

[88] P. Gonzalez-Gómez, J. Gómez-Hernández, J. Briongos and D. Santana, "Thermo-economic optimization of molten salt steam generators," *Energy Conversion and Management, 146,* pp. 228-243, 2017.

[89] S. Donnola, A. Maccari, F. Matino and S. Tamano, *Archimede Solar Energy Molten Salt Parabolic Trough Demo Plant: improvements and second year of operation,* Cape Town: Archimede Solar Energy, 2015.

[90] P. H. Wagner, M. Wittmann, C. Wieland and H. Spliethoff, "Thermodynamic simulation of solar thermal power stations with liquid salt as heat transfer fluid," 2012.

[91] M. Z. Yilmazoglu, "Effects of the selection of heat transfer fluid and condenser type on the performance of a solar thermal power plant with technoeconomic approach," *Energy Conversion and Management, 111 ,* pp. 271-2787, 2016.

[92] M. Falchetta and A. G. Rossi, "Dynamic simulation of the operation of a molten salt parabolic trough plant, comprising draining procedures," *Energy Procedia 49,* pp. 1328-1339, 2014.

[93] S. Sau, N. Corsaro, T. Crescenzi, C. D'Ottavi, R. Liberatore, S. Licoccia, V. Russo, P. Tarquini and A. Tizzoni, "Techno-economic comparison between CSP plants presenting two different heat transfer fluids," *Applied Energy, 168,* pp. 96-109, 2016.

[94] exxaro, "South Africa's grid emissions factors," 2013.

[95] K. Riffelmann, T. Richert, P. Nava and A. Schweitzer, "Ultimate Trough® – A Significant Step towards Cost-competitive CSP," *Energy Procedia, 49 ,* pp. 1831-1839, 2014.

[96] P. Kurup and C. S. Turch, "Parabolic Trough Collector Cost Update for the System Advisor Model (SAM)," NREL, 2015.

[97] Bloomberg, "Currencies," 2 June 2017. [Online]. Available: https://www.bloomberg.com/markets/currencies. [Accessed 2 June 2017].

[98] G. Towler and R. Sinnott, "Chapter 7 - Capital cost estimating," in *Chemical Engineering Design: Principles, Practice and Economics of Plant and Process Design*, Elsevier, 2013, pp. 307-354.

[99] C. Turchi, "Parabolic Trough Reference Plant for Cost Modeling with the Solar Advisor Model (SAM)," NREL, 2010.

[100] K. Damerau, K. Williges, A. G. Patt and P. Gauché, "Costs of reducing water use of concentrating solar power to sustainable levels Scenarios for North Africa," *Energy Policy, 39 ,* pp. 4391-4398, 2011.

[101] Eskom, "List of fact sheets," 2015.

[102] S. Tolksdorf and F. Dinter, "Design of a solar field for a 100 MWe molten salt parabolic trough power plant with TES in Upington, South Africa with a novel freeze protection approach (Pre-publishing)," Stellenbosch University, Stellenbosch, South Africa, 2017.

[103] T. P. Fluri, "The potential of concentrating solar power in South Africa," *Energy Policy, 37,* pp. 5075-5080, 2009.

[104] H. Zhang, J. Baeyens, J. Degreve and G. Caceres, "Concentrated solar power plants_ Review and design methodology," *Renewable and Sustainable Energy Reviews, 22 ,* pp. 466-481, 2013.

[105] Klaus and Riffelmann, "Suitable Solar Field Layout For The Ultimate Trough Collector," 2012.

[106] S. J. Smith, "The long-term market potential of concentrating solar power (CSP) technology," in *Concentrating solar power technology*, New Delji, India, Woodhead Publishing, 2012, pp. 437-465.

[107] R. Boyd, A. Rosenberg and A. Hobbs, "The Role of Public Finance in CSP Case Study: Eskom CSP, South Africa," 2014.

[108] WWF, "Concentrated Solar Power – A strategic industrial development opportunity for South Africa," 2015.

[109] A. Amato, M. Compare, M. Gallisto, A. Maccari, M. Paganelli and E. Zio, "Business interruption and loss of assets risk assessment in support of the design of an innovative concentrating solar power plant," *Renewable Energy, 36,* pp. 1558-1567, 2011.

[110] D. Vallentin and P. Viebahn, "Economic opportunities resulting from a global deployment of concentrated solar power (CSP) technologies—The example of German technology providers," *Energy Policy, 38,* pp. 4467-4478, 2010.

[111] E. R. G. Eckert and R. M. Drake, Analysis of heat and mass transfer, New York: McGraw-Hill, 1972.

[112] solargis, "GeoSUN Africa," 2014. [Online]. Available: http://geosun.co.za/maps/. [Accessed 12 May 2017].

Annexes

Annex I: Coefficients for the calculation of the Nusselt number in equation (2.28)

In the following table, the coefficients *C* and *m* needed for the calculation of the convective heat transfer coefficient between the glass and the external environment are report as function of the Reynolds number.

Table 0.1: Values of C and m for different Reynolds number [64]

Reynolds number range	C	m
1-40	0.75	0.4
40-1 000	0.51	0.5
1 000-200 000	0.26	0.6
200 000-1 000 000	0.076	0.7

Annex II: Air properties

The air properties utilized in section 2.2.6 have been taken from [111] and they are hereafter report, as function of the temperature *T*, expressed in Kelvin and the pressure, *p,* expressed in Pascal.

Thermal conductivity:

$$k_{air} = \frac{2.648 \cdot 10^{-3}\sqrt{T}}{1 + (\frac{245.4}{T}) \cdot 10^{-12/T}}$$

Density:

$$\rho_{air} = \frac{p}{287 \cdot T}$$

Viscosity:

$$\mu_{air} = \frac{1.458 \cdot 10^{-6} \cdot T^{1.5}}{T + 110.40}$$

Specific heat capacity:

$$c_{p,air} = 1034.09 - 2.849 \cdot 10^{-1} \cdot T + 7.817 \cdot 10^{-4} \cdot T^2 - 4.971 \cdot 10^{-7} \cdot T^3 + 1.077 \cdot 10^{-10} \cdot T^4$$

Annex III: Validation of the model

No test results were available regarding the use of molten salt in the chosen collector and receiver. On the other hand, many sources report these values when the thermal oil is used. Since the model presented can be virtually used with any kind of HTF, [72] is used as a reference to compare experimental data with the obtained values. The test is performed utilizing the LS-2 collector and Syltherm 800 as operating fluid. The geometric characteristics of the collector and the thermophysical properties of the oil are reported in the following:

Table 0.2: Geometrical characteristics of the LS-2 collector [72]

Parameter	Symbol	Value	Unit
Focal length	f	1.84	m
Net aperture width	W	5	m
Rim angle	Ψ	70°	/
Number of SCE per assembly	/	6	/
Net aperture area of the SCA	A_{SCA}	234	m^2
Gross SCA length	l_{tube}	46.8	m

The tests were performed with the Schott receiver, whose properties have been already described in the main part of the report. The collector was tested in different conditions of ambient temperature, solar radiation and wind speed. In the following table, five different situations are reported, highlighting fluid inlet and outlet temperature, inlet velocity and relative error of the calculation. As it can be appreciated, it is always very low: the model utilized is consistent and realistic. The incidence angle is always kept equal to 0° [72].

Table 0.3: Thermophysical properties of the Syltherm 800 [64]

Property	Symbol	Function	Unit
Density	ρ	$1015.7 - 0.4153 \cdot \mathrm{T} - 6.0617 \cdot 10^{-4} \cdot T^2$	kg/m^3
Specific heat capacity	c_p	$1107.798 + 1.708 \cdot T$	J/kgK
Viscosity	μ	$0.0848 - 5.54 \cdot 10^{-4} \cdot T + 1.38 \cdot 10^{-6} \cdot T^2 - 1.56 \cdot 10^{-9} \cdot T^3$	$Pa \cdot s$
Conductivity	k	$0.19 - 1.87 \cdot 10^{-4} \cdot T$	W/mK

Table 0.4: Comparison between experimental data and values from the model

Solar radiation [W/m^2]	Air temperature [°C]	Wind speed [m/s]	Fluid inlet velocity [m/s]	Fluid inlet temperature [K]	Fluid outlet temperature (experimental) [K]	Fluid outlet temperature (model) [K]	Relative error
999.45	17.98	2.10	0.18	294.5	306.28	304.2	-0.7%
1044.73	4.83	2.77	0.27	474.38	495.77	491.36	-0.9%
953.29	7.63	1.34	0.27	571.42	591.35	592.69	0.2%
1016.51	10.64	1.74	0.27	621.34	643.45	644.82	0.2%
1015.78	11.98	3.53	0.27	636.12	658.07	659.59	0.2%

Annex IV: Coefficients for the calculation of the insulation thickness

In the following tables, the coefficients used for the calculation of the insulation thickness for the solar field piping are reported.

Table 0.5: Coefficients for the calculation of the insulation thickness in the solar field piping [76]

Coefficient	Value
A_0	-1.306428735
B_0	$1.636801061 \cdot 10^{-2}$
C_0	$-1.927263416 \cdot 10^{-3}$
D_0	$6.081932874 \cdot 10^{-4}$
A_1	$2.149490799 \cdot 10^{-2}$
B_1	$-7.236908659 \cdot 10^{-2}$
C_1	$6.252139677 \cdot 10^{-3}$
D_1	$-1.77029853 \cdot 10^{-5}$
A_2	$-1.257195231 \cdot 10^{-3}$
B_2	$3.687234096 \cdot 10^{-4}$
C_2	$-3.183035693 \cdot 10^{-5}$
D_2	$9.014140246 \cdot 10^{-6}$
A_3	$1.498173167 \cdot 10^{-5}$
B_3	$-4.256243216 \cdot 10^{-6}$
C_3	$3.670609916 \cdot 10^{-7}$
D_3	$-1.03922241 \cdot 10^{-8}$

Annex V: Coefficients for the calculation of Colburn and friction factors

The coefficients needed for the evaluation of the Colburn and friction factors are reported in the following Table. They refer to the 30° pitch arrangement and they are expressed as function of the Reynolds number (Re).

Table 0.6: Coefficients for the calculation of the Colburn and friction factor inside shell-and-tube heat exchangers [82]

Re	a_1	a_2	a_3	a_4	b_1	b_2	b_3	b_4
10^5-10^4	0.321	-0.388	1.450	0.519	0.372	-0.123	7.000	0.500
10^4-10^3	0.321	-0.388	0	0	0.486	-0.152	0	0
10^3-10^2	0.593	-0.477	0	0	4.570	-0.476	0	0
10^2-10	1.360	-0.657	0	0	45.100	-0.973	0	0
< 10	1.400	-0.677	0	0	48.000	-1.000	0	0